Mechanobiological predictions of fetal joint morphogenesis

By

MARIO GIORGI

Imperial College London

Department of Bioengineering

This dissertation is submitted in partial fulfilment of the requirements for the degree of Doctor of Philosophy

Mario Giorgi

Supervised by Dr. Niamh C. Nowlan and Dr. Sandra J. Shefelbine

Imperial College London, United Kingdom

Declaration of Originality

I hereby certify that this thesis is my own work. I declare that this work is original and that I only used the sources and means which are mentioned throughout the thesis. All other sources of information are clearly identified and references are fully cited.

This thesis was carried out between October 2011 and March 2015 under the supervision of Dr. Niamh C. Nowlan and Dr. Sandra J. Shefelbine in the Department of Bioengineering at Imperial College London (UK).

London, 27/03/2015 Signature

_____ _____

Copyright Declaration

Abstract

This PhD thesis explores, through the use of a mechanobiological simulation of prenatal joint morphogenesis, the hypotheses on how fetal movements, shapes and position impact on the shape of the developing joint.

A novel mechanoregulation algorithm specific for cartilage growth was developed and, for the first time, a 3D mechanobiological simulation of joint morphogenesis in which the effects of a range of movements and different initial joint shapes was proposed. Both pre- and post-cavitational phases of joint development were simulated and the effect of rigid paralysis on joint shape was also explored. This study concluded that the starting joint configuration and applied movement are fundamental for the development of specific and anatomically recognisable joint shapes.

Moreover, for the first time, a mechanobiological simulation of prenatal hip joint morphogenesis was used to investigated the effects of reduced, or asymmetric, movement at various stages of fetal hip joint development. This study concluded that normal fetal movements are important for the emergence of a physiological hip joint shape and that movements during development tend to minimise the natural trend of decreasing stability. Results showed that reduced movements at an early stage of development lead to decreased sphericity and acetabular coverage of the femoral head, increasing the risk of subluxation or dislocation of the hip. It also shows that, in the case of mal-positioning or joint laxity in utero, movements may actually lead to an abnormal hip joint shape with characteristics of developmental dysplasia of the hip (DDH).

This PhD thesis has advanced the basic understanding of prenatal joint shape development and the implication that different mechanical environments within the joint region, might have on developmental skeletal diseases such as DDH.

Acknowledgements

This PhD thesis would not have been possible without the support and encouragement of many people.

First of all, I wish to express my sincere gratitude to both my supervisors, Dr. Niamh C. Nowlan and Dr. Sandra J. Shefelbine, who have mentored, guided and believed in me throughout my time at Imperial College London. You have both taught me so much.

I would like to thank everyone from Niamh's lab, Vikesh Chandaria, Stefaan Verbruggen, Samantha Martin and Lisa Abela, and everyone from Sandra's lab, Naiara Rodriguez-Florez, Alessandra Carriero and Andre Pereira.

Very special thanks goes to Naiara Rodriguez-Florez, Alessandra Carriero and Vikesh Chandaria for being amazing colleagues and friends.

I also want to thanks everyone who throughout the years contributed to making London my second home. Thanks to Mercedes Mateos, Gianmarco Mengaldo, Daniele De Grazia, Alessando Bolis, Sahir Gandhi, Gabriella Raimondo, Umberto Callegari and Guido Goggi for being fantastic companions during this journey.

This PhD thesis has been possible especially thanks to Mercedes, who strongly supported me during these (almost) four years. A new chapter is now starting, and this time will be with you.

Last but not least, a special thanks goes to my family, who throughout my life, and particularly during this period, have always shown faith in me and encouraged me to persist and succeed through both the good and difficult times I was faced with.

Publications and presentations resulting from this study

Giorgi, M., Carriero, A., Shefelbine, S.J., Nowlan, N.C., 2014. *"Effect of Normal and Abnormal Loading on Morphogenesis of the Prenatal Hip Joint: Application to hip Dysplasia"*, Journal of Biomechanics, in review.

Giorgi, M., Carriero, A., Shefelbine, S.J., Nowlan, N.C., 2014. *"Mechanobiological simulations of prenatal joint morphogenesis"*. Journal of Biomechanics 47, 989-995.

Giorgi, M., Carriero, A., Shefelbine, S.J., Nowlan, N.C. *"The role of prenatal movements in promotion postnatal hip joint stability"*. BSMB, 01-03 September, 2014, Norwich, UK (Podium).

- Winner of the Best Oral Presentation prize.

Giorgi, M., Carriero, A., Shefelbine, S.J., Nowlan, N.C. *"Mechanobiological simulations of prenatal joint morphogenesis"*. 7th World Congress of Biomechanics, 6-9 July, 2014, Boston, USA (Podium).

- Winner of the ESB (European Society of Biomechanics) award.

Giorgi, M., Carriero, A., Shefelbine, S.J., Nowlan, N.C. *"Mechanobiological simulations of prenatal joint morphogenesis"*. Muscoskeletal Technology Network, 27 February, 2014, London, UK (Podium).

Giorgi, M., Carriero, A., Shefelbine, S.J., Nowlan, N.C. *"Fetal movements play an important role in joint morphogenesis"*. 59th Annual Meeting of the Orthopaedic Research Society, 26-29 January, 2013, San Antonio, USA (Poster Presentation).

Giorgi, M., Carriero, A., Shefelbine, S.J., Nowlan, N.C. *"Fetal movements play an important role in joint morphogenesis"*. Pre-Orthopaedic Research Society, 25 January, 2013, San Antonio, USA (Podium).

Giorgi, M., Carriero, A., Shefelbine, S.J., Nowlan, N.C. *"Mechanobiological prediction of foetal joint morphogenesis"*. Bioenginnering13, 16-17 September, 2013, Glasgow, UK (Podium).

Giorgi, M., Carriero, A., Shefelbine, S.J., Nowlan, N.C. *"Influence of mechanical forces on joint morphogenesis"*. Bioengineering 2012, 6th – 7th Sept 2012, Oxford University, UK. (Podium).

Table of Contents

Table of Figures

1 Introduction and Objectives

1.1 Introduction

During prenatal joint development, the two opposing cartilaginous rudiments of a joint develop their reciprocal and interlocking shapes through a process known as morphogenesis (Pacifici et al., 2005). Pacifici et al. (2005) describe the process of synovial joint formation as a well-defined sequence of three events: 1) a layer of compact and closely associated mesenchymal cells form the interzone, 2) cavitation results in the physical separation of the adjacent skeletal elements within the interzone, and 3) joint shape occurs through the process of morphogenesis. Recent studies, however, have shown that joint morphogenesis is a continuous process which commences prior to, and continues after, joint cavitation (Nowlan and Sharpe, 2014).

The consequences of incomplete or abnormal morphogenesis can be debilitating, such as in the case of musculoskeletal diseases. A number of experimental studies have shown that fetal immobilisation can alter joint shape development (Kahn et al., 2009; Mikic et al., 2000; Nowlan et al., 2010b; Osborne et al., 2002; Roddy et al., 2011b), therefore shedding light on the influence of fetal movements on joint formation. However, the mechanism by which these movements affect joint morphogenesis is still unknown (Pacifici et al., 2005).

A lack of movements or an abnormal mechanical environment during prenatal development have been strongly linked to developmental dysplasia of the hip, also known as DDH, which is the most common congenital abnormality of the hip joint. DDH occurs when the hip joint is malformed, unstable or dislocated (Aronsson et al., 1994), and occurs in 1.3 per 1000 births (Leck, 2000). Two types of dislocation have been defined (Ponseti, 1978), one known as teratologic dislocation which occurs early *in utero* and is usually associated with neuromuscular problems (Aronsson et al., 1994; Nowlan et al., 2014), and one known as typical dislocation which occurs *in utero* or after birth and is usually associated with breech position or oligohydramnios (Aronsson et al., 1994; Nowlan et al., 2014).

Thanks to the growing literature regarding material properties and mechanics of the human body, the use of computational models in the field of biomechanics is

growing rapidly. However, only one computational study has explored the role of motion on joint morphogenesis (Heegaard et al., 1999), using an idealised planar biomechanical model of the proximal interphalangeal joint in which epiphyseal growth was simulated using a modified version of the endochondral ossification theory proposed by Carter et al. (1987).

In this thesis, a novel mechanobiology theory for cartilage growth is proposed and employed, through the use of mechanobiological simulations, to provide new and important insights into normal and abnormal joint development. This study delivers a deeper understanding of the importance of fetal movements in promoting normal and abnormal joint morphogenesis and their implications in musculoskeletal diseases such as the developmental dysplasia of the hip (DDH).

1.2 Objectives

The consequences of an incomplete or abnormal process of morphogenesis can be debilitating, such as in the case of musculoskeletal diseases. For example, the fetal akinesia deformation sequence (FADS), which occurs when little or no fetal movements take place (Witters et al., 2002); arthorogrypososis, which is due to a substantial reduction in fetal movements (Bamshad et al., 2009) and, the developmental dysplasia of the hip (DDH) which is the most common congenital abnormality strongly linked to abnormal movements or intrauterine conditions (Aronsson et al., 1994). Therefore, understanding the factors driving joint morphogenesis during prenatal development is critical for developing strategies for early diagnosis and preventative treatments for these diseases.

The first objective and challenge of this work is to develop a novel mechanobiological simulation of prenatal joint morphogenesis based on a mechanoregulation theory developed specifically for cartilage growth. A secondary objective of the work is to propose and test hypotheses on how fetal movements and position impact upon the shape of the developing hip joint. The body of work involved the following steps:

1. *Understanding the effectiveness of the endochondral ossification mechanobiological theory proposed by Carter et al. (1987) as an algorithm to predict prenatal joint development.* The study of the mechanobiological growth theory began by presenting and replicating the first computational

model developed for prenatal joint morphogenesis (Heegaard et al., 1999), and then described the growth theory evolution through the different models: “rectangular shape”, “proximal interphalangeal joint”, and “hinge joint motion”. (Chapter 3).

2. *Proposing a novel mechanobiological simulation of prenatal joint morphogenesis.* A novel mechanobiology theory for cartilage growth was developed and used in the first 3D mechanobiological simulation of joint morphogenesis which included the effects of a range of movements (or lack of movement) and different initial joint shapes is developed (Chapter 4).
3. *Sensitivity analysis,* there are many parameters in the model that played an important role in the resultant shapes and therefore, this chapter aimed to provide additional evidence for the choices made within the model (Chapter 5).
4. *Proposing and testing hypotheses on how fetal movements impact upon the shape of the developing hip joint.* A dynamic mechanobiological simulation of the prenatal hip joint was used to explore the effects of normal, reduced and asymmetric fetal movements on hip joint growth and morphogenesis (Chapter 6).

Finally, conclusions are drawn in Chapter 7. The main outcomes of this thesis as well as contributions to the field of developmental mechanobiology are discussed, and perspectives for future research are presented.

2 Background

2.1 Prenatal development & fetal growth

The prenatal development of the human skeleton is divided into two periods, the embryonic and fetal phase. Embryonic development is defined as the first 8 weeks of intra-uterine life and fetal development is the remaining period until birth (Scheuer and Black, 2004). The embryonic development of the skeleton has been thoroughly described by Bardeen and Lewis in 1901 in a study observing the typical stages during the development of the back, limbs and the body-wall in humans. They reported that in an embryo of approximately 2 weeks of gestational age (~2.1mm embryos length), its axis is curved and it contains the neural tube, notochord, mesenchyme and myotomes in the cervical region. The limb buds start to be present around gestational week 3, when the embryo length is approximately 4.3mm. Between gestational weeks 4 and 5 (~11mm embryos length) several anatomical features start to be more visible. The segmentation of the limbs has begun; the arm is in an advanced stage showing flatter hands, which are now clearly distinguishable from the forearm, the swellings of the digits are visible and the first sign of the shoulder can be detected. At this stage the lower limb shows differentiation of foot and leg. Between gestational weeks 5 and 6, while the digits in the hand are well marked, digitation on the foot has just begun. Within the same period ribs extend ventrally and the vertebral bodies have chondrified. By gestational week 7 (~20mm embryos length) most of the adult anatomical skeletal structures have appeared (Bardeen and Lewis, 1901); the intervertebral discs are present and the vertebrae, as well as the ribs, are composed of hyaline cartilage. At this stage both, vertebrae and ribs are surrounded by a dense mesenchyme, the musculature of the back and abdominal walls, and the main blood-vessels resemble those of the adult. The posterior limb is well differentiated and all its rudiments are present in cartilaginous form with exception for the terminal phalanges of the three outer toes which are still not present at this time. Torsion of the ankle joint has not begun yet at this stage. Likewise, the rudiments of the arm are all made of hyaline cartilage except for the distal phalanges of the 2nd, 3rd, 4th and 5th digits, which are made of undifferentiated condensed tissue. From now on, the fetal phase begins and further development depends mainly on growth and relative shifting of parts (Bardeen and Lewis, 1901).

Progressive growth, formation and progression of the primary and secondary ossification centres, and further shape development are the main events of the fetal development of the skeleton. The development of long bones, during their fetal period, has been studied in detail by several researchers (Bagnall et al., 1982; Gardner and Gray, 1953, 1970) and has been shown that the primary ossification centres for the major long bones (femur, tibia, fibula, humerus, radius and ulna) can be identified histologically in the center of the shaft around gestational week 9 (Bardeen and Lewis, 1901; Gardner and Gray, 1970; Scheuer and Black, 2004), while the appearance of the secondary ossification centres varies among bones. For example, at birth, the proximal end of the femur is entirely cartilagineous and the secondary ossification centre for the femoral head starts to be detectable by the age of 1 year (Elgenmark, 1945; Ryder and Mellin, 1966). Different timings can be seen for the distal femur and the proximal tibia, which are usually present at birth (Christie, 1949; Hill, 1939; Scheuer and Black, 2004). Moreover, the rate of fetal growth, which can be determined by the weight (Doubilet et al., 1997) or the length (O'Rahilly and Müller, 1996) of the fetus, has been reported, by researcher, to slow down over the gestation period (Table 2-1) (Doubilet et al., 1997; O'Rahilly and Müller, 1996). Morphogenesis, the biological process through which an organism develops its shape, will be addressed in detail, with focus on joint morphogenesis, in section 2.3.1.

Table 2-1 Average fetal weight adapted from (Doubilet et al., 1997).

Gestational age	Mass (g)	Gestational age	Mass (g)	Gestational age	Mass (g)
8 weeks	1	20 weeks	300	32 weeks	1702
9 weeks	2	21 weeks	360	33 weeks	1918
10 weeks	4	22 weeks	430	34 weeks	2146
11 weeks	7	23 weeks	501	35 weeks	2383
12 weeks	14	24 weeks	600	36 weeks	2622
13 weeks	23	25 weeks	660	37 weeks	2859
14 weeks	43	26 weeks	760	38 weeks	3083
15 weeks	70	27 weeks	875	39 weeks	3288
16 weeks	100	28 weeks	1005	40 weeks	3462
17 weeks	140	29 weeks	1153	41 weeks	3597
18 weeks	190	30 weeks	1319	42 weeks	3685
19 weeks	240	31 weeks	1502		

2.2 Cartilage & synovial joints

2.2.1 Cartilage

Cartilage is a highly specialized, resilient connective tissue consisting of dispersed chondrocytes, derived from embryonic mesenchyme and embedded in an extracellular matrix (ECM) (Hall, 1983). Cartilage has a relatively simple structure, which does not contains blood vessels (avascular) and progenitors cells (Hunziker, 2000; Mankin, 1982; Silver and Glasgold, 1995). The biochemical composition of the extracellular matrix, which is mainly composed of collagen, proteoglycans and water, determines the biomechanical characteristics of the tissue and is directly responsible for the unique functional properties of cartilage providing resilience and resistance against compression and shear (Lorenzo et al., 2004; Mow et al., 1984). There are three types of cartilage: hyaline cartilage, fibrocartilage and elastic cartilage (Figure 2-1), which differ in functional properties and biochemical contents. Hyaline cartilage is involved in skeletal development in the process of endochondral ossification, and therefore the type of cartilage of interest for this project (from now on simply called cartilage). It is rich in Type II collagen and proteoglycans with an amount of water that constitutes 60% to 80% of its total weight (Dijkgraaf et al., 1995). Fibrocartilage mainly contains Type I collagen, or a combination of Type I and Type II collagen (Dijkgraaf et al., 1995). Fibrocartilage is considered the strongest kind due to the alternating layers of hyaline cartilage matrix and dense collagen fibres oriented in the direction of functional stresses and it is found mainly in tissues that are subject to tensile forces such as the intervertebral disk (Fisher et al., 2007). Elastic cartilage consists of a network of elastic fibres, not exclusively collagen which provides strength and elasticity. The elastic fibres give this type of cartilage the ability to be deformed and return to shape. Examples of elastic cartilage include external ear, epiglottis, and upper portion of larynx (Fisher et al., 2007).

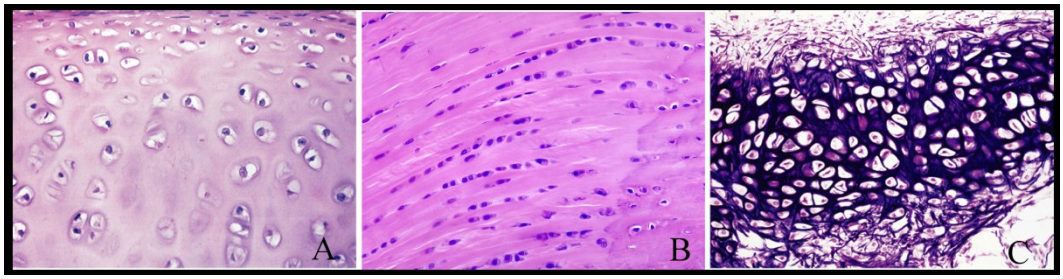

Figure 2-1 Different types of cartilage. A) Hyaline cartilage; B) fibrocartilage; C) elastic cartilage. Images adapted from http://medcell.med.yale.edu

One of the primary functions of hyaline cartilage is to support load. Cartilage can respond to its loading environment by producing more matrix (anabolic), by causing tissue destruction (catabolic) or by calcifying and turning to bone (endochondral ossification). These mechano-adaptive processes indicate that chondrocytes are able to respond to mechanical forces and, in the past years, researchers have studied cellular mechano-transduction in different connective tissues (Carter et al., 1998b; Gillard et al., 1979; Koob et al., 1992; Woo and Buckwalter, 1988).

2.2.2 Mechanobiology of cartilage

During embryonic development, cartilage undergoes numerous changes in cellular and extracellular composition. Various experimental studies suggested that an appropriate mechanical environment is crucial to develop a proper fully functioning joint. For example, paralysis of embryonic chicks limbs may block joint cavity formation or lead to abnormal joint shape (Mikic et al., 2000; Ward and Pitsillides, 1998). These studies indicate that mechanical loading has an important effect on cartilage during development and that growth and ossification of this tissue are locally regulated by the stresses and strains generated by muscle contractions, pre- and post-natally (Carter and Wong, 2003).

A mature version of hyaline cartilage, known as articular cartilage, is found in the mature skeleton, primarily at the joints surfaces, and has been used by several researchers to understand how cartilage is affected by different mechanical loading conditions (Beaupré et al., 2000; Carter and Wong, 2003; Grodzinsky et al., 2000; Lu and Mow, 2008). Articular cartilage is known to experience a wide range of static and dynamic mechanical loads in synovial joints (Correia et al., 2012; Herberhold et al., 1998; Maxian et al., 1995) and its ability to resist to compressive, tensile and

shear forces depends on the composition and integrity of its ECM (Asanbaeva et al., 2008; Grodzinsky et al., 2000). In vitro models such as cartilage explants were used to study the mechanisms by which chondrocytes respond to mechanical stimuli, and by using these models, the effect of static and dynamic compression have been studied. Li et al. (2001), looked at the biosynthetic and proliferative response of different stages of bovine cartilage maturation (fetal, calf and adult) to well defined static and dynamic unconfined loading protocols. The results showed that cartilage synthesis was inhibited in all tissues by static loading and it was stimulated by the dynamic load in calf cartilage. No significant effects, due to dynamic load on glycosamionglycans synthesis were found on fetal and adult cartilage. A subsequent study (Davisson et al., 2002), focused on determining the effects of static and dynamic compression on the metabolism of sulfated glycosamionglycans (S-GAG) and proteins in tissue engineered cartilage, showed that static compression suppressed the synthesis by 35% and 57% respectively while dynamic compression stimulated synthesis. If researchers agree on the inhibitive effects of static compression on the synthesis of cartilage, contradictory results can be found in literature regarding the effects on biosynthesis due to dynamic compression which have been reported several times as stimulatory (Davisson et al., 2002; Farquhar et al., 1996; Korver et al., 1992; Larsson et al., 1991; Palmoski and Brandt, 1984; Sah et al., 1989) as well, in some cases, as inhibitory (Palmoski and Brandt, 1984; Steinmeyer et al., 1997; Torzilli et al., 1997). However, a large number of studies showed that the application of mechanical compression directly to cartilage explants with specific range of amplitudes and frequencies inhibits cartilage growth when statically loaded (Burton-Wurster et al., 1993; Grodzinsky et al., 2000; Guilak et al., 1994) while promotes cartilage growth under cyclic compressive loads (Grodzinsky et al., 2000; Kim et al., 1994; Korver et al., 1992; Parkkinen et al., 1992).

2.2.3 Synovial joints

Synovial joints are the most movable type of joints and the differences which distinguish synovial joints from other type of joints, such as cartilaginous joints (e.g. intervertebral discs) and fibrous joint (e.g. suture between bones of the skull), lie in its structure and function. Unlike cartilaginous and fibrous joints, the articulating surfaces of a synovial joint are surrounded by a capsule filled with synovial fluid. The articular capsule consists of an external fibrous membrane which contains the

ligaments, and an internal synovial membrane that secretes the lubricating and shock absorbing synovial fluid. This fluid is secreted within the synovial cavity, the characteristic space between the two opposing rudiments typical of synovial joints (Figure 2-2, A). Examples of synovial joints are the elbow, the wrist, the shoulder, the hip and the knee joint.

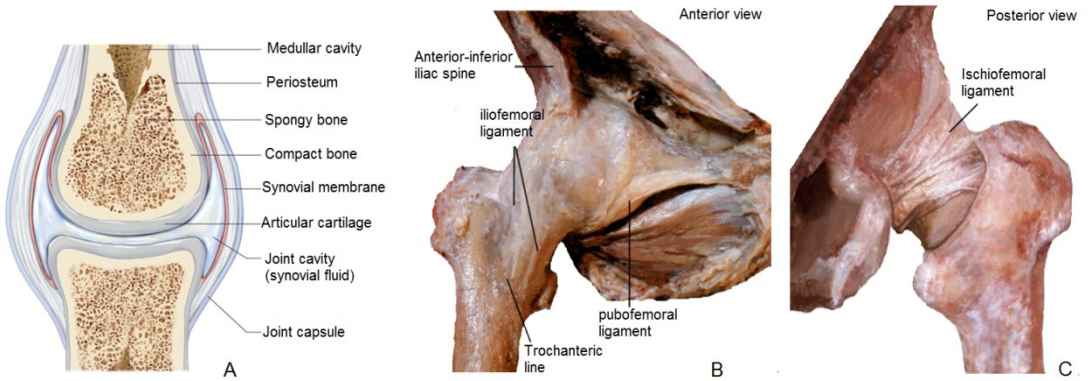

Figure 2-2 A) Example of a synovial joint including its main structural components such as the joint cavity, synovial fluid, joint capsule, synovial membrane and articular cartilage. Image adapted from http://biology-forums.com/index.php?action=gallery;sa=view;id=8793; B) Anterior view of an hip joint where the iliofemoral and pubofemoral ligaments can be seen (Image adapted from http://www.gla.ac.uk/t4/~fbls/files/fab/tutorial/anatomy/hipt.html); C) Posterior view of an hip joint where the Ischiofemoral ligament can be seen (Image adapted from http://www.gla.ac.uk/t4/~fbls/files/fab/tutorial/anatomy/hipt.html).

2.2.4 Hip joint: Synovial capsule

The joint capsule is vital to the function of synovial joints. It seals the joint space and provides for its stability by, for example, limiting movements. In adults it is a dense fibrous connective tissue that is attached to the bones via specialised attachment zones and it forms a cover around the joint. Inside the capsule, the surfaces of the hip joint are covered by a thin tissue called the synovial membrane as shown in Figure 2-2, A (Ralphs and Benjamin, 1994).

There are three main ligaments which play an important role in joint stability:

- Iliofemoral ligament, which passes over the front of the hip joint and connects the ilium to the femur. The iliofemoral ligament restrains the movement of the hip joint in the pelvic region by preventing overextension. This ligament also restrains external rotation of the hip joint when flexed, and it restrains both internal and external rotation when the joint is extended (Platzer and Spitzer, 2003) (Figure 2-2, B).

- Pubofemoral ligament, which is located on the interior side of the hip joint and extends from the pubic portion of the acetabular rim passing below the neck of the femur. The pubofemoral ligament prevents joint hyperextension and over-abduction, and it also limits external rotation (Platzer and Spitzer, 2003) (Figure 2-2, B).
- Ischiofemoral ligament, which is a band of very strong fibres located on the posterior side of the hip joint that connect the pelvis and the femur. Its main function is to stabilise the hip joint and limits extension and medial rotation of the hip (Platzer and Spitzer, 2003) (Figure 2-2, C).

The integrity of the synovial capsule is of paramount importance; if injured, it can induce, for example, joint laxity and therefore leading to important rheumatic disease such as arthritis and osteoarthritis (Ralphs and Benjamin, 1994).

2.3 Prenatal joint development

Embryonic joint formation has been described by Pacifici et al. (2005) as a well-defined sequence of four events: joint site determination, interzone formation, cavitation and joint morphogenesis (Figure 2-3). Joint development starts with formation of uninterrupted mesenchymal condensations within the limb bud forming the template of the future limb rudiments which undergoes chondrification. The future joint location, known as interzone, becomes evident as a layer of compact and closely associated mesenchymal cells (Khan et al., 2007; Pacifici et al., 2005). This is the control centre for further joint development from which signalling molecules, growth and transcription factors are expressed (Archer et al., 2003; Storm and Kingsley, 1996). Chondrocyte proliferation drives growth of the skeletal elements while the joint undergoes cavitation and morphogenesis (Bellairs and Osmond, 2005). Cavitation is the physical separation of the adjacent skeletal elements within the interzone creating two articular surfaces and a joint cavity (Pacifici et al., 2005). Joint morphogenesis, described by Pacifici et al. (2005) as the final step involved during joint development, is the process in which distinct and functional joint shape start to appear. Contrary to what was said by Pacifici et al. (2005), Nowlan and Sharpe (2014) recently have studied the development of the prenatal hip joint shape

in embryonic chicks using 3D imaging, with their histological results suggesting that morphogenesis precedes cavitation and continues to mould the joint shape after it.

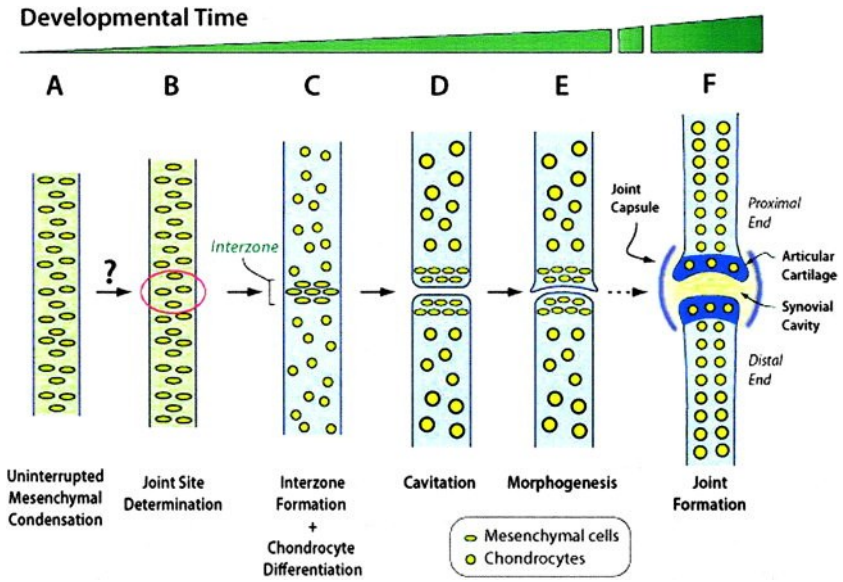

Figure 2-3 Scheme depicting the major steps in digit synovial joint formation. A-B) Uninterrupted mesenchymal condensation; C) interzone formation; D) cavitation; E) morphogenesis; F) schematic example of a synovial joint including all its major structure. Image adapted from (Pacifici et al., 2005)

2.3.1 Joint morphogenesis & fetal movements

Many studies have shown fusion across the joint site and abnormal joint shape under immobilised conditions suggesting that the stages of cavitation and morphogenesis are dependent on mechanical forces generated by prenatal movements (Drachman, 1966). Contrarily, joint site determination and interzone formation are not believed to be mechanobiologically determined since they remained unaltered in experimentally immobilised embryos (Kahn et al., 2009; Murray and Drachman, 1969; Osborne et al., 2002). The mechanisms by which these movements affect morphogenesis are still unknown. Immobilisation techniques have been used to address some questions on the importance of prenatal movements on joint morphogenesis. Drachman and Sokoloff (1966) were among the first to study the effect of paralysis on joint formation and they used pharmaceutical agents and spinal cord extirpation to eliminate muscular contraction in developing chick embryos. Their study showed absent or minimal joint cavity formation, joint fusion and flattened articular surfaces in immobilised joints, compared with embryos developed under normal conditions (Figure 2-4).

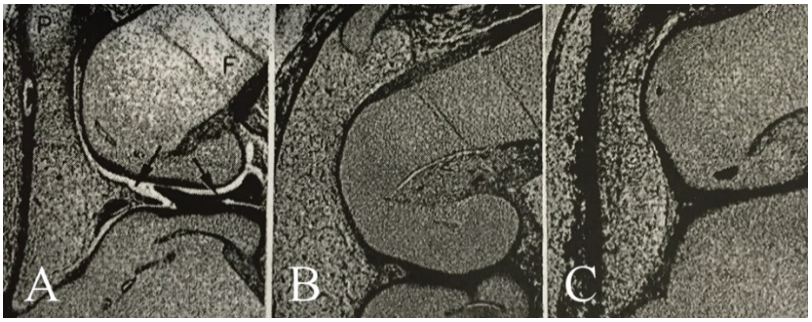

Figure 2-4 Effect of paralysis on the developing chick knee joint. A) Sagittal histological section of control, joint cavities are clearly seen (white regions); B) pharmaceutically immobilization, joint cavities are absent; C) spinal cord expiration, joint cavities are absent. Image adapted from (Drachman, 1966)

Similar results were reported in following studies where neuromuscular blocking agents were used on chick embryos to investigate patterns of extracellular matrix proteins during joint formation (Mikic et al., 2000), or to explore the effects of rigid and flaccid paralysis on joint development during pre and post cavitation (Osborne et al., 2002). The former found, in the immobilized embryos, the generation of a non-interlocking joint shape with partial or absent cavitation (Figure 2-5) during the post-cavitational stages of joint development. The latter showed a loss of joint cavity when induced before the normal period of cavitation while only flaccid paralysis led to the loss of joint cavity in post-cavitation phase.

More recent studies, using similar techniques, studied the effects of prenatal movements during knee (Roddy et al., 2011b) and hip (Nowlan et al., 2014) joint development in chick embryos. Roddy et al. (2011b) showed, when chicks were immobilised up to 5 days, 1) a reduction in width of the intercondylar fossa of the distal femur and of the proximal epiphysis of the tibiotarsus and fibula, 2) flattened articular surfaces of the condyles and 3) an overall simplified joint shape. Nowlan et al. (2014), induced immobilisation from day 4 and looked at its effects over the period between 7 and 9 days of incubation. The results showed minor impact of absent movements on joint morphogenesis prior to cavitation. At day 7 they reported no effect on any aspect of hip joint shape due to immobilisation while at day 8 a decrease in length of the pre-acetabular portion of the ilium was observed. However, massive changes on joint shape were observed after cavitation should have arisen (day 9), the joint showed abnormal positioning and orientation of the pelvis and abnormal shaping of the femoral head and acetabulum. Similarly, studies of genetically modified “muscleless limb” mice have revealed changes in joint morphogenesis. Kahn et al (2009) used mouse models to demonstrate that

contracting musculature is crucial to maintain joint progenitor's cell fate reporting the failure of joint formation in absence of contracting musculature. Nowlan et al. (2010a), studying skeletal development of mutant muscleless limb mouse, revealed abnormal growth and ossification in the scapular blade, humerus, ulna and femur but no significant changes in the tibia.

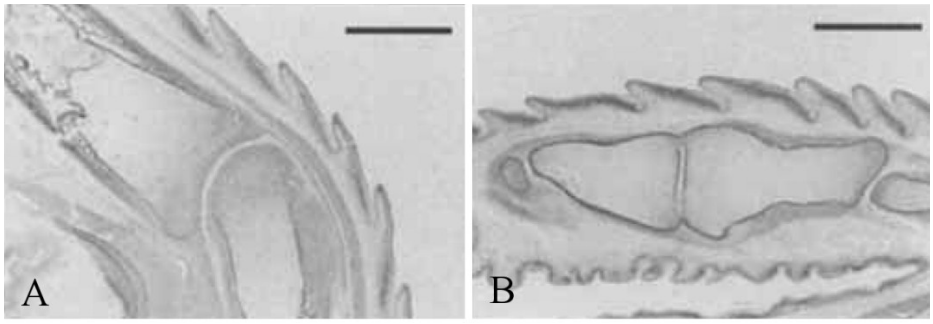

Figure 2-5 Interphalangeal joint development at day 16th. A) Sagittal section of the control joint showing the development of a functioning and congruent joint; B) sagittal section of the immobilised joint showing the development of an abnormal joint shape. Scale bar=0.54mm. Imaged adapted from (Mikic et al., 2000)

2.4 Prenatal Hip joint development & Developmental Dysplasia of the Hip (DDH)

2.4.1 Introduction to prenatal hip joint development

Hip joint development is a complex phenomenon which includes two parts, a growing proximal femur, and a growing acetabulum. Clarifying the steps involved during hip development is important to understand the mechanism which leads to hip diseases and deformities.

The prenatal development of the human hip joint has been well described by several researchers over the past 70 years (Gardner and Gray, 1950; O'Rahilly and Gardner, 1975; Scheuer and Black, 2004; Strayer Jr, 1943). In humans, the lower limb buds start to appear around day 28 (O'Rahilly and Gardner, 1975) in a form of a concentration of mesenchymal cells lying within a border of ectoderm (O'Rahilly et al., 1956). By the sixth week of intrauterine life, the lower limb buds have elongated, a shallow acetabulum is visible, proximal to the head of the femur, and condensation of cartilage cells first appear in the primitive ilium, and then in the pubis and ischium (Lee and Eberson, 2006). In the iliac mass the chondrification process starts around weeks 6^{th} - 7^{th} of the intra uterine development (O'Rahilly and Gardner, 1975), whereas the pubis and the ischium start to chondrify around weeks 7^{th} - 8^{th} (O'Rahilly and Gardner, 1975). At the end of the eighth week, the three chondrification centres fuse forming a shallow acetabulum (Figure 2-6) (Tachdjian and Wenger, 1983).

Figure 2-6 Complete cartilaginous differentiation of the os innominatum and femur showing the shallow acetabulum. Image from (Tachdjian and Wenger, 1983)

The junction of the cartilaginous ends of the ilium, ischium and pubis is known as triradiate cartilage, an expanding structure composed by three growth plates, which is believed to be responsible for the acetabular growth during its fetal life (Portinaro et al., 1994). The joint cavity initiates around the 7th and 8th gestational weeks and it is well defined and fully opened around the 11th gestational week. By the eight week of development, the primary ossification centre of the femur appears in its shaft and ossification proceeds proximally and distally from this centre (Lee and Eberson, 2006). Around the 11th gestational week (the first trimester), a globular femoral head is almost completely enclosed by a deep-set acetabulum (Ráliš and McKibbin, 1973) (Figure 2-7) and the infantile configuration of the hip joint is achieved (Lee and Eberson, 2006).

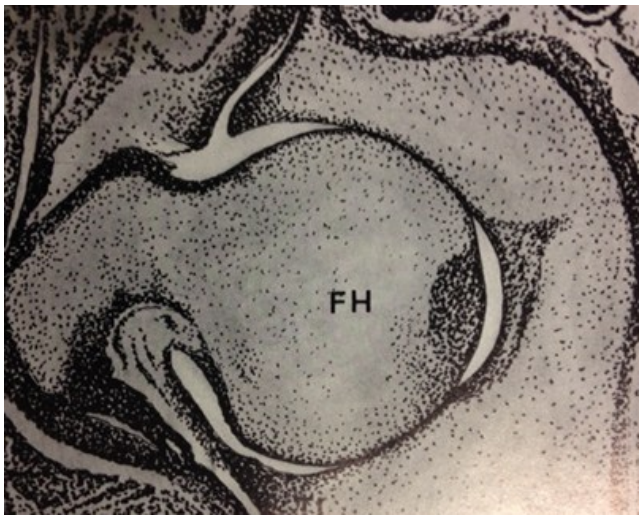

Figure 2-7 Hip joint at the twelfth week of gestation. The femoral head (FH) is almost completely enclosed by a deep-set acetabulum. Image from (Tachdjian and Wenger, 1983)

By week 16 of development, the ossification of the femur has reached the lesser trochanter and meanwhile, the primary ossification centres have appeared in the ilium, ischium and pubis (Lee and Eberson, 2006). The ossification centre of the acetabulum will not appear until adolescence (Lee and Eberson, 2006).

Week 11 is believed to be the most stable period during hip joint development (Ippolito et al., 1984; Ráliš and McKibbin, 1973). From that time until birth, the acetabulum becomes shallower and the femoral head loses substantial sphericity, becoming more hemi-spherical (Figure 2-8).

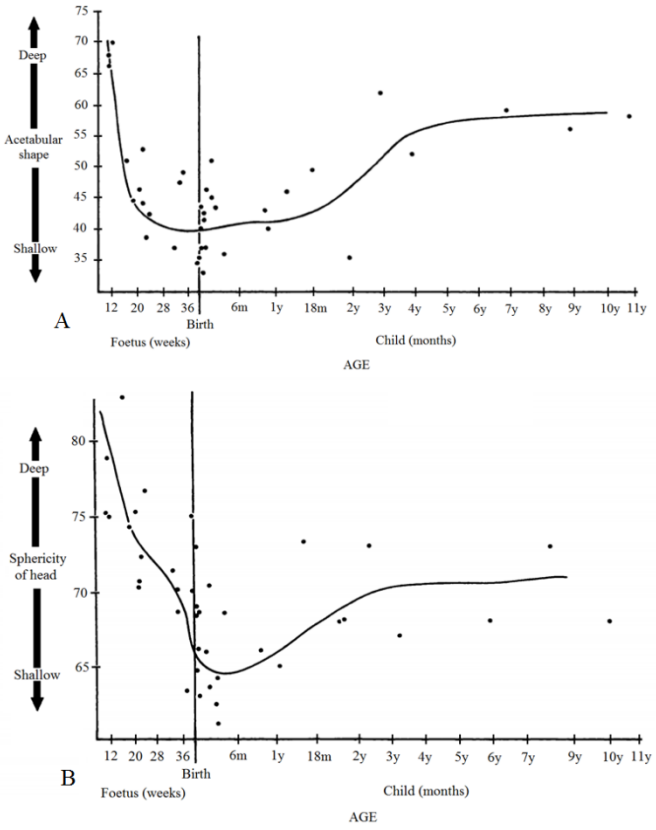

Figure 2-8 A) Changes in acetabular shape in relation to age, measured as ration of the height to diameter of its concave; B) changes in femoral head shape in relation to age, measured as the ration of the height to diameter of its rounded end. Image from (Ráliš and McKibbin, 1973)

An increase in femoral head sphericity and coverage by the acetabulum is then regained after birth, although never to the extent evident in early development (Figure 2-8). Therefore, the coverage of the femoral head is never as low as it is at birth, which most likely means that the hip joint is at its most unstable shape at this time. Alterations of the normal process of joint morphogenesis are highly relevant to postnatal skeletal malformations, particularly to developmental dysplasia of the hip (DDH). Figure 2-9 shows different stages of fetus development with focus on hip joint development.

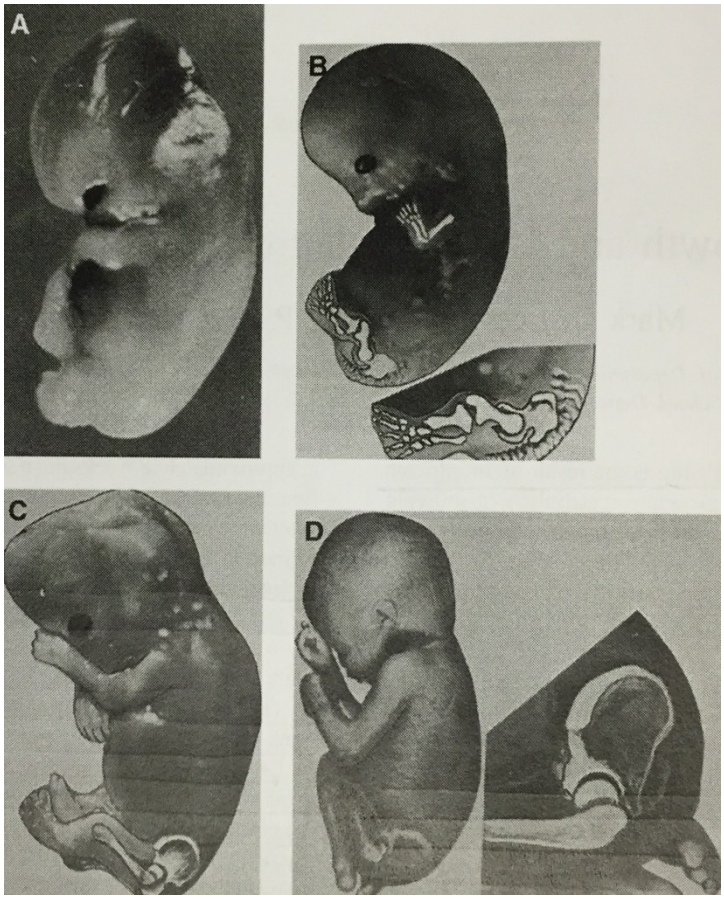

Figure 2-9 A) Fetus at the age of 6 weeks, the limbs bus have begun the process of differentiation; B) fetus at the age of 8 weeks, differentiation is more advanced; C) fetus at the age of 11 weeks, the infantile configuration of the hip joint is now present; D) fetus at the age of 16 weeks, the lower extremities lie in a position of stability. Image adapted from (Lee and Eberson, 2006)

2.4.2 Developmental dysplasia of the hip (DDH)

Developmental dysplasia of the hip, also known as DDH, is the most common congenital abnormality of the hip joint, which is thought to be strongly linked to abnormal fetal movement. As deeply described in Section 1.1, two types of dislocation have been defined (American Academy of Pediatrics, 2000), one known as paralytic dislocations, and one known as typical dislocations. In the most severe cases of DDH, the femoral head is completely dislocated from the acetabulum (Figure 2-10, type 3), while in less severe manifestations, the femoral head is partially dislocated (Figure 2-10, type 2) or easily dislocatable from the acetabulum (Figure 2-10, type 1) (Ponseti, 1978; Tachdjian and Wenger, 1983). Both environment and genetic factors are thought to play a role in DDH; the former is usually referred to as abnormal mechanical environment (Stevenson et al., 2009) and/or a lack of physiological fetal movement patterns (Muller and Seddon, 1953),

the latter to genetic risks associated with positive family history (Stevenson et al., 2009; Wynne-Davies, 1970) and female gender (Chan et al., 1997).

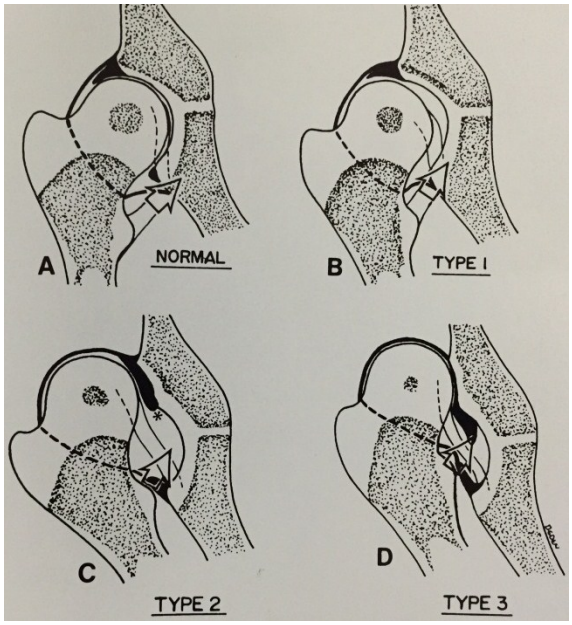

Figure 2-10 A) Normal hip joint; B) type 1 dislocation; C) type 2 dislocation; D) type 3 dislocation. Image adapted from (Tachdjian and Wenger, 1983)

An interesting study has been done by Bialik et al. (1999) where two categories of neonatal hip pathology were distinguished, once that regress naturally developing into a normal hip and another which develops into DDH, showing that many detected cases of hip instability in newborns progress into a normal hip without any medical intervention. It has also been shown that some geographical regions and ethnicities have higher incidence rates of DDH, such as the Northern Italian (Riboni et al., 2003) and the Japanese (Yamamuro and Ishida, 1984) populations. Moreover, the risk of the condition increases with abnormal movements or intrauterine conditions that reduce or restrict the movements *in utero*. For example fetal breech position (Figure 2-11), particularly extended breech where the hips are flexed and knees extended, has been shown to increase the risk of hip instability and dysplasia (Luterkort et al., 1986). Portinaro et al. (1994), hypothesised that ligamentous laxity or malpositioning in utero leads to abnormal loading allowing the femoral head to displace and encourage deformity. It has been also proposed that the reason why the left hip has a higher risk of DDH is due to the position of the left leg beside the mother's spine, which limits hip abduction (Aronsson et al., 1994; Homer et al., 2000).

Figure 2-11 Schematic representation of particularly extended breech with flexed hips and extended knees. Image adapted from (Health, 2003)

Oligohydramnios, which is a condition during pregnancy where a deficiency of amniotic fluid occurs, has been also associated to abnormalities in fetal movements which may lead to DDH. Sival et al. (1990) monitored 19 fetuses affected by oligohydramnios weekly and found that moderate and severe loss of amniotic fluid have an influence on fetal movements. Moderate loss impacted the amplitude of the movements, while severe loss impacted the speed and amplitude of movements. Despite the likely influence of fetal movements on hip joint formation, the mechanism by which these movements affect hip morphogenesis is still unknown.

2.4.3 From Developmental Hip Disorders to Osteoarthritis

Osteoarthritis (OA) is the most common disabling joint disease observed worldwide (Sandell, 2012). The primary risk factor for OA is age, however altered mechanical loading, joint injury and genetics mutation have been strongly linked with this disease (Hogervorst et al., 2012; Sandell, 2012).

Developmental hip disorders such as DDH, Femoroacetabular Impingement (FAI) or Slipped Capitis Femoris Epiphysis (SCFE), all conditions which share a common mechanism of local cumulative mechanical overload, and which lead to an altered joint morphology, are strongly linked to OA (Hogervorst et al., 2012). For example, in DDH, the presence of a maloriented and/or insufficient articular surface, with decreased contact area and increased shear force at the acetabular rim, leads to

excessive and eccentric loading on the acetabular rim. If DDH remains undetected, it will lead to OA later in life (Sandell, 2012).

Because OA development is related to morphology variants of developmental hip disorder, understanding the mechanism involved during hip joint morphogenesis will help to decrease developmental hip disorders incidence and therefore decrease the chance to develop OA.

2.5 Computational models

2.5.1 Introduction to FEM/FEA

Finite-element method (FEM) is a numerical technique that provides solutions to boundary value problems based on approximation of differential equations (Reddy, 1993). Established in the 1960s, FEM is best understood for its practical application: Finite-element analysis (FEA). FEA is a computational tool for engineering analysis which uses mesh generation techniques to divide complex geometries into small discrete problems. The geometric representation consists of a mesh of polygonal or polyhedral elements interconnected at points called nodal points. Strains and stresses of the whole structure are calculated from the nodal displacement which will deform the elements in a specific way dictated by the element formulation (Reddy, 1993). Due to the fast evolution of these techniques and the growing literature regarding material properties and boundary conditions, which are becoming day by day more reliable, FEA is nowadays widely used in the field of biomechanics to create accurate numerical representations of organs, tissues, and joints with complex geometries.

2.5.2 Computational models in developmental biomechanics

As explained in section 2.2.1 and 2.2.2, during embryonic development cartilage undergoes numerous changes in cellular and extracellular composition based on the type of loading environment it experiences. The mechanisms behind these mechano-adaptive processes are still not very well understood. Several mechano-regulation algorithms for investigating the influences of mechanical stimuli on tissue differentiation have been proposed (Carter and Wong, 1988b; Claes and Heigele, 1999; Lacroix et al., 2002; Prendergast et al., 1997) and computational models have been used to examine different aspect of skeletal development, such as ossification (Carter et al., 1987), evolution of long bone epiphyses (Tanck et al., 2000), alteration of ossification in culture (Wong and Carter, 1990a), sesamoid bone formation (Sarin and Carter, 2000), developmental bone deformities, such as post natal DDH (Shefelbine and Carter, 2004) or the fracture healing process (Isaksson et al., 2006). However, only one mechanobiological simulation of prenatal joint development has been proposed (Heegaard et al., 1999).

In 1987, Carter et al. (1987) proposed a theory to describe the influences of mechanical stress on chondrosseous biology. The mechano-regulation algorithm developed suggested that intermittent hydrostatic pressure inhibits degeneration and ossification of cartilage, while intermittent strain or shear stresses accelerate ossification and degeneration. A single phase 2D plane strain model of the human femur was generated and used to simulate 3 embryonic stages, and 2 postnatal stages. Although a much simplified model, it gave insightful results. Initially, high strain energy density values were predicted at the mid shaft region in all cartilage model, but in later stages regions of high strain energy shifted to the center of the chondroepiphysis, where the secondary ossification centres appeared. Compressive stresses were predicted near the joint surface and therefore the authors proposed that this stimulus inhibited ossification, therefore maintaining the articular cartilage. However no quantitative limits were set for when the various tissues were from.

Following this mechanobiological theory, or a variation of it, several studies have been performed. Wong and Carter (1990b), conducted a finite element analysis of *in vitro* organ culture experiments done by Klein-Nulend et al. (1986). They predicted ossification patterns by calculating an osteogenic index as a combination of the influence of tissue shear and hydrostatic stresses based on the previous mechanobiological theory. They hypothesised that the local shear stress at the mineralisation front may lead to increased calcification. The osteogenic index was given by:

$$I = \sum_{i=1}^{c} n_i(S_i + kD_i)$$

, where n_i= number of load cycles, S_i= cyclic octahedral stress, D_i= dilatational hydrostatic stress, k= empirical constant, and c= total number of load cases. However, when a model of the same experiment was created with poroelastic material properties (Tanck et al., 1999) the hypothesis of Wong and Carter could not be confirmed.

Sarin and Carter (2000) used 2D finite element analysis to predict the distribution of octahedral shear and hydrostatic stresses in an idealised model of a sesamoid cartilage subjected to *in vivo* loading. They found that regions with high octahedral

stresses were likely sites where the process of endochondral ossification could begin, and that high contact pressures inhibited ossification.

Shefelbine and Carter (2004) implemented a finite element model to predict the rate of progression of the growth plate and formation of coxa valga in DDH. They developed a 3D single phase model of an approximately two month old proximal femur and hip joint forces with different angles were tested. The specific growth rate was a function of biological and mechanobiological growth where the mechanobiological growth was determined from the maximum octahedral shear stress (σ_s) and the minimum hydrostatic stress (σ_h) throughout the load history as shown in the following equation:

$$\dot{\varepsilon_m} = aMax\sigma_s + bMin\sigma_h$$

, with *a* and *b* as constant. The biological growth rate was assumed to be constant too. Their simulations showed that hydrostatic compression on the lateral side inhibited growth, while octahedral shear and hydrostatic tension promoted growth and ossification on the medial side (Figure 2-12). However, because the loading conditions of the fetal and neonatal hip are still unknown, several assumptions on the loading conditions were made on the model, such as that the angle of the resultant hip force was greater in the dysplastic hip than in the normal hip.

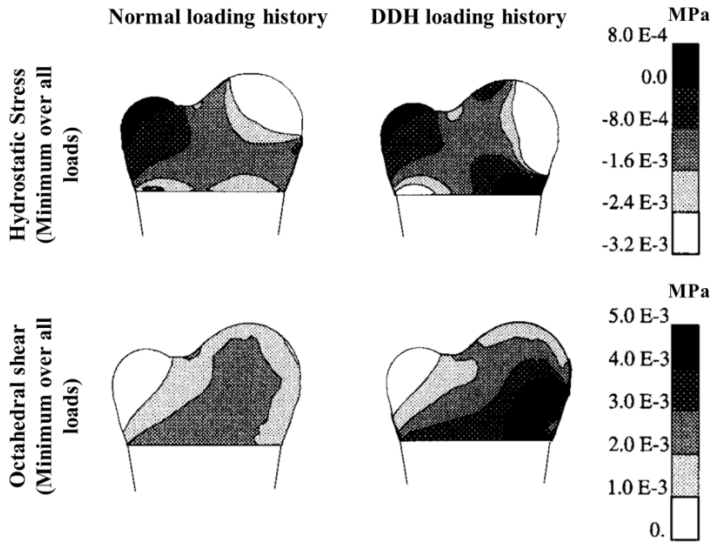

Figure 2-12 Minimum hydrostatic stress and octahedral shear stress patterns for normal and DDH conditions. Image adapted from (Shefelbine and Carter, 2004)

In 1997, Prendergast et al. (1997) introduced a new model of tissue differentiation based on poroelastic FE analysis. They proposed two biophysical stimuli as mechano-transduction variables: shear strain and fluid velocity. Following this mechanobiology theory, Lacroix et al (2002) investigated the fracture healing process of a long bone using an axisymmetric finite element model. Their model simulated periosteal bone formation, endochondral ossification in the external callus and resumption of the external callus. Tanck et al. (2000) used a 3D poroelastic finite element model of a fetal mouse metatarsal rudiment in order to explore the result of an organ culture experiment where a curved mineralisation front was found. Their simulations showed that during flexion and extension, fluid pressure was approximately the same at the centre and at the periphery. A high rate of mineralisation was observed at the centre, leading the authors to conclude that pressure was unlikely to be involved in the regulation of growth of the mineralisation front.

While computational models have been used to examine different aspect of skeletal development, only one mechanobiological simulation of prenatal joint development has been proposed so far. Heegaard et al. (1999), used a mechanobiological simulation to predict finger joint morphogenesis. The authors used an idealised planar biomechanical model of the proximal interphalangeal joint and simulated rudiment growth using a mechanoregulation theory for endochondral ossification (Stevens et al., 1999) in which growth and shape depends on the biological growth (i.e. the intrinsic growth due to hormones, genes and nutrients), and mechanical growth (i.e. region-specific growth due to muscle, ligament and joint forces). The model predicted joint shape changes between 55 and 70 embryonic days and revealed the development of congruent surfaces within the joint region with the acquisition by the distal phalanx of a slightly concave surface (Figure 2-13). This study was pioneering in that and it was the first ever mechanobiological simulation of any aspect of prenatal joint development. However, it is important to note that, at

the stage of development modelled by them, the joints are entirely cartilaginous and there is no experimental evidence to suggest that endochondral ossification has an influence on prenatal joint shape development. The mechanical stimulus for cartilage during growth (where ossification does not occur) is likely to be different than the mechanical stimulus during endochondral growth and ossification (where cartilage growth occurs but the endpoint is ossification). In the former, the cartilage is trying to make more cartilage; in the latter it is trying to turn into bone.

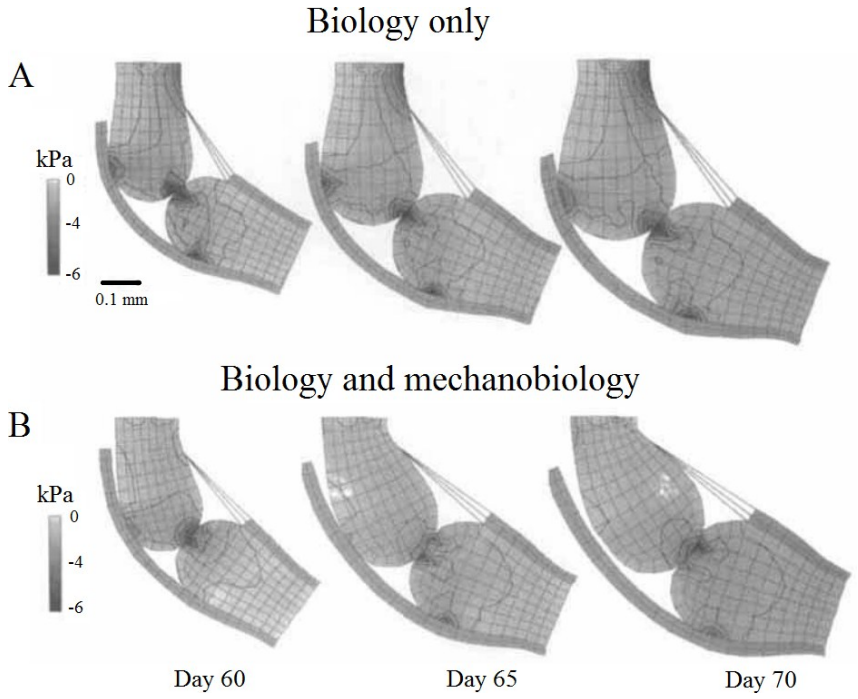

Figure 2-13 A) Predicted geometry (only biological contribution) of the chondroepiphysis ad different stage of development (60, 65, 70 days); B) predicted geometry (both biological and mechanobiological contribution) of the chondroepiphysis ad different stage of development (60, 65, 70 days). From (Heegaard et al., 1999)

2.5.3 Growth-generated biophysical stimuli

During early development, cells receive extrinsic signals that lead to particular changes in cell behaviour, such as differentiation, migration or proliferation. In addition, morphogenesis is regulated by inductive signals transmitted within cells through direct contact, diffusible molecules, and gap junctions (Henderson and Carter, 2002). During development, different tissues form and begin to grow at different rates. The tissue with faster growth will experience compression, while the slower growing tissue will experience tension (Figure 2-14).

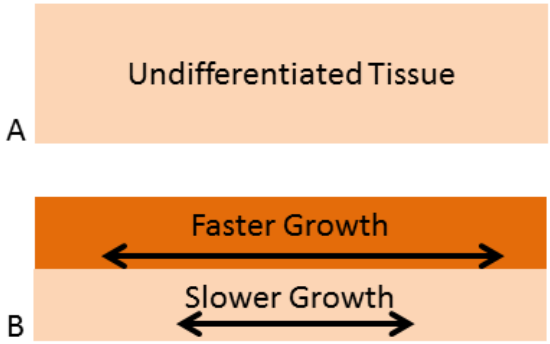

Figure 2-14. A) example of regions of undifferentiated tissue; B) differentiate tissue which leads to alteration in rate of growth.

The growth-generated strain and pressures are used to refer to the local deformation and corresponding forces generated by this differential growth. Four ways were proposed on how growth-generated strain and stresses can send inductive signals to the cells (Figure 2-15): 1) direct contact, 2) diffusible molecules, 3) gap junctions, and 4) imposed tension and pressures.

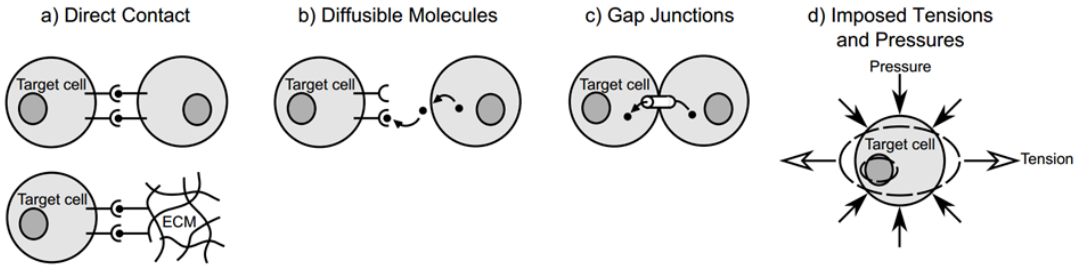

Figure 2-15 Four ways on how growth-related strain and stresses send inductive signals to cells: A) Direct contact; B) inductive signal; C) gap junctions; D) imposed tension and pressure. Image from (Henderson and Carter, 2002).

Direct contact occurs when a receptor on the target cell surface connect to a ligand on another cell or in the Extra Cellular Matrix (ECM); inductive signals occur when a diffusible molecule connect to a receptor on the target cell; gap junctions consist of channel-forming proteins that allow the passage of small molecules, such as ions, between the two cells; imposed tension and pressure occur due to tension and pressure generated in other sites and then transmitted to the cells by anatomical structures.

It has been suggested that growth-generated strains and pressures may influence the process of morphogenesis by modulating growth rates (Henderson and Carter, 2002).

Mechanical modulation of growth rate occurs when a cell receives a signal in the form of an imposed strain or pressure from the mechanical environment and the signal is transduced into an alteration of the cells rate of hypertrophy, mitotic rate, or rate of ECM production.

2.6 Summary

This chapter has presented a review of prenatal development, cartilage and synovial joint with detailed focus on prenatal joint development, mechanobiology of cartilage, developmental dysplasia of the hip (DDH) and mechanoregulation algorithms used in computational modelling.

Now is known that cartilage is a mechano-adaptive tissue able to respond to mechanical forces, for example, by producing more matrix, by causing tissue destruction or by calcifying and turning into bone. An abnormal mechanical environment can incorrectly stimulate the cartilaginous tissue, altering the process of morphogenesis and leading to postnatal skeletal malformations, particularly to developmental dysplasia of the hip (DDH). FEA can be used to model and better understand the influence of mechanics during joint development and therefore, in this thesis a novel mechanoregulation algorithm for cartilage growth wad proposed and used: 1) in 3D mechanobiological simulations of joint morphogenesis to explore the effects of a range of movements and different initial joint shapes for both pre- and post-cavitational phases and, 2) in dynamic mechanobiological simulations to explore the effects of normal, reduced and abnormal prenatal movements on hip joint shape.

3 Models and Algorithms

In this section the evolution of the algorithms used to model joint morphogenesis is discussed. A model very similar to that of Heegard et al. (1999) was initially used. Their work was the first computational model developed for prenatal joint morphogenesis and the achievements and limitations of this pioneering study will be explored by re-implementing it. The evolution of the model presented in this thesis will be described through three phases: "rectangular shape", "proximal interphalangeal joint", and "hinge joint motion". For each model its purpose, its defining features and the results will be described. Given the exploratory nature of this chapter, some boundary conditions, such as loads or displacements, are arbitrarily chosen at this stage.

3.1 Introduction

3.1.1 First simulation for prenatal joint morphogenesis

As described in Section 2.5.2, Heegaard et al. (1999) developed the first computational model for joint morphogenesis. This model explores how the stresses generated by joint motion may modulate the growth of the cartilaginous rudiments and lead to the development of a congruent articular surface.

They developed a planar biomechanical model of the proximal interphalangeal joint (idealised shape between 55 and 70 days of fetal life) (Figure 3-1) to simulate, using finite element analysis, the joint kinematics resulting from muscles contraction, as well as the corresponding stress distribution (Figure 3-2). The model consisted of two cartilaginous phalanges of the same dimension connected by an array of nine fibres representing a retinacular ligament. The extensor and flexor tendons were also modelled and the joint motion was obtained by the application of a force on the extensor tendon (Figure 3-1).

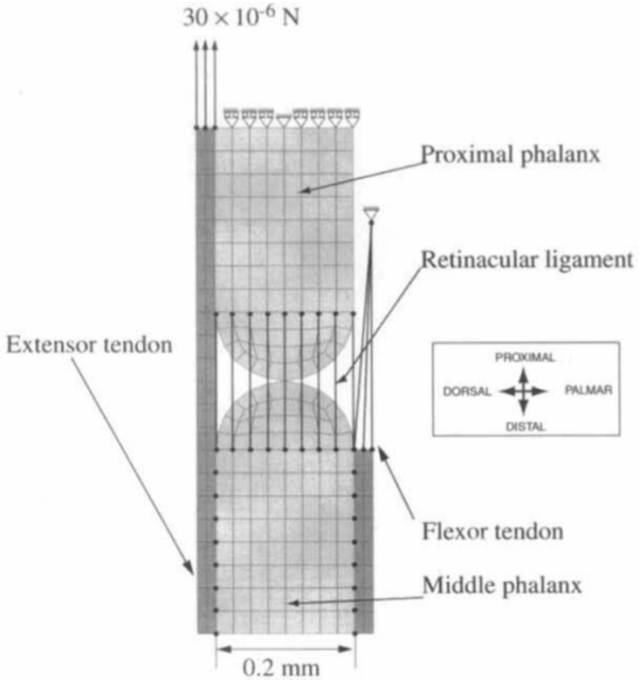

Figure 3-1 Model with all its components and boundary conditions of the proximal interphalangeal joint at day 55. Image taken from (Heegaard et al., 1999)

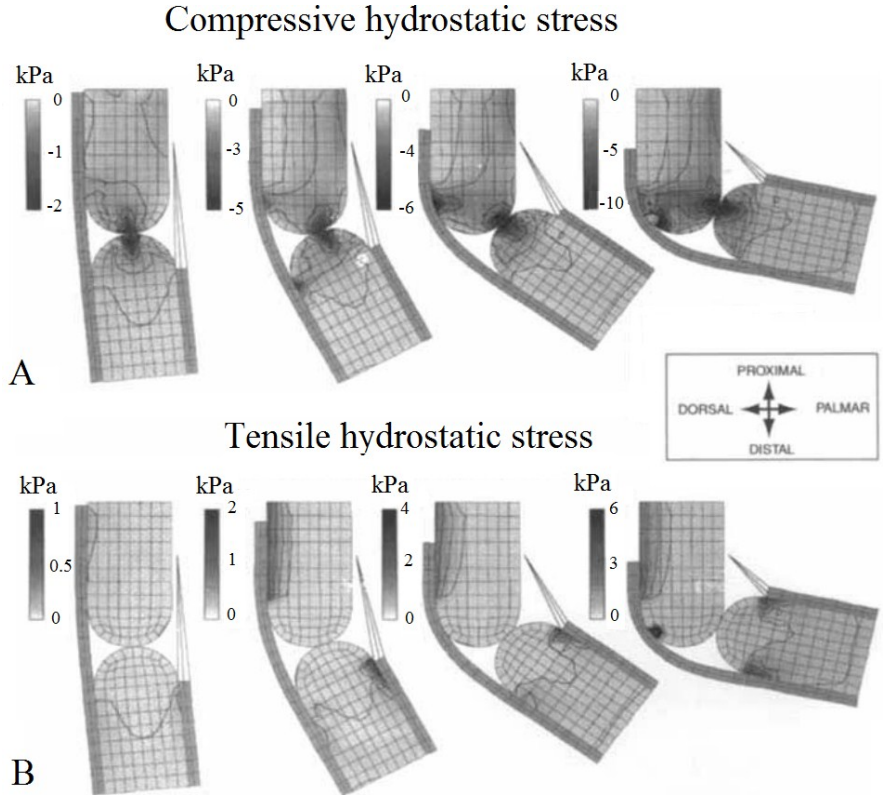

Figure 3-2 A) Compressive hydrostatic stress distribution over a joint flexion; B) Tensile hydrostatic stress distribution over a joint flexion. Image adapted from (Heegaard et al., 1999)

The growth rate was a function of: (1) a biological growth rate, and (2) a mechanobiological growth rate. The changes in shape were obtained through a

procedure similar to the thermal expansion allowing isotropic growth of the proximal and distal rudiments with the sum of the biological and mechanobiological growth rate used as the "temperature" for expansion. The model revealed the development of congruent surfaces within the joint region with the acquisition by the distal phalanx of a slightly concave surface making this study the first ever mechanobiological simulation of prenatal joint development (Figure 2-13).

3.2 Models

In this section the three main models developed to understand and investigate the effectiveness of the endochondral ossification growth theory to predict prenatal joint morphogenesis are described.

3.2.1 Model 1, Rectangular shape: Introduction

This model was created to better understand the contribution to growth due to compressive and tensile hydrostatic stresses and octahedral shear stresses using the mechanoregulation theory for endochondral ossification presented by Carter et al. (1987). An iterative simulation was developed, which allowed simulation of growth from multiple load cycles. This simple model allowed to explore separately the biological and mechanobiological contribution to growth. Given its simplicity, it allowed to check the proper functioning of the framework and the correct behaviour of the model.

3.2.2 Model 1, Rectangular shape: Material and methods

A simple rectangular shape model with arbitrary dimensions (0.2*0.25mm) was created in Abaqus (Dassault Systemes, CAE module, version 6.12) (Figure 3-4, A). A pressure of 1N, chosen to test the reliability of the model, was applied in the middle of the top edge as shown in Figure 3-4 A and the bottom edge was fixed in all directions. The material properties were assumed to be linear elastic with E=1.0 MPa and υ=0.4 (Heegaard et al., 1999). The mesh model was generated by using linear plane stress quadrilateral elements (CPS4) and the stress components were calculated at the integration points. The overall mechanobiological contribution to growth, obtained using Matlab (R2011b, The MathWorks, Inc.), was calculated at each node of the model as a function of biological growth and mechanobiological growth. The former was not influenced by mechanical loading while the latter was

influenced by mechanical loading. The total growth was expressed by the equation below:

$$\frac{d\varepsilon}{dt} = \frac{d(\varepsilon_b)}{dt} + \frac{d(\varepsilon_m)}{dt}$$

Where $\dot{\varepsilon}_b$ and $\dot{\varepsilon}_m$ are the biological and mechanobiological contribution to growth respectively (Shefelbine and Carter, 2004). At this stage, the biological growth was assumed to be constant while the mechanical contribution at each node was defined as:

$$\frac{d(\varepsilon_{mi})}{dt} = (a\sigma_{si} + b\sigma_{hi})$$

Where σ_s and σ_h are the octahedral shear stress and the hydrostatic stress calculated at each node i. "a" and "b" are constants used to determine the relative influence of octahedral shear and hydrostatic stress and a ratio of b/a=0.5 was used in this model based on previous parametric studies which have shown that this value produces accurate prediction of articular cartilage thickness and secondary ossification center appearance (Carter and Wong, 1988a; Wong and Carter, 1990a). Morphological changes due to growth were obtained using the orthonormal thermal expansion capabilities of the FE solver Abaqus which allowed, for this simple model, orthotropic expansion along the "y" axis with the sum of the biological and mechanobiological growth rates used as the 'temperature' for expansion. In order to simulate the growth resulting from multiple load cycles, the new geometry was then re-loaded and prepared for another step of growth. Three loading cycles were simulated with this model. A graphical representation of the process explained above can be seen in Figure 3-3.

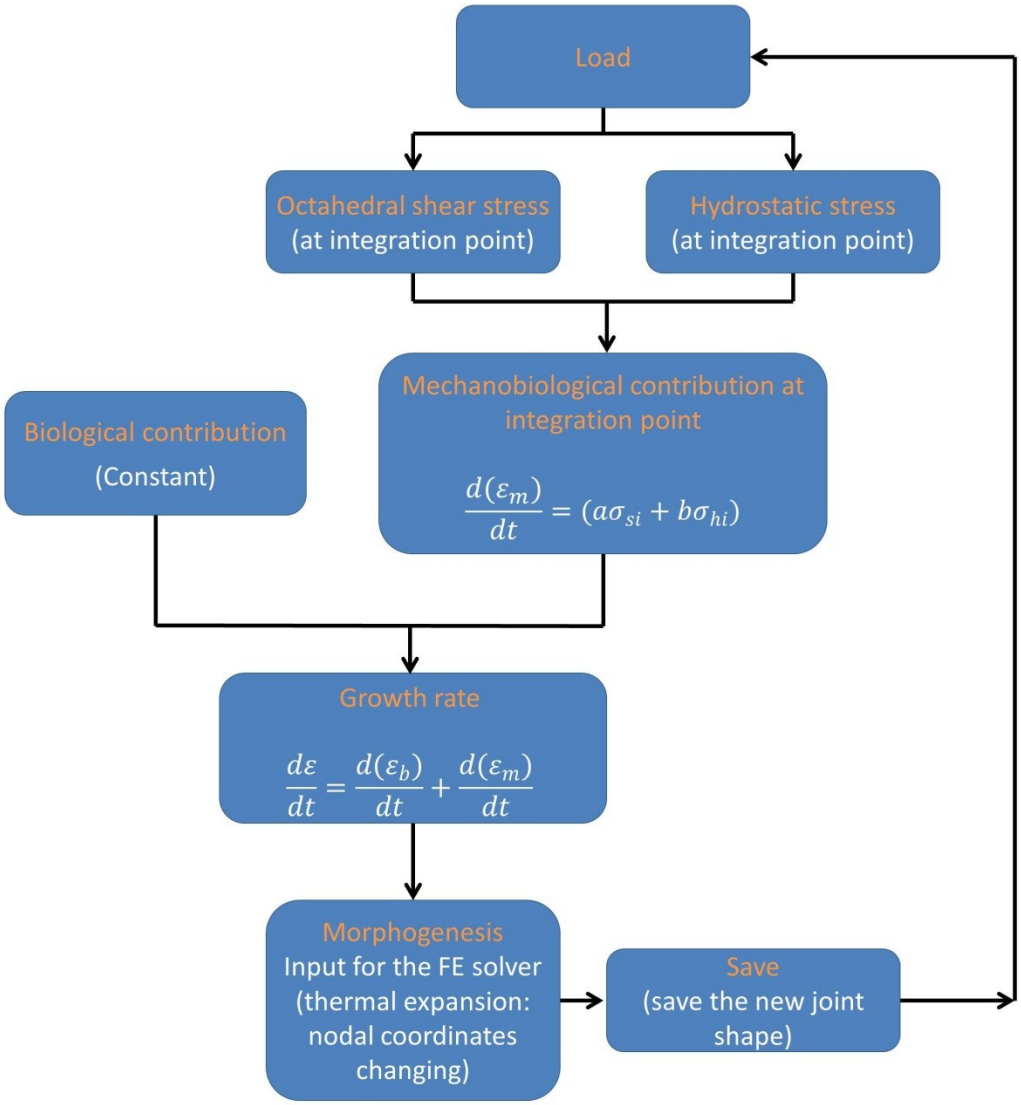

Figure 3-3 Graphical representation of the process used to predict the changes in shape of the rectangular model.

3.2.3 Model 1, Rectangular shape: Results

Following the endochondral theory, hydrostatic compressive stresses occurred directly under the applied load and, inhibited growth in this region. Hydrostatic tensile stresses, which promote cartilage growth, were seen along the sides of the model with high values on the left and right top corners (Figure 3-4 B). Octahedral shear stress had a similar distribution with higher values in the region under the applied load (Figure 3-4 C). When morphogenesis was simulated, the model increased its size along the y direction due to the orthonormal properties and the

onset of a concave profile was visible on its top region (Figure 3-4) showing a reasonable shape according to the computational framework developed.

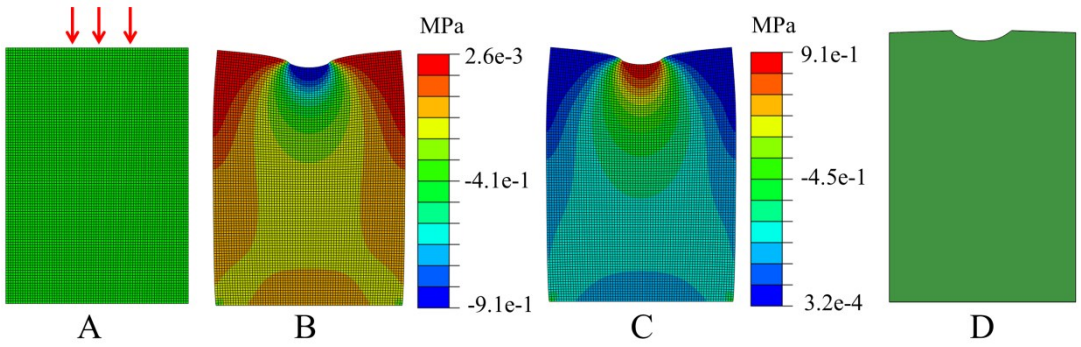

Figure 3-4 A) Initial rectangular model with the applied load; B) hydrostatic stress distribution; C) Octahedral shear stress distribution; D) resulting shape predicted by the simulation.

This simulation was then run for three loading cycles and the model increased its size at each step (Figure 3-5, A, B). When only the biological contribution was included, the model grew along the "y" direction while at the same time maintained its original shape (Figure 3-5, A). The biological contribution was constant and was not influenced by the applied load. When both biological and mechanobiological contributions were included, the model grew even more, developing a growing concave surface on its top region (Figure 3-5, B).

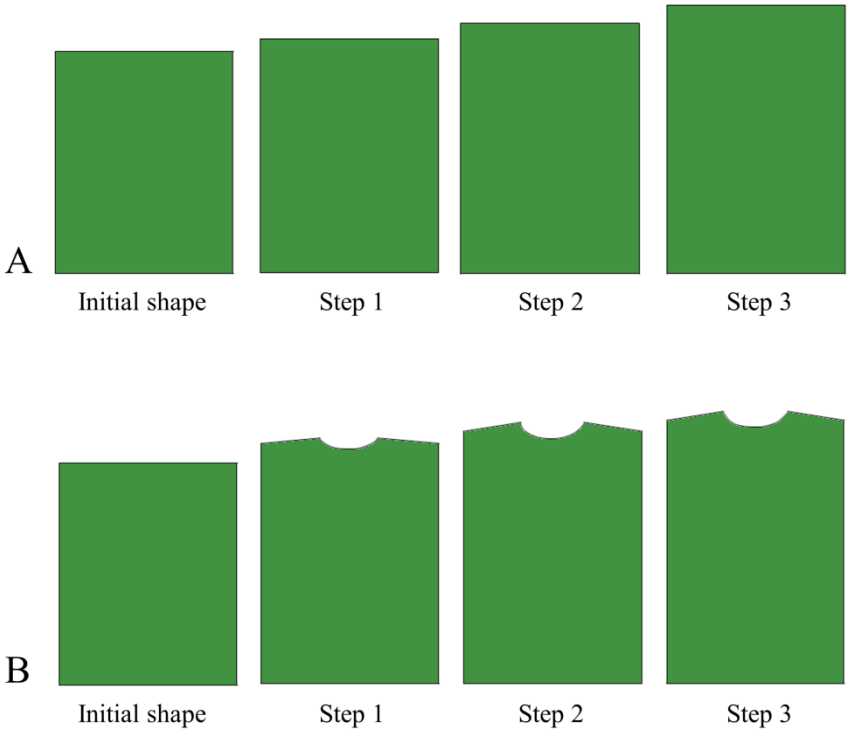

Figure 3-5 A) Initial shape and development over 3 steps (loading cycles) when only the biological contribution was included; B) initial shape and development over 3 steps (loading cycles) when both, biological and mechanobiological contribution were included.

3.2.4 Model 1, Rectangular shape: Conclusion

With this model the mechanobiological theory presented in literature (Carter et al., 1987) was tested on a model representing a region of cartilage and a better understanding of the influence to growth due to the biological and mechanobiological contributions was achieved. Biological growth was not influenced by the applied load, and did not change shape over successive iterations. With the addition of the mechanobiological factor, local changes in shape occurred. Moreover, by separating the mechanobiological contribution in its components, the compressive and tensile hydrostatic stresses and octahedral shear stresses, a better picture of their local contribution on shape changes was gained. The simplicity of this model helped to have a better understanding on how the mechanoregulation theory for endochondral ossification presented by Carter et al. (1987) works, and where to expect shape changes and direction of growth. Thanks to this model, enough knowledge was acquired to apply this algorithm to a more complex simulation representing a joint. With this new simulation the reliability of this algorithm in predicting prenatal joint morphogenesis was explored.

3.2.5 Model 2, Proximal interphalangeal joint: Introduction

This model was created to verify the reliability of the computational framework previously developed and to increase the overall knowledge in joint modelling. By replicating, as closely as possible, the computational model proposed by Heegaard et al. (1999), I wanted to achieve comparable results to their in order to understand the difficulties involved in simulating prenatal joint development and understand where/how improve it.

3.2.6 Model 2, Proximal interphalangeal joint: Material and methods

A planar model of the proximal interphalangeal joint was developed to calculate the joint kinematics resulting from muscle contraction as well as the corresponding stress distribution. A hinge joint configuration was composed of two cartilaginous phalanges of the same dimensions with convex opposing ends (Heegaard et al., 1999) as shown in Figure 3-6 A. The material properties were assumed to be linear elastic with E=1.0 MPa and υ=0.4. The rudiments were initially connected by an

array of nine fibres simulating a retinacular ligament (Heegaard et al., 1999), and then reduced to only one fibre tied, at its extremities, with the centre of the two hemispherical ends as shown in Figure 3-6 A. One fibre allowed mobility of the joint, whereas nine fibres held it rigidly in place in my model. The single fibre, which represented the joint ligaments, was modelled with the same material properties as the rudiments. Both the tendons, the extensor and flexor, were added to the model and tied with the distal phalange as shown in Figure 3-6, A. Their material properties were assumed to be linear elastic with E= 3.0 MPa and υ=0.2. All components were meshed using linear plane stress quadrilateral elements (CPS4) and the stresses were calculated at the integration points. A displacement of 0.1mm was applied on the tendons with opposite directions in order to obtain the finger joint motion as shown in Figure 3-6 B. Frictionless, impenetrable contact was modelled between the two components of the model. Growth and morphogenesis of the rudiments were controlled by biological and mechanical growth rates so that the growth rate $\dot{\varepsilon}$ was as described in Section 3.2.2. The equation for the local chondrocyte density along the axis of a rudiment was calculated by Heegaard et al. (1999) by fitting a polynomial curve to the grey level distribution on a sagittal micrograph of a joint, where darker areas indicated higher chondrocyte density (Figure 3-7). The chondrocyte density C_d is greater towards the ends of the rudiments and lower towards the diaphysis, and therefore expressed by the formula:

$$\dot{\varepsilon}_b = C_d = k * (0.14 - 0.87\xi + 4.40\xi^2 - 2.66\xi^3)$$

with C_d being the chondrocyte density, k = 0.04 being a constant determining the amount of biological growth (Heegaard et al., 1999) and ξ the distance along the proximal-distal axis of the rudiment starting from the distal end (Heegaard et al., 1999).

$\dot{\varepsilon}_m$, the mechanobiological contribution to growth, was calculated at each node of the model as the local peak hydrostatic stress obtained throughout a full joint motion. When the joint motion was simulated, high tensile stresses appeared in areas where the tie condition was present (Figure 3-6 B – black arrows), causing an excessive deformation of the adjacent elements during growth. In order to eliminate these high tensile hydrostatic stresses, which are clearly visible between the flexor tendon and the distal phalange, and at the attaching points between the fibre and the proximal phalange (Figure 3-6, B – black arrows), given the exploratory nature of this chapter,

the hydrostatic stresses were scaled down using the maximum and minimum value of the biological contribution in order to obtain comparable values. A graphical representation of the process explained above can be seen in Figure 3-8.

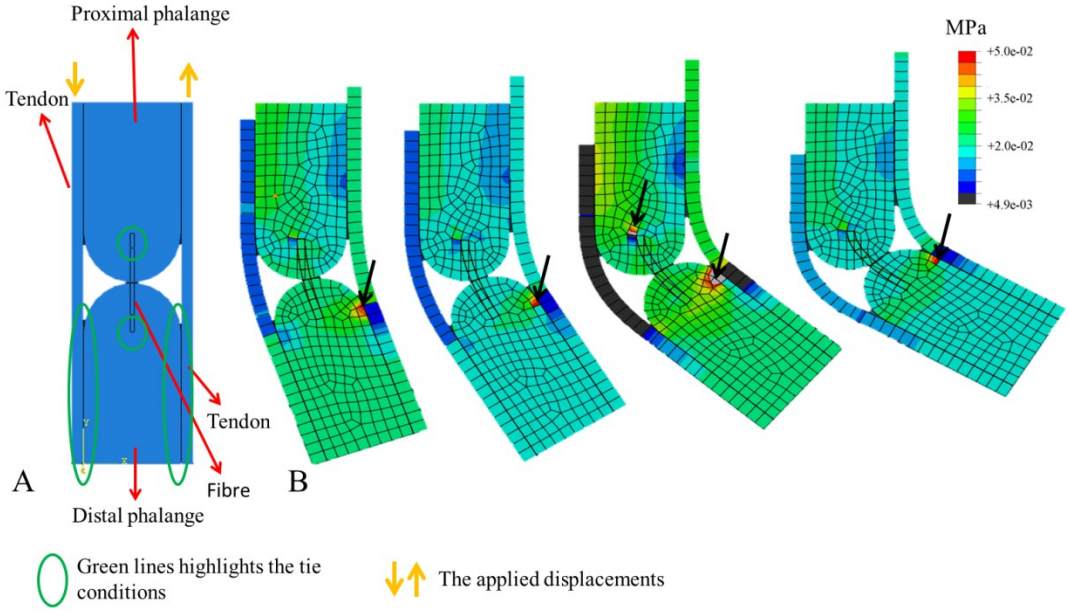

Figure 3-6 A) Planar model of the proximal interphalangeal joint showing the initial model configuration and boundary conditions; B) joint motion due to the applied boundary conditions; the colour plot shows the Von Mises stress.

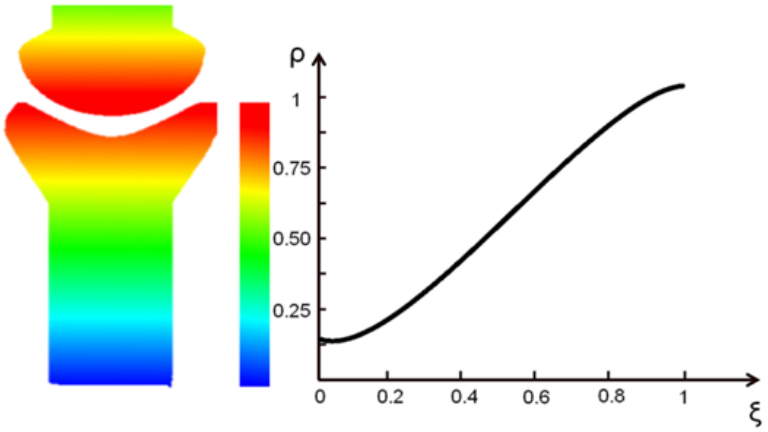

Figure 3-7 Polynomial curve representing the biological contribution which was considered to be proportional to the chondrocyte density. Image adapted from (Heegaard et al., 1999)

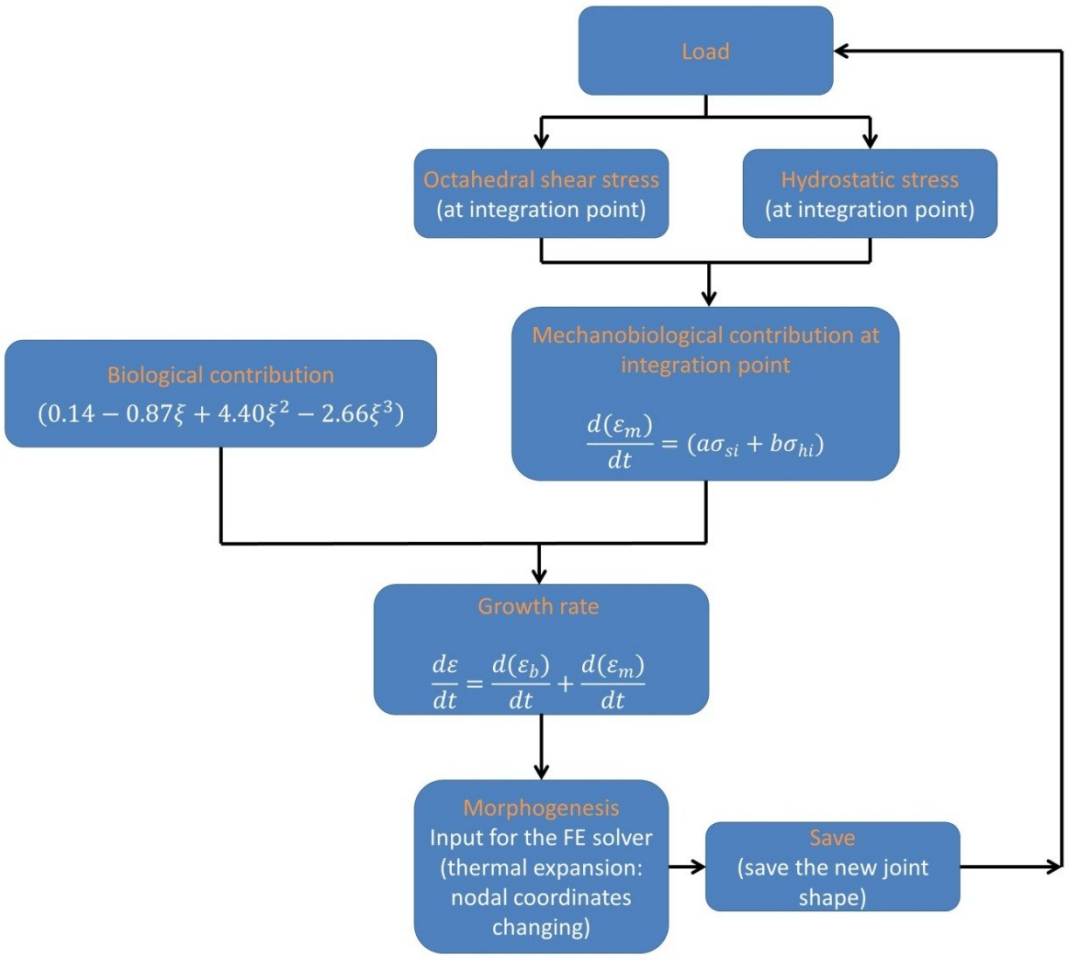

Figure 3-8 Graphical representation of the process used to predict the changes in shape of the proximal interphalangeal joint model.

3.2.7 Model 2, Proximal interphalangeal joint: Results

When only the biological growth was applied, as expected, the chondrocyte density increased as it approached the epiphysis of the rudiments (Figure 3-9 A). When the mechanobiological contribution was included (Figure 3-9 B), high stresses were concentrated within the joint region (red circle), on the left side of the proximal phalange (purple arrow) and at the attaching point between the flexor tendon and the distal phalange (black arrow). By comparing the stress distribution obtained with the stresses predicted by Heegaard et al. (1999) (Figure 3-10 A - B), an almost identical stress distribution for the two conditions can be clearly seen: 1) only the biological contribution (Figure 3-10 A) and 2) the mechanobiological contribution (Figure 3-10 B). Then, three steps of growth were simulated and the model progressively changed

its shape ending with a right side bend of the proximal rudiment and the formation of a slightly concave surface at the top of the distal phalange (Figure 3-11). The predicted joint shape matched with the shape presented by Heegaard et al. (1999) (Figure 3-12).

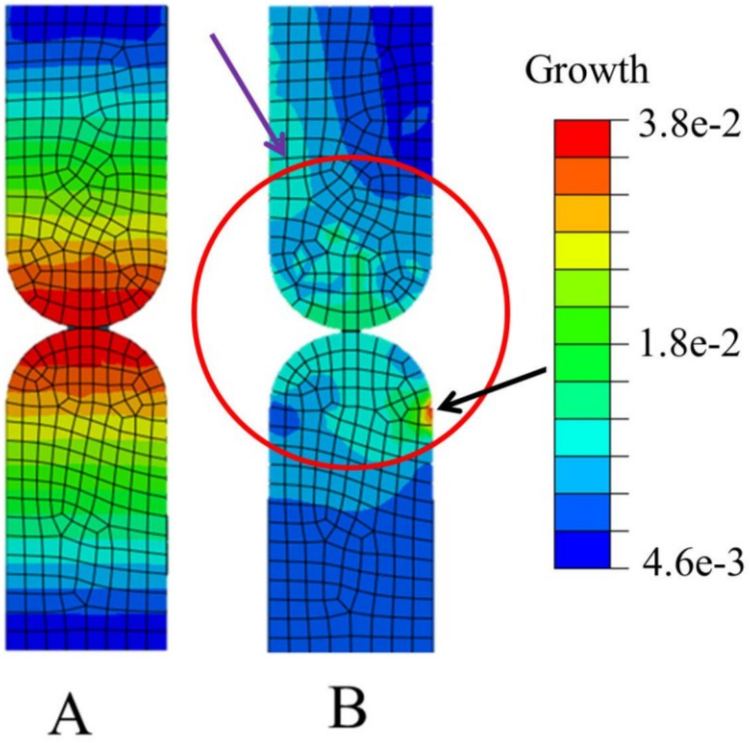

Figure 3-9 A) Biological contribution to growth; B) biological + mechanobiological contribution to growth.

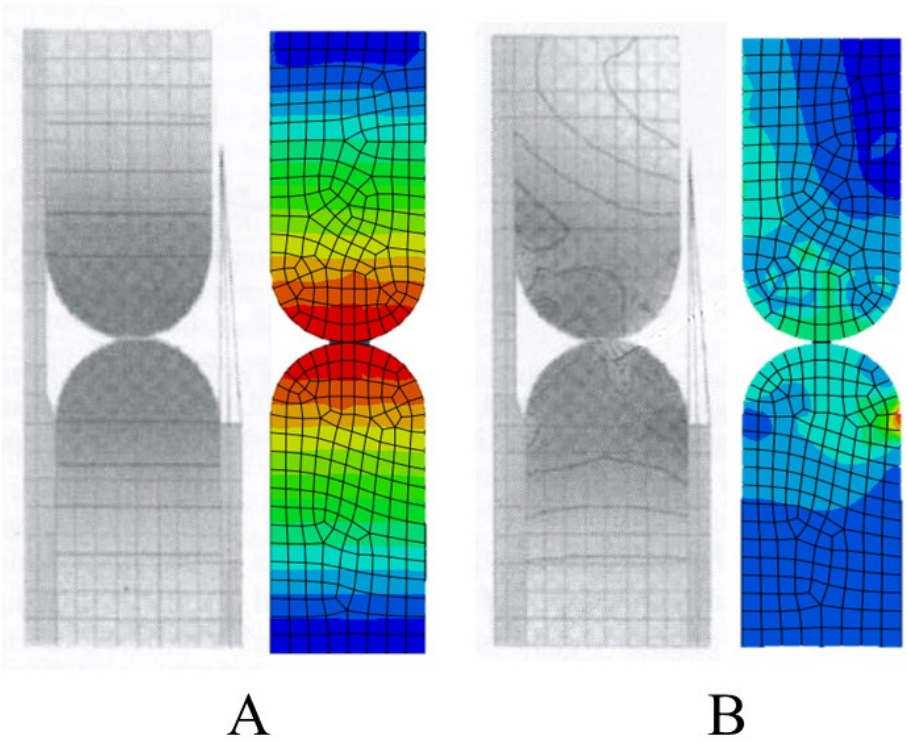

Figure 3-10 A) Biological contribution comparison between the Heegaard et al. (1999) and our prediction; B) Biological + mechanobiological comparison between the two models.

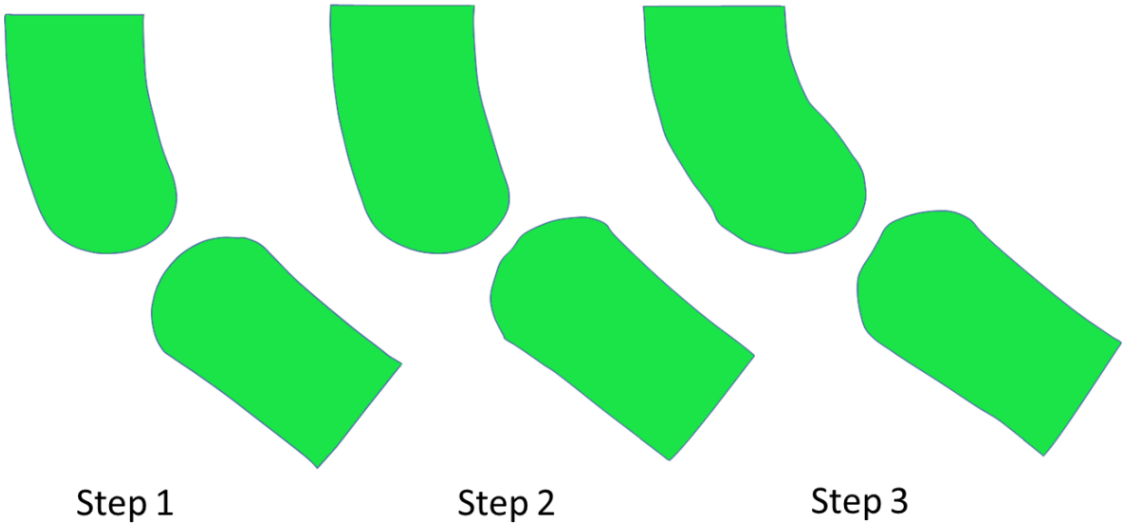

Figure 3-11 Joint morphogenesis over 3 steps of growth. The joint progressively changed its shape acquiring a right side bend of the proximal rudiment and the formation of a slightly concave surface at the top of the distal phalange.

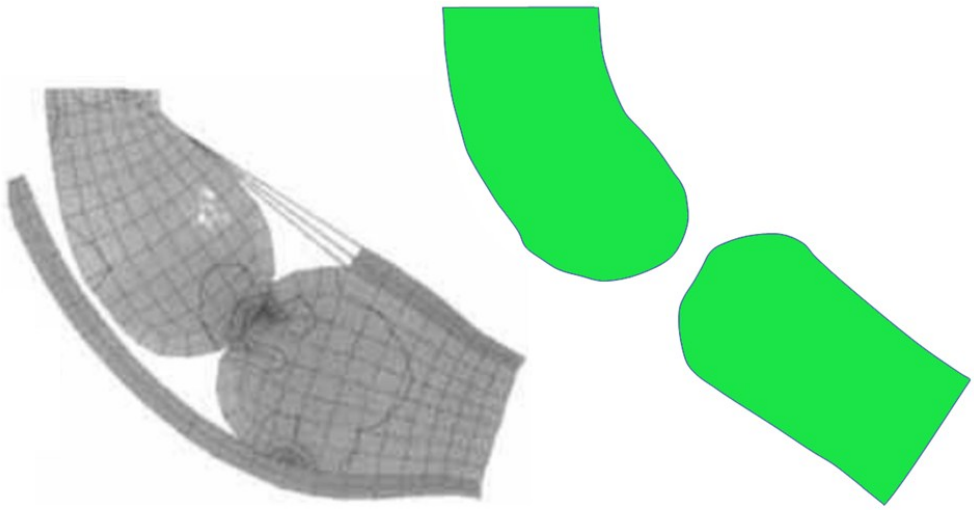

Figure 3-12 Joint morphogenesis comparison between Heegaard et al. (1999) and our model; both models acquired a right side bend of the proximal rudiment and the formation of a slightly concave surface at the top of the distal phalange.

3.2.8 Model 2, Proximal interphalangeal joint: Conclusion

The biological and mechanobiological contribution showed comparable patterns with the Heegaard et al. (1999) model. The final shape, predicted after 3 steps of growth, presented a right side bending of the proximal rudiment and the onset of a concave surface at the top of the distal rudiment. There are some limitations in this study. Because of the 8 linear plane stresses quadrilateral elements (CPS4) used to model the fibre which connected the rudiments, high stresses were generated close the region of interest. The use of springs would have probably reduced this effect. However, the stress distribution and the predicted joint shape matched with the shape presented by Heegaard and therefore no further investigation was necessary at this stage. Interestingly, no high stresses were shown by Heegaard et al. (1999) in the regions where the nine fibre array was connected with the rudiments (Figure 3-1, Figure 3-2). Heegaard et al. (1999) may have modelled the connection differently. In the model, which is presented next, I addressed my concerns to the right side bend of the model. I believe this may be a consequence of the stresses generated by the tendons during motion instead of a result of the applied mechanoregulation algorithm. I will also address my concern regarding the acquisition of the concave/convex profile in the joint region, which I think to be due to the contacts conditions during expansion. In summary, I believe that, in the Heegaard et al.

(1999) model, the boundary conditions during movement and the contact conditions during growth were likely to play more of a role in shape change than the growth law itself.

3.2.9 Model 3: Hinge joint: Introduction

In the next stage of model development, a different method was used to simulate the joint motion. Joint motion was represented by a number of steps during which a displacement was applied to the lower surface of the distal rudiment towards the proximal element, with the angle and position of the displacement determined by the type of movement being applied. With this new method I reduced to a minimum the effects of boundary conditions on the growth. This allowed me to appreciate the effects on growth due to the growth law itself and to study the effects of a range of movements (or lack of movement) and different initial joint shapes during the process of prenatal joint morphogenesis. 3D models were also developed to gain insight to the complexities of 3D joint development and its volumetric changes.

3.2.9.1 Model 3: 2D - Material and methods

The same two-dimensional biomechanical model previously presented, but with different boundary and loading conditions, was used to simulate a *single plane motion* from 0 to 120 degrees mimicking a hinge movement (Figure 3-13, B). The process used to simulate the joint morphogenesis is the same presented in section 3.2.6, Figure 3-8. Motion was no longer obtained through the use of tendons and fibres but by the application of a displacement of 0.01mm on the lower surface of the bottom phalange. The bottom phalange was then rotated by 0, 40, 60, 90 & 120 degrees relative to the vertical axis of the top phalange in order to simulate the knee bending. General contact conditions with frictionless interaction properties were maintained to model surface contact between the two joint surfaces, and linear plane stress triangle elements (CPS3) were used to mesh both rudiments. The stresses were calculated at the integration points.

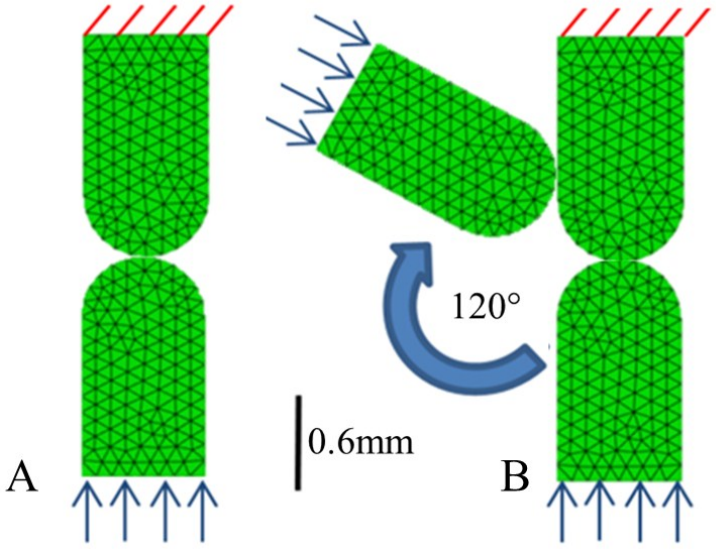

Figure 3-13 A) two-dimensional biomechanical model theoretical joint shape with boundary conditions; B) representation of the hinge movement (rotation between 0 and 120 degrees);

The direct contact between the two rudiments led to the generation of high stresses in small regions (Figure 3-14). These stresses caused an excessive localised morphogenesis instead of a well distributed pattern within the entire joint region.

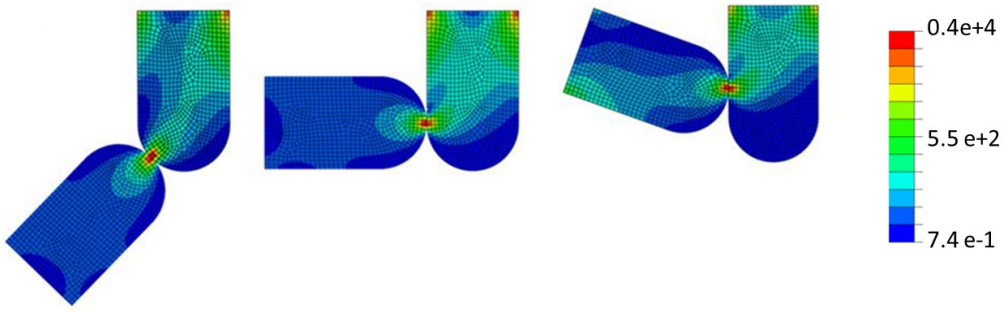

Figure 3-14 2D hinge joint motion showing the high stresses generated on the contact nodes.

To avoid this problem I decided to introduce a third component to the model, the inter-rudiment space (Figure 3-15, A). The inter-rudiment space, which is a physiological component of synovial joints (Chapter 2, Section 2.2), was included in my simulations to avoid direct contact between the two rudiments. This function is performed biologically by the interzone during early joint development and by the synovial fluid during later development. Mathematically, it acted as a smoothing function to spread the loads, therefore eliminating areas of high stress due to direct

contacts between the two rudiments; condition which is unlikely to happen in healthy joints (Figure 3-15, B; Figure 3-16). The material properties of the interzone are still unknown. However, Roddy et al. (2011a) tried to measure and analyse its properties by using AFM (Atomic Force Microscopy) and the Hertz model respectively. In their analysis, up to 40% of the force curves were removed for technical reasons and approximately a further 20% of curves were eliminated from the analysis because did not fit the Hertz model. Therefore, based on their work, the material properties of the interzone were assumed to be single phase, linear elastic, isotropic and homogeneous with E=0.287 kPa (Roddy et al., 2011a) and υ=0.4 (McCarty et al., 2011).

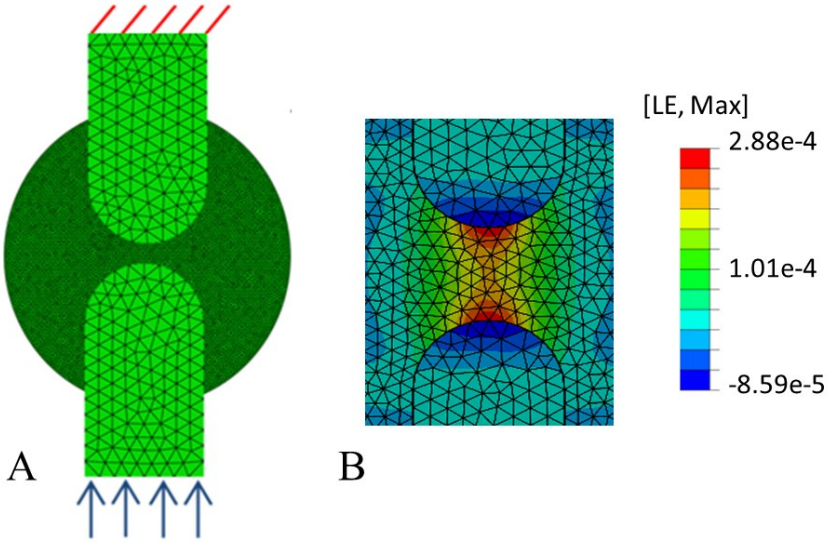

Figure 3-15 A) new model with the inter-rudiment space included between the two rudiments; B) example of the well distribute strain achieved with the inter-rudiment space; figure shows the maximum strain on principal plane.

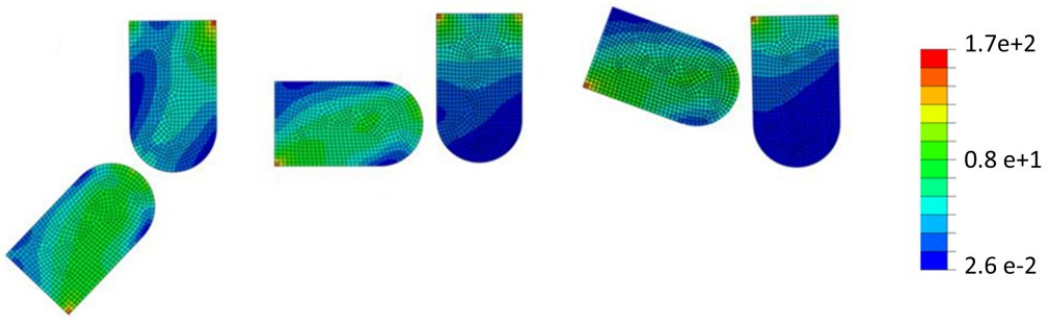

Figure 3-16 Stress distribution comparison when the inter-rudiment space included in the model; The capsule is acting as a smoothing function to spread the loads avoiding high stresses due to direct contact.

Inclusion of the inter-rudiment space spread the stresses more evenly across the joint. However, the results indicated that peak stresses occurred primarily at the

initial contact region (Figure 3-17). I expected to see stresses distributed across the surface of the proximal rudiment and at the centre of the surface of the distal rudiment. I then altered the formulation to obtain average, rather than peak, stresses throughout the full joint motion:

$$\dot{\varepsilon}_m = C_d * \left(\frac{\sum_{i=1}^{N} (a\,\sigma_{si} + b\,\sigma_{hi})}{N} \right)$$

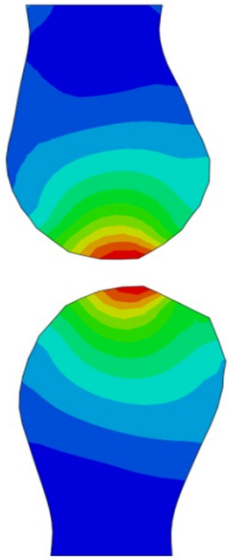

Figure 3-17 the shape obtained after five steps of growth showing high values of growth concentrate mainly on the initial contact region.

With this updated version of model 3, I ran four different simulations: (1) a *single plane motion* from 0 to 120 degrees mimicking a hinge movement, (2) a *rotational movement* from 60 to -60 degrees mimicking a ball and socket joint, (3) *rigid paralysis* condition, where axial force was applied but muscle contractions were inhibited, mimicking chicks immobilisation experiments (Mikic et al., 2000) and (4) only biological growth (Figure 3-18). In all cases, except when only the biological contribution was simulated, a displacement of 0.01mm was applied on the lower surface of the bottom phalange. While during the *single plane* and the *rotational movement*, the bottom phalange was rotated relative to the vertical axis of the top phalange in order to simulate the appropriate movement, in the immobilized case, no

movement was applied. General contact conditions with frictionless interaction properties were added to model impenetrability between all the components.

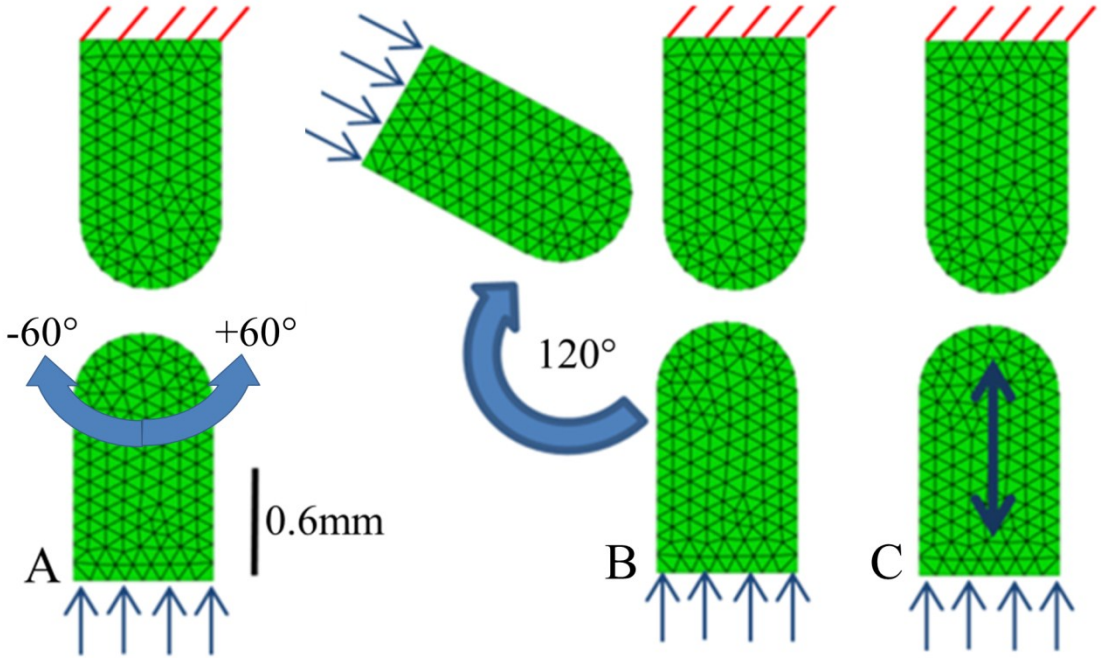

Figure 3-18 A) representation of the rotational movement between -60 and +60 degrees; C) representation of the single plane motion between 0 and 120 degrees; D) model used when muscle contraction are inhibited.

3.2.9.2 Model 3: 2D - Results

With *rotational movement*, the hydrostatic stress distribution was mostly compressive at the proximal region of the distal rudiment, while on the proximal rudiment, the hydrostatic stresses followed the movement of the distal rudiment (Figure 3-19). The top phalange acquired a more rounded convex profile whereas the bottom phalange acquired a concave profile showing the onset of a ball and socket joint (Figure 3-19). When the s*ingle plane motion* was simulated, tensile hydrostatic stresses showed a tendency for the proximal rudiment to growth more on its right side, while compressive hydrostatic stresses were seen on the top region of the distal rudiment (Figure 3-20). The top phalange bent toward the right side and it acquired a more rounded convex profile whereas, the bottom phalange acquired a flatter profile on its top region. The shape obtained was similar to a sagittal view of a hinge joint such as the knee (Figure 3-20) but, in my model the condylar shape formed on the side opposite to the motion (this will be discussed later in the thesis). In real knee

joints the condylar shape develops on the side where contact occurs. When the *rigid paralysis* was simulated, a symmetric pattern of compressive hydrostatic stress can be seen on both rudiments with the highest values on the sides (Figure 3-21). Both the rudiments acquired a concave shape (Figure 3-21). When only the biological growth was applied, as expected both the rudiments acquired a convex profile as shown in Figure 3-22.

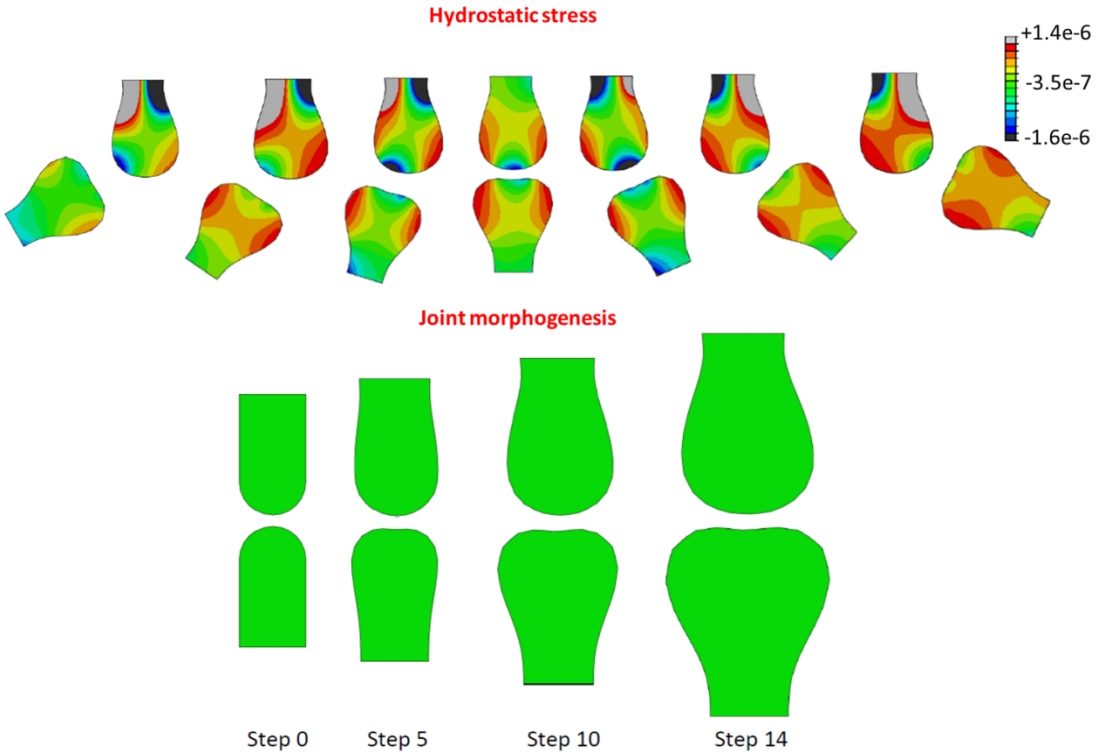

Figure 3-19 hydrostatic stress distribution at step 14 when rotational movement was simulated. Predicted joint morphogenesis over development.

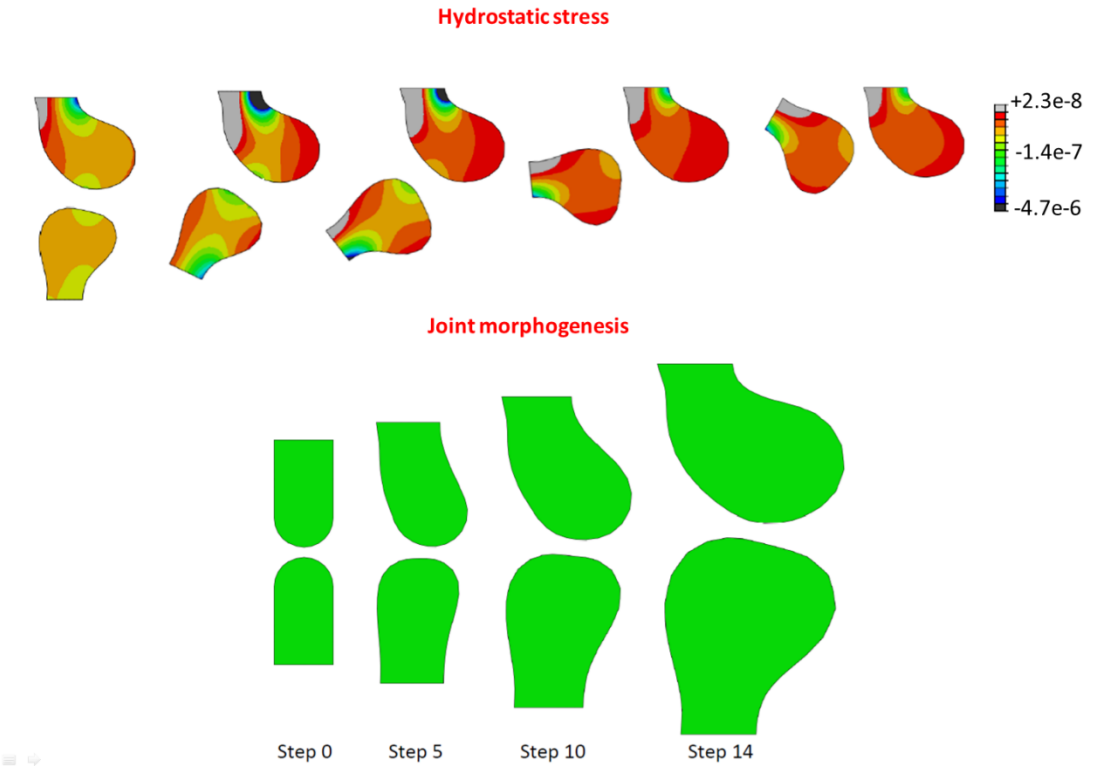

Figure 3-20 Hydrostatic stress distribution at step 14 when the hinge motion was simulated. Predicted joint morphogenesis over development.

.

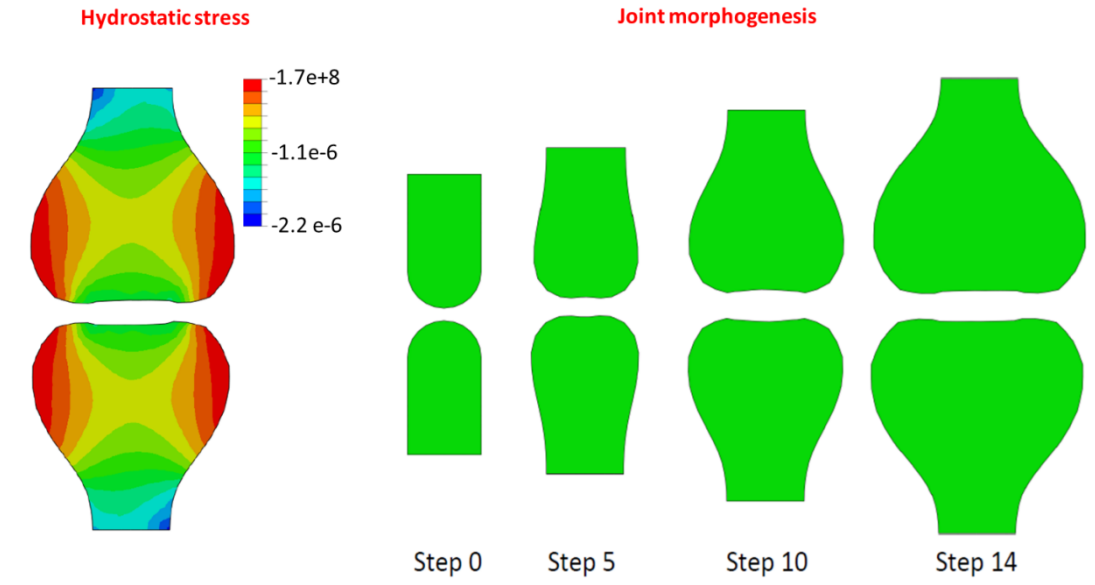

Figure 3-21 Hydrostatic stress distribution at step 14 when muscle contraction are inhibited. Predicted joint morphogenesis over development.

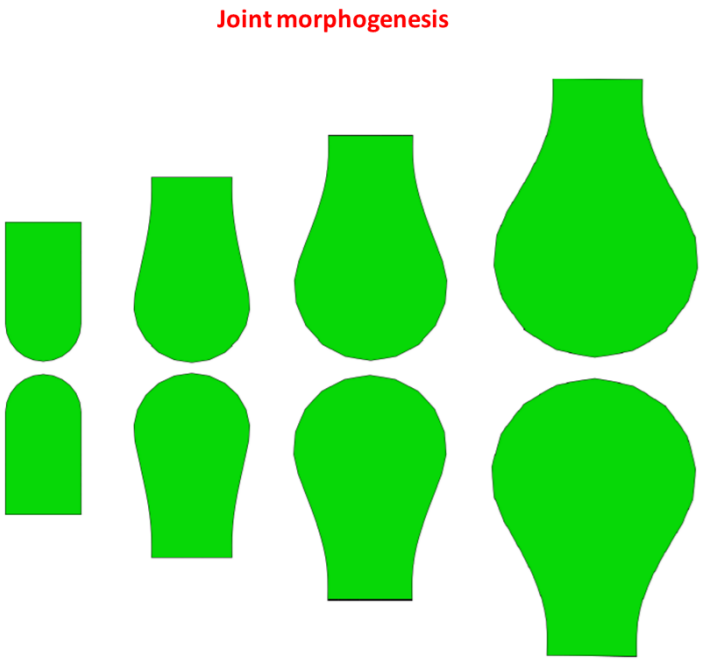

Figure 3-22 Joint morphogenesis when only the biological contribution to growth was applied. Both rudiments acquired a convex profile.

3.2.9.3 Model 3: 3D - Material and methods

3D models of the same simulations were developed in order to appreciate the complexities of 3D joint shape and its volumetric changes. The mechanoregulation algorithm, material properties and boundary conditions were the same used for the 2D version. All configurations consisted of two opposing cylindrical cartilaginous rudiments of the same dimensions with hemispherical opposing ends (Figure 3-23, A) and the inter-rudiment space. For both rudiments and the inter-rudiment space the meshes were generated by using tetrahedral quadratic elements (C3D10) and the stresses were calculated at the integration points. This model have been used to simulate a *single plane motion* from 0 to 120 degrees, a *multi-plane motion* from 60 to -60 degrees, a *rigid paralysis* condition and when only the biological growth was applied (Figure 3-23, B, C, D).

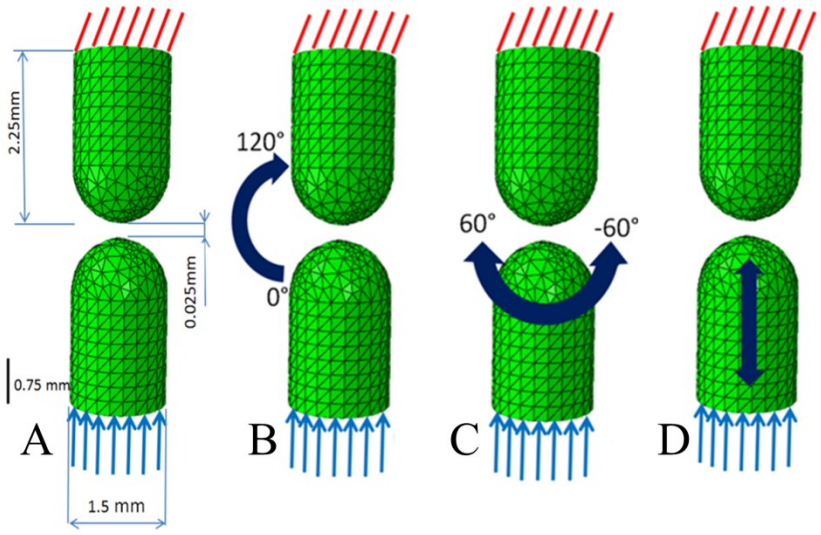

Figure 3-23 A) 3D model of an idealised prenatal joint; B) representation of the 3D hinge movement; C) representation of the multi-plane motion from 60 to -60 degrees mimicking a rotational movement; D) 3D model used for the experimental condition.

3.2.9.4 Model 3: Results

After 10 loading cycles, the shapes of the growing joints were noticeably altered and similar features with the 2D versions of the same simulations were seen. When only the biological contribution was applied, as expected, the joint expanded acquiring a rounded profile at the joint region showing a non-interlocking joint shape (Figure 3-24, A, B). When the s*ingle plane motion* was simulated, the top phalange acquired a more rounded convex profile whereas the bottom phalange acquired a flatter profile. Though the shape obtained was similar to a sagittal view of a hinge joint such as the knee (Figure 3-25), it should be noted that, the condylar outgrowth occurs on the anterior side of the joint in our model. This however is not the case in a physiological knee joint, where the outgrowth should appear on the posterior side (the side on which contact occurs during flexion). This will be discussed below. When *rigid paralysis* was simulated, both the phalanges acquired a concave shape similar to the experimental results of Mikic et al. (2000) (Figure 3-26). When the *multi-plane motion* was simulated, the top phalange acquired a more rounded convex profile whereas the bottom phalange acquired a concave profile. The shape obtained showed the onset of a ball and socket joint such as the hip (Figure 3-26).

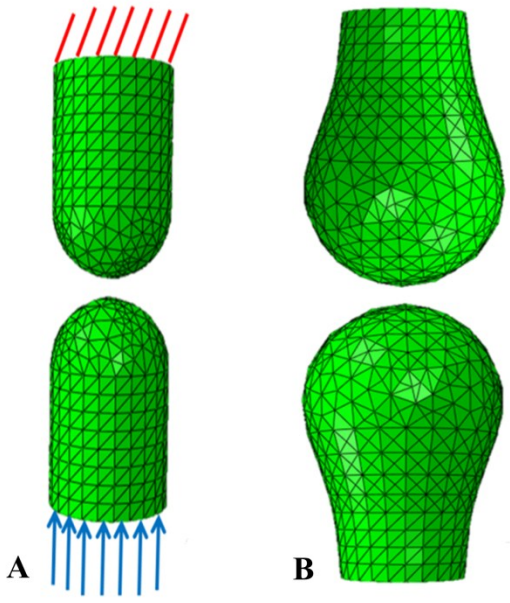

Figure 3-24 A) Theoretical shape of a joint at the beginning of the simulation; B) predicted joint morphogenesis after 10 loading cycles when only the biological growth was applied.

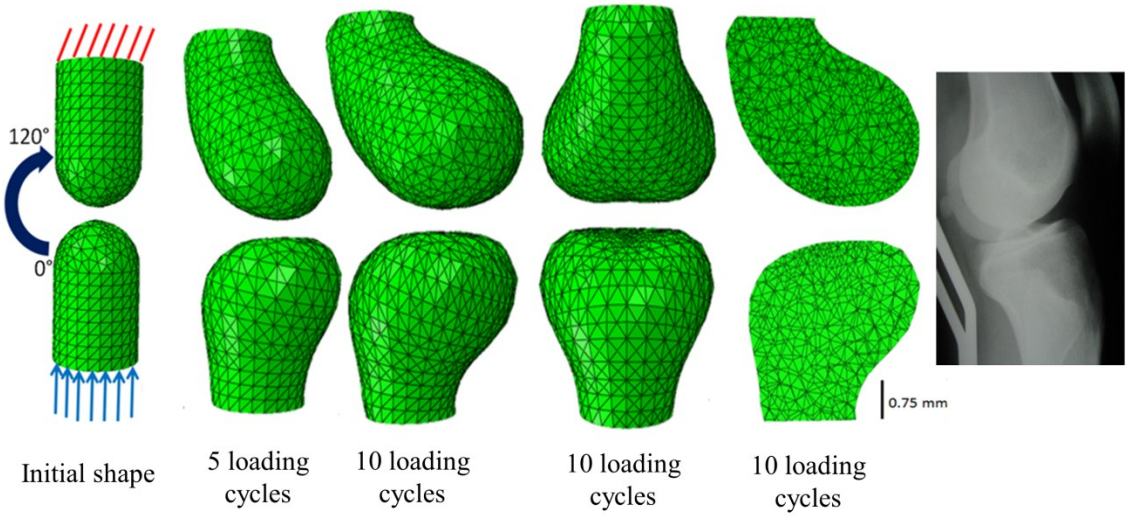

Figure 3-25 Single plain motion from 0° to 120° mimicking a hinge movement; the top phalange acquired a more rounded convex profile whereas the bottom phalange acquired a flatter profile. X-ray of a knee joint (adapted from (Ares et al., 2009)).

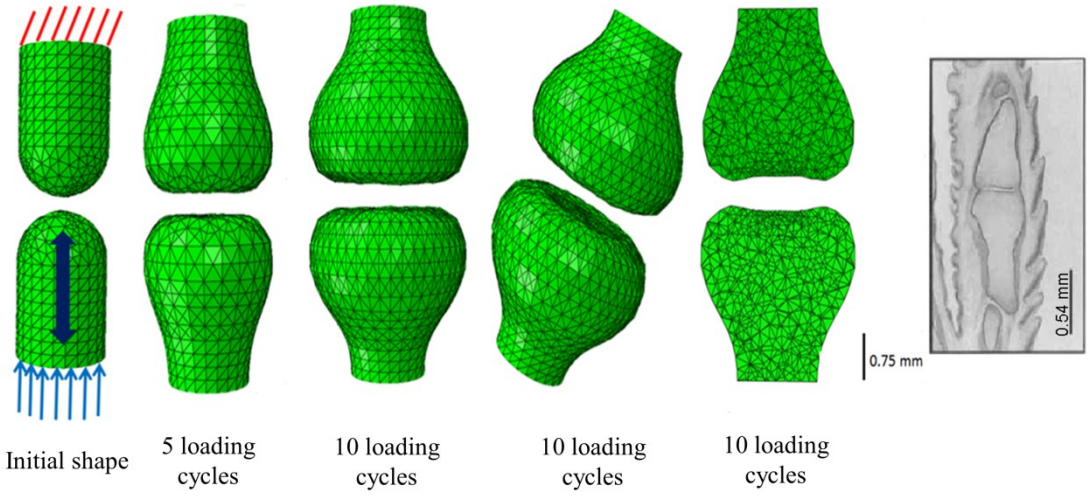

Figure 3-26 Rigid paralysis (axial force is applied but muscle contractions are inhibited); both the phalanges acquired a concave shape. X-ray of an immobilised joint (adapted from (Mikic et al., 2000)).

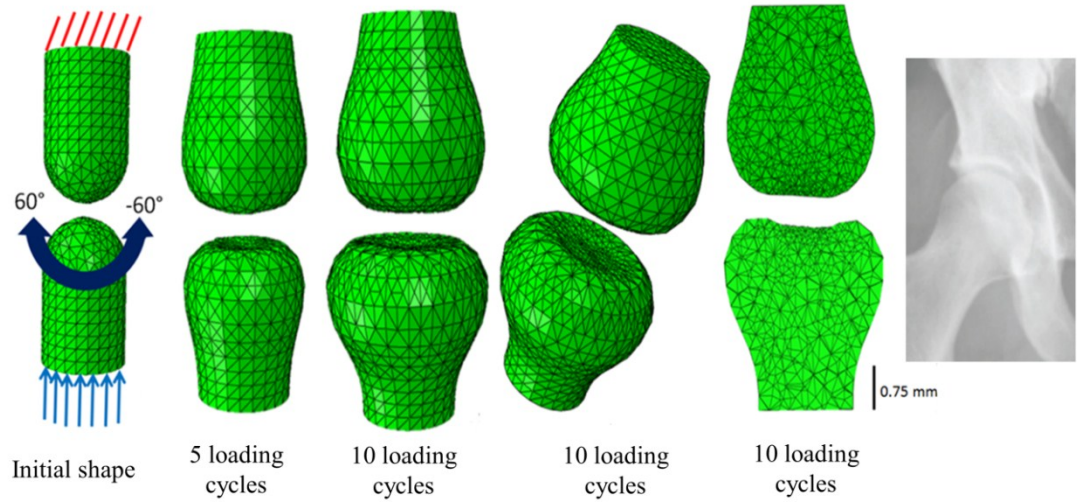

Figure 3-27 Multi-plane motion from 60° to -60° mimicking a rotational movement; the top phalange acquired a more rounded convex profile whereas the bottom phalange acquired a concave profile. X-ray of a knee joint (adapted from (Schuh et al., 2009)).

3.2.9.5 Model 3: 2D & 3D conclusion

Similar changes in shape were achieved by both 2D and 3D models. The rounded convex profile on the proximal rudiment, instead appearing on the side where the motion was applied (as in Heegaard et al. (1999)), it developed on the opposite side (Figure 3-28).

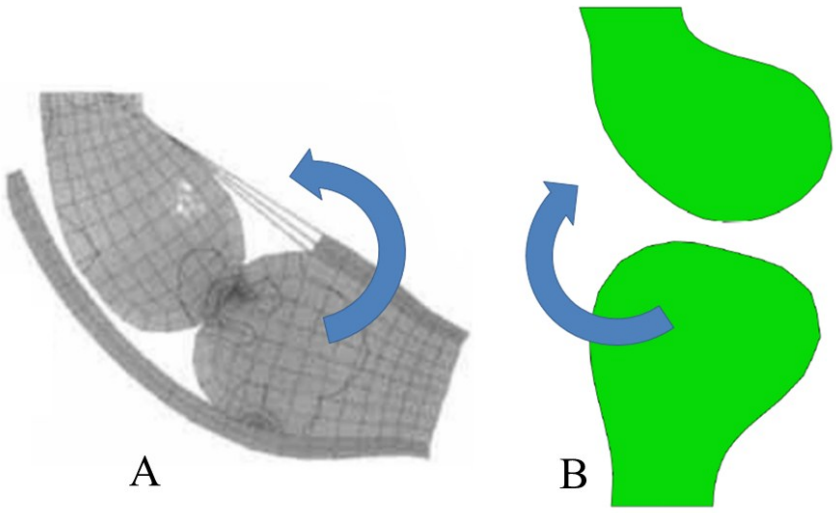

Figure 3-28 A) Heegaard simulation where the proximal rudiment is bending on the same side of the joint motion; B) our simulation where the right bending of the proximal rudiment is opposite to the joint motion.

These results made me examine the algorithm more closely. I investigated the contact conditions during growth, which constrained the volume during expansion, and influenced the final joint shape. A 2D simulation was generated and when the rudiments were allowed unconstrained expansion during growth, both acquired a convex profile within the joint region as shown in Figure 3-29, A. When the rudiments were constrained during growth, two flat surfaces developed (Figure 3-29, B). Therefore, the mechanoregulation algorithm used predicted growth on the opposite side of the rudiment suggesting that the results showed by Heegard et al. (1999), and the ones of our previous model (model: 2) (3.2.5), were probably due to the stresses generated by the tendons during motion instead of the growth law used.

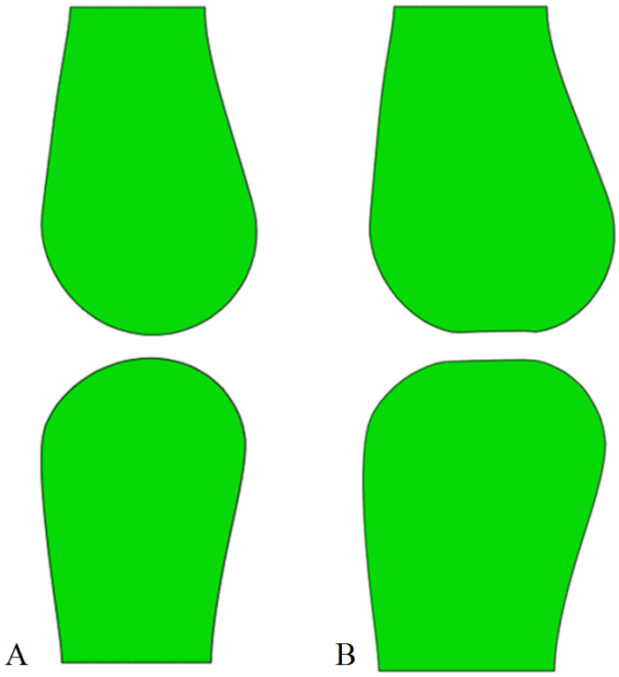

Figure 3-29 A) When the rudiments were allowed unconstrained expansion (no contact with opposing rudiment), both resultant shapes were convex; B) When we imposed an enforced contact condition in the model, two flat surface within the joint region were found to develop.

3.3 Summary

In this chapter I introduced the evolution of my prenatal joint morphogenesis simulations. I based my initial models on that of the pioneering study of Heegaard (1999), which uses the endochondral ossification growth law of Carter et al. (1987). I found that the onset of the interlocking joint shape presented by Heegaard et al. (1999) was promoted by the boundary conditions instead of by the mechanoregulation theory. In fact, in an attempt to reduce to a minimum the effect to growth due to external factors (boundary conditions), I was unable to replicate their findings (Heegaard et al., 1999).

It is important to note that, at the stage of development modelled by Heegaard et al. (1999) and us, the joints are entirely cartilaginous and there is no experimental evidence to suggest that endochondral ossification has an influence on prenatal joint shape development. The mechanical stimulus for cartilage during growth (where ossification does not occur) is likely to be different than the mechanical stimulus during endochondral growth and ossification (where cartilage growth occurs but the endpoint is ossification). In the former, the cartilage is trying to make more cartilage; in the latter it is trying to turn into bone. Two main limitations were present in this

study in order to understand the effectiveness of the endochondral ossification algorithm in predicting prenatal joint development. As already explained in Section 3.2.9.1 the material properties used for the inter-rudiment space are still unknown and therefore the values used may not be fully realistic. However, at this stage it was added to evenly spread the load between the two rudiments and not to simulate any physiological phenomenon. Tendons and ligaments were not included in the model even if, as shown in Section 3.2.5 they have an important effect on the direction of growth. However, to understand the solely contribution due to the mechanoregulation algorithm, their removal from the simulation was necessary.

All these simulations were a key point for the entire project and these findings made us question the effectiveness of the endochondral ossification law proposed by Carter et al. (1987) as algorithm to predict prenatal joint development. Therefore, a new mechanobiology theory specific for cartilage growth and morphogenesis was needed.

4 Simulation of Prenatal Joint Development

This chapter present the first 3D mechanobiological simulation of joint morphogenesis for which the effects of a range of movements (or lack of movement) and different initial joint shapes were explored. A novel mechanobiology theory for cartilage growth, where static hydrostatic compression inhibits cartilage growth while dynamic hydrostatic compression promotes cartilage growth, was proposed and tested. Both pre-cavitational (no muscle contractions) and post-cavitational (with muscle contractions) phases of joint development were simulated. These models demonstrate how mechanical factors influence early joint morphogenesis. An enhanced understanding of how prenatal joints form is critical for developing strategies for early diagnosis and preventative treatments for congenital musculoskeletal abnormalities such as developmental dysplasia of the hip. This chapter presents an adapted version of work previously published in the Journal of Biomechanics (Giorgi et al., 2014) (see Appendix 10).

4.1 Introduction

As described in Section 2.3, the process of synovial joint formation is a well-defined sequence of events: 1) Joint site determination, 2) interzone formation, 3) cavitation, and 4) morphogenesis (Pacifici et al., 2005). Recent studies, however, have shown that joint morphogenesis starts before cavitation (Nowlan and Sharpe, 2014). Only one computational study, previously presented (Heegaard et al., 1999), has explored the role of motion on joint morphogenesis. Here I advance the model of Heegaard et al. (1999) to include static loads that occur pre-cavitation and may play a role in early joint shape. I also examine the effects of different movement regimes and simulate growth over a longer time period so that a realistic joint shape is obtained.

4.2 Cartilage growth law

During early prenatal development, the joints are entirely cartilaginous. Differentiation of cartilage to bone through endochondral ossification is a biologically distinct process to the region-specific growth of proliferating cartilage that leads to joint shape morphogenesis. During prenatal development, the primary

centre of ossification may be present at the mid-diaphysis, which is far from the developing joint, and is not likely to affect joint morphogenesis. *In vitro* studies indicate that static compressive loading inhibits cartilage growth (Burton-Wurster et al., 1993; Guilak et al., 1994) while cyclic compressive loading promotes growth (Kim et al., 1994; Korver et al., 1992; Parkkinen et al., 1992). I propose a mechanobiological theory specific to these properties of cartilage growth (and distinct from growth that occurs during endochondral ossification). In proposing and testing this novel mechanobiological theory for cartilage, my models give a greater insight into the process of joint morphogenesis.

4.2.1 Growth rate

Growth and morphogenesis of the rudiments were controlled by biological and mechanical growth rates so that the growth rate $\frac{d\varepsilon}{dt}$ was as follows (as described in Section 3.2.2):

$$\frac{d\varepsilon}{dt} = \frac{d(\varepsilon_b)}{dt} + \frac{d(\varepsilon_m)}{dt}$$

with $\dot{\varepsilon}_b$ being the biological contribution to growth and $\dot{\varepsilon}_m$ the mechanical contribution to growth (Shefelbine and Carter, 2004). Following Heegaard et al. (1999), $\dot{\varepsilon}_b$ was considered to be proportional to the chondrocyte density. The equation for local chondrocyte density along the long axis of a rudiment was calculated by Heegaard et al (1999) by fitting a polynomial curve to the grey level distribution on a sagittal micrograph of a joint, where darker areas indicated higher chondrocyte density. The chondrocyte density C_d is greater towards the ends of the rudiments and lower towards the diaphysis, and therefore expressed by the formula (see Section 3.2.6):

$$\dot{\varepsilon}_b = C_d = k * (0.14 - 0.87\xi + 4.40\xi^2 - 2.66\xi^3)$$

with C_d being the chondrocyte density, $k = 11*10^3$ being a constant determining the amount of biological growth, which is maintained in the range of 75-85% of the total growth (Hill, 1939), and ξ the distance along the proximal-distal axis of the rudiment starting from the distal end (Heegaard et al., 1999). The biological contribution to growth was assumed to be same during static and dynamic loading phases. The

effects of alternative equations for the chondrocyte density were also analysed in 2D versions of the hinge simulation and are discussed in the next chapter (Chapter 5).

The mechanical growth rate, $\dot{\varepsilon}_m$, was proportional to the compressive hydrostatic stress, σ_h. I implemented a mechanobiological theory in which static hydrostatic compression inhibits cartilage growth (Burton-Wurster et al., 1993; Guilak et al., 1994) while dynamic hydrostatic compression promotes cartilage growth (Kim et al., 1994; Korver et al., 1992; Parkkinen et al., 1992). The mechanobiological growth rate was weighted by the chondrocyte density, based on the assumption that the greater the number of cells, the greater the adaptation to mechanical loading. The overall mechanobiological contribution to growth was therefore calculated at each node of the model as the average stresses throughout a full joint motion using the formulae below:

$$\dot{\varepsilon}_m = C_d * \left(\frac{\sum_{i=1}^{N} \sigma_{hi}}{N} \right), \text{ pre-cavitation}$$

$$\dot{\varepsilon}_m = -C_d * \left(\frac{\sum_{i=1}^{N} \sigma_{hi}}{N} \right), \text{ post-cavitation}$$

where σ_h is the compressive hydrostatic stress, N the number of movement per step and C_d the chondrocyte density.

4.3 Mechanobiological simulations of prenatal joint morphogenesis

4.3.1 Material and methods

Three idealised geometries of common joint configurations were created in Abaqus (Dassault Systemes, CAE module, version 6.12), where all configurations consisted of two opposing cartilage rudiments and an inter-rudiment space. A hinge joint configuration was composed of two cylindrical rudiments of the same dimensions with hemispherical opposing ends, with the distal rudiment at an initial angle of 45°

to the vertical proximal rudiment to represent a more physiological initial joint position (Figure 4-1, A). A ball-and-socket configuration was composed of a distal cylindrical rudiment opposed to a flat proximal rudiment representing a bone such as the pelvis or shoulder, as shown in Figure 4-1, B. A similar configuration to the hinge was used for the rigid paralysis configuration, except that the two rudiments were aligned, as shown in Figure 4-1, C. As these configurations are intended to be generic and not to be representative of any particular species or animal, the initial dimensions (as shown in Figure 4-1) were arbitrary, and size changes due to growth or adaptation were analysed as relative to the initial size. The inter-rudiment space was modelled as a sphere surrounding the joint, (truncated at its extremes in order to decrease the number of elements) with a maximal diameter of 10 mm and large enough to contain the joint throughout movement sequences (Figure 4-1, D). Based on the stage of joint development being modelled, the rudiments were assumed to be fully cartilaginous (Gardner and O'Rahilly, 1968). All cartilage material properties were assumed to be linear elastic, isotropic and homogeneous. The Young's modulus for cartilage (E= 1.1 MPa) was taken from four-point bending tests on un-mineralised embryonic mouse ribs (Tanck et al., 2004) and the cartilage Poisson's ratio taken as v=0.49 to reflect the incompressibility of the fluid in the cartilage at short time scales (Armstrong et al., 1984; Carter and Beaupre, 1999; Wong et al., 2000). The Young's modulus of the inter-rudiment space was E=0.287 kPa (Roddy et al., 2011a), and its Poisson's ratio was v=0.4 (McCarty et al., 2011). For both rudiments and the inter-rudiment space the meshes were generated by using tetrahedral quadratic elements (C3D10) and the stresses were calculated at the integration points.

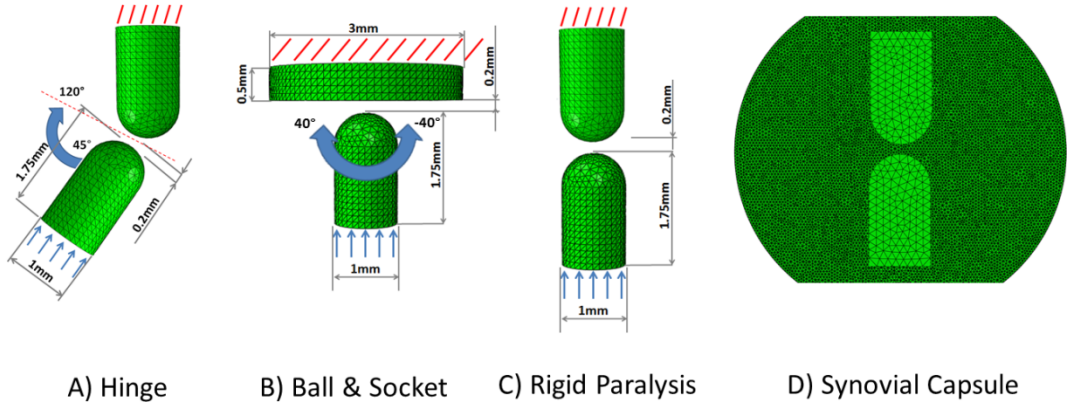

Figure 4-1 A) Initial hinge model configuration; B) ball-and-socket configuration; C) rigid paralysis configuration; D) section of the rigid paralysis configuration with inter-rudiment space.

4.3.1.1 Loading conditions

In all models, the proximal rudiment was fixed at its proximal end. At rest, the bottom rudiment was located 0.2 mm from the top rudiment's lower surface (Figure 4-1, A). Static and dynamic loading were represented by an applied displacement of the distal rudiment towards the proximal (upper fixed) rudiment. In the pre-cavitational phase, prior to the onset of muscle contractions, static loading was represented by the constant application of an axial displacement on the distal rudiment towards the proximal rudiment in the starting configuration. In the post-cavitational phase, after the onset of muscle contractions, joint loads were represented by a number of discrete steps during which a displacement was applied to the lower surface of the distal rudiment towards the proximal element, with the angle and position of the displacement determined by the specific movement. The magnitude of the displacement applied, 10µm, remained constant throughout all simulations. Based on approximations of muscle cross sectional area (as a percentage of rudiment width) and a maximum embryonic muscle stress of S = 1.11mN/mm^2 (Nowlan et al., 2008), I estimated the likely muscle force to be on the order of 0.1 mN. An applied displacement of 10µm resulted in a force of approximately this magnitude on the fixed region of the proximal rudiment. In the absence of data on the magnitude of growth related strains in the developing joint, the same displacement was used for the static phase. Two static iterations (pre-cavitation with no motion) and eight dynamic iterations (post-cavitation with motion) were included in the hinge and the ball-and-socket simulation. In the hinge model, a single plane

motion was applied from 45° to 120° in each iteration, as shown in Figure 4-1, A, at angles of 45°, 90° and 120°, while the ball-and-socket model was loaded under a multi-plane motion from 40° to 0° to -40° in two planes perpendicular to each other as shown in Figure 4-1, B. Rigid paralysis, where the muscles are in continuous tetanus (Roddy et al., 2011b), was represented by the constant application of an axial displacement, as shown in Figure 4-1, C, assumed to be static loading due to the lack of dynamic muscle contractions. The paralysis model was also run in 2D with the distal rudiment at -60° to the proximal rudiment. Frictionless impenetrable contact was modelled between all the components of the models.

4.3.1.2 Model Implementation

During each iteration, the orthonormal thermal expansion capabilities of the FE solver were utilised to allow isotropic expansion of the proximal and distal rudiments with the sum of the biological and mechanobiological growth rates used as the 'temperature' for expansion. This expansion occurred within an unconstrained volume, representing the growth of the entire limb, which ensured that the mechanical stresses due to motion were the dominant stimulus for shape change rather than stresses due to contact of the two rudiments during growth. The new geometry was then re-meshed and the two rudiments were automatically realigned based on the initial axis position ensuring that the initial distance of 0.2mm, between the bottom rudiment and the top rudiment's lower surface, was maintained. With this configuration the loading conditions could be applied again for another step of growth. The size and shape of the synovial capsule remained the same for the entire simulation. A simulation using biological growth rates only was also performed for comparative purposes. A graphical representation of the entire process is shown in Figure 4-2.

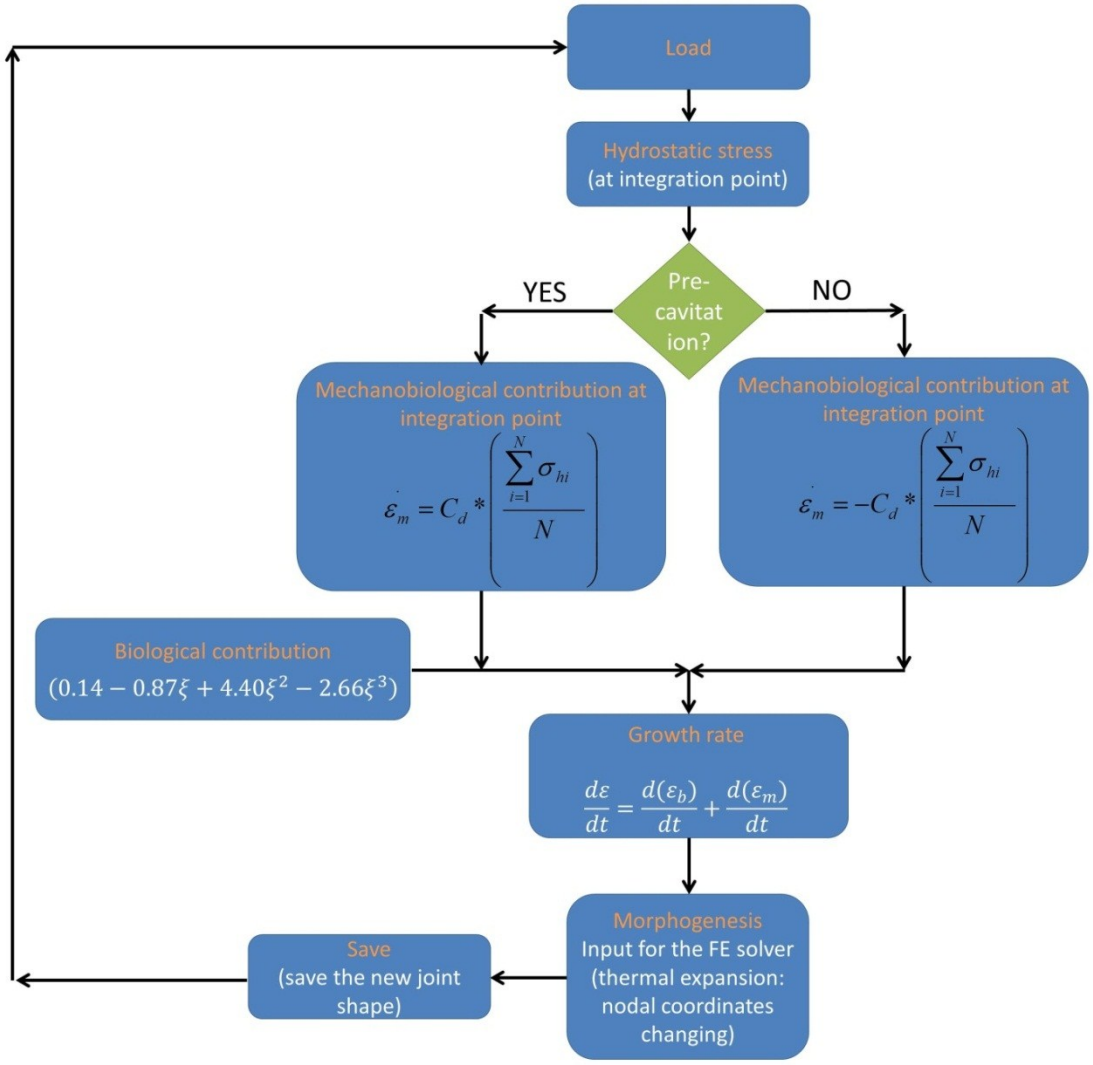

Figure 4-2 Graphical representation of the steps involved to simulates prenatal joint development.

4.3.2 Results

4.3.2.1 Hydrostatic stress distribution

In all the models, the hydrostatic stresses close to the contact regions were always compressive, as shown in Figure 4-3. High compressive hydrostatic stresses were also seen at the anterior corner of the proximal rudiment of the hinge model due to the fixed boundary condition (Figure 4-3, arrows). The simulation in which rigid paralysis was modelled induced a symmetric stress pattern on the rudiments, as shown in the first (static) phase of the hinge simulation (Figure 4-3, left).

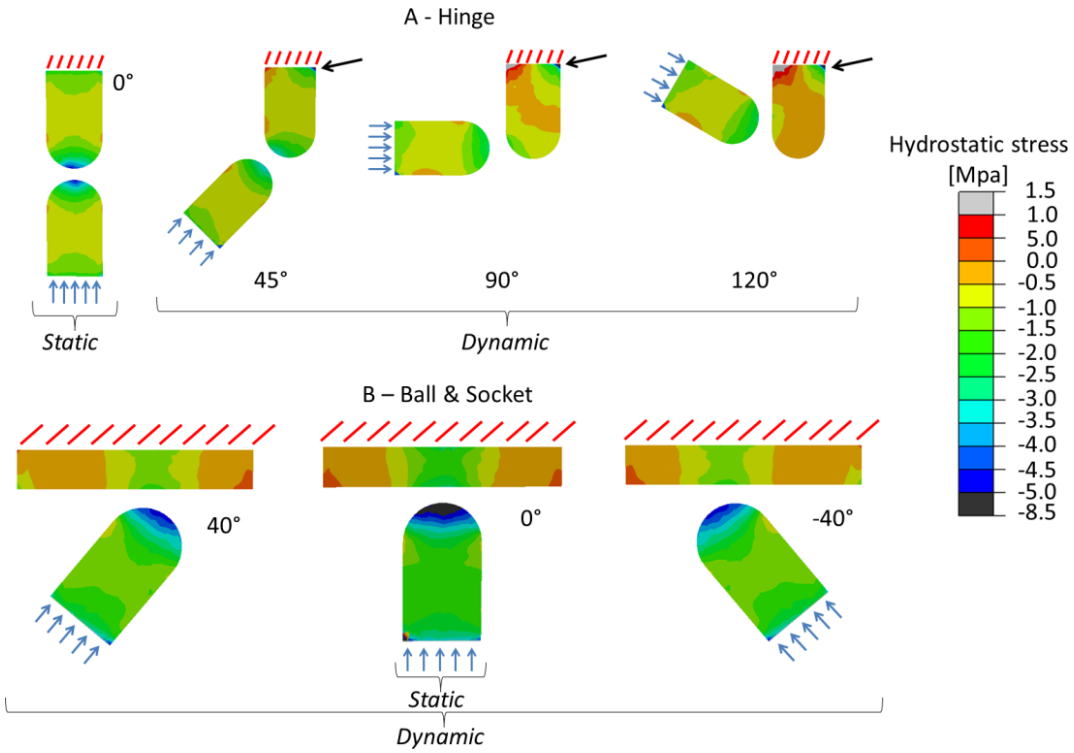

Figure 4-3 Hydrostatic stress distribution during the first step of static and dynamic loading for the A) hinge and the B) ball-and-socket joint, respectively.

4.3.2.2 Morphogenesis

When biological growth alone was applied, the rudiments preserved their initial opposing convex surfaces as shown in Figure 4-4. In contrast, when the mechanical stimulus was included in the simulation, the shape of the predicted growing joints changed according to the movement pattern applied. When a single plane motion from 45° to 120° was applied, the proximal rudiment showed a rounded convex profile in both posterior and anterior regions, with more pronounced growth posteriorly (Figure 4-5, arrowhead). The distal rudiment showed similar features with a less pronounced rounded convex profile in its posterior region and the acquisition of a slight concave profile in the mid-line section (Figure 4-5, arrow). The final joint shape suggests the generation of an interlocking joint shape such as the knee, where the condylar shape formed on the same side of the motion (see Section 3.2.9.2). When a multi-plane motion from 40° to -40° degrees was applied between a flat and a cylindrical rudiment, the flat rudiment showed a concave profile which partially enclosed the rounded convex profile of the cylindrical rudiment (Figure 4-6) suggesting the generation of an interlocking joint shape such as the hip or shoulder joint. When only axial forces were applied under static loading

conditions, reproducing rigid paralysis, both the rudiments acquired a flat shape within the joint region as shown in Figure 4-7, similar to the experimental results of Mikic et al. (2000) (see Section 2.3.1, Figure 2-5 B).

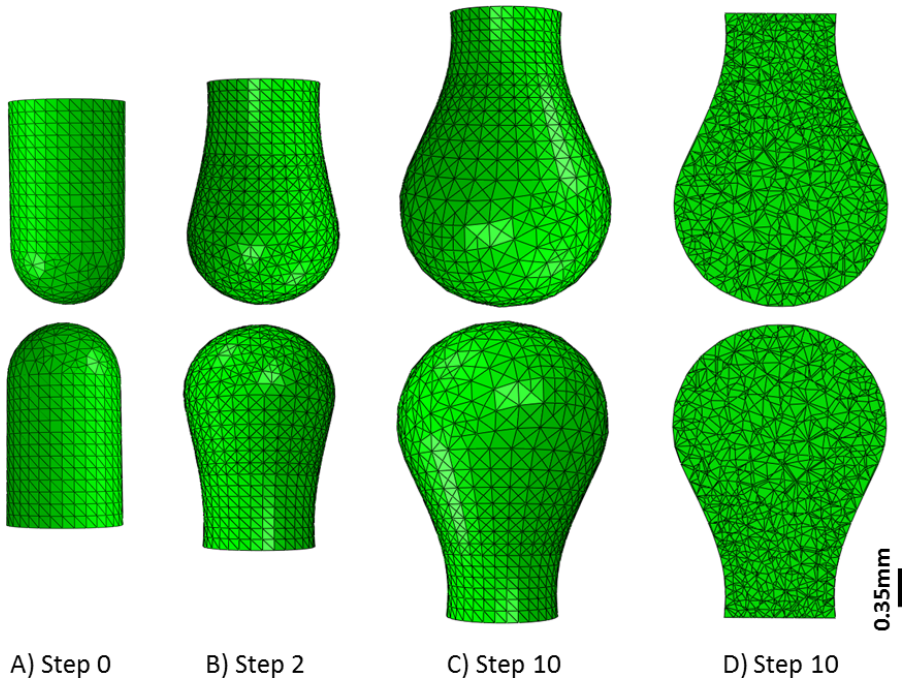

Figure 4-4 Joint morphogenesis prediction when only the biological contribution to growth was considered. A) Sagittal view of the initial model. B) Sagittal view of the predicted joint shape after 2 steps. C) Sagittal view of the predicted joint shape after 10 steps of growth. D) Sagittal section after 10 steps of growth.

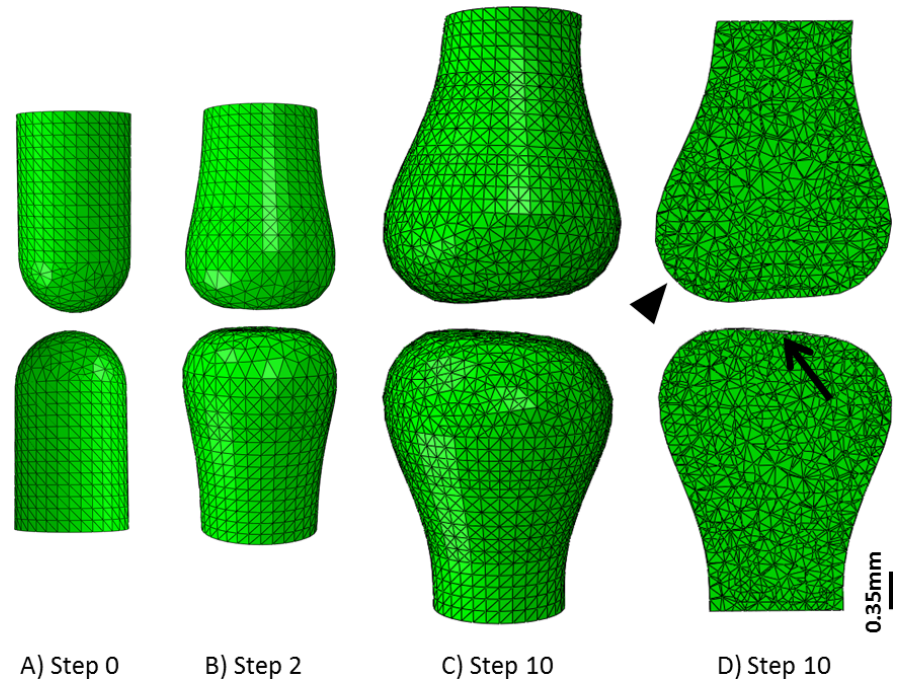

Figure 4-5 Joint morphogenesis prediction when a single plane motion from 45° to 120° is applied. A) Sagittal view of the initial model. B) Sagittal view of the predicted joint shape after 2 static steps of growth. C) Sagittal

view of the predicted joint shape after 2 static and 8 dynamic steps of growth. D) Sagittal section after 2 static + 8 dynamic steps of growth.

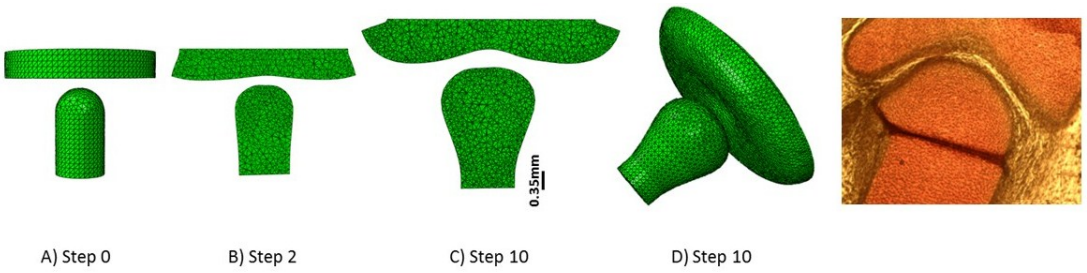

Figure 4-6 Joint morphogenesis prediction when a multi plane motion from 40° to -40° is applied. A) Sagittal view of the initial model. B) Sagittal section of the predicted joint shape after 2 static steps of growth. C) Sagittal section of the predicted joint shape after 2 static and 8 dynamic steps of growth. D) Rotated view after 2 static + 8 dynamic steps of growth. Histological images of day 9 of chick (adapted from Nowlan et al., 2014).

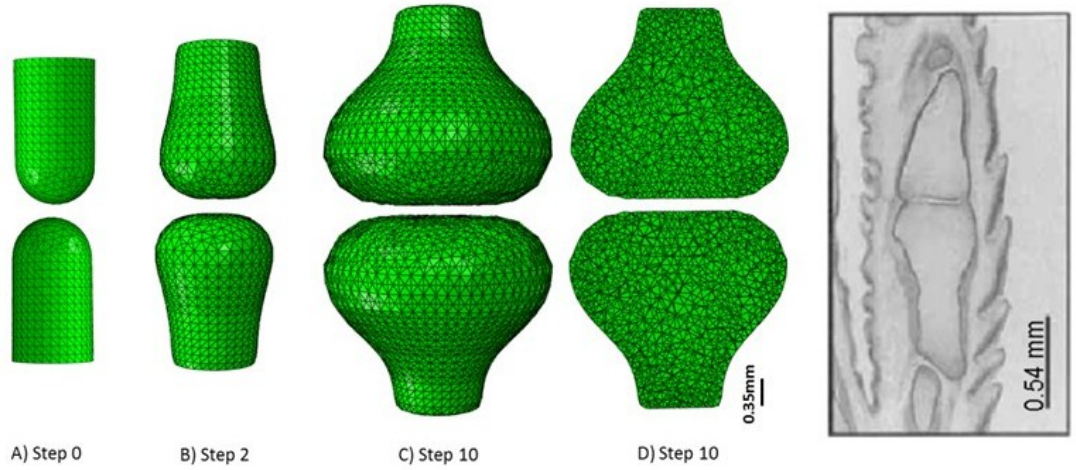

Figure 4-7 Joint morphogenesis when the rigid paralysis was simulated. A) Sagittal view of the initial model. B) Sagittal view of the predicted joint shape after 2 static steps of growth. C) Sagittal view of the predicted joint shape after 10 static steps of growth. D) Sagittal section after 10 static steps of growth. X-ray of an immobilised joint (adapted from (Mikic et al., 2000)).

4.3.3 Conclusion

I have developed the first 3D mechanobiological models of prenatal joint shape development, which are capable of predicting a range of joint shapes based on the starting joint configuration and applied movements. Both hinge and ball and socket movements predicted physiological interlocking shapes (Figure 4-5, Figure 4-6) and, when only axial forces were applied under static loading conditions, reproducing rigid paralysis, both the rudiments acquired a flat shape within the joint region

(Figure 4-7) similar to the experimental results of Mikic et al. (2000) for the immobilised interphalangeal joint (see Section 2.3.1, Figure 2-5).

Based on recent evidence that joint shape initiates prior to cavitation (Nowlan and Sharpe, 2014), I have modelled the development of the joint under both static and dynamic loads, characteristic of pre- and post- cavitation, respectively. I have developed a novel mechanobiology theory of cartilage growth, based on experimental evidence from *in vitro* stimulation of chondrocytes (Burton-Wurster et al., 1993; Guilak et al., 1994; Kim et al., 1994; Korver et al., 1992; Parkkinen et al., 1992). Despite the abundance of mechanobiological theories and mechanobiological simulations relating to endochondral ossification (Carter et al., 1998a; Claes and Heigele, 1999; Huiskes et al., 1997; Lacroix and Prendergast, 2002; Lacroix et al., 2002; Prendergast et al., 1997; Sarin and Carter, 2000; Stevens et al., 1999), I am unaware of any mechanoregulation algorithm specific to cartilage growth in a non-endochondral ossification context. The growth law proposed by Heegaard et al. (1999) was based upon a theory developed for endochondral ossification (Carter et al., 1987), where hydrostatic compressive stress inhibits and tensile stress promotes cartilage growth and ossification. In contrast, my simulations focus specifically on joint epiphyses which are entirely cartilaginous at the stages modelled (Gardner and O'Rahilly, 1968), and it is likely that the mechanical stimuli for growth and adaptation of epiphyseal cartilage are different than those which influence endochondral growth and ossification. These two processes are biologically distinct, as growth at the growth plate is primarily due to chondrocyte hypertrophy (Kronenberg, 2003), while cartilage growth at the epiphysis is likely due to cell proliferation (Pacifici et al., 2005). Therefore, the mechanobiological growth law proposed here is specific to epiphyseal cartilage and is based upon experimental data showing that cyclic hydrostatic compression stimulates matrix production (Kim et al., 1994; Korver et al., 1992; Parkkinen et al., 1992) and static compression inhibits the synthesis of cartilage matrix proteins (Burton-Wurster et al., 1993; Guilak et al., 1994). However, the new theory which I propose is not in conflict with the theories previously proposed for growth plate cartilage, as in both cases, compression provides a favourable environment for cartilage. In endochondral ossification, hydrostatic compression maintains the cartilage at the growth plate, while during epiphyseal cartilage growth, hydrostatic compression promotes the formation of

more cartilage. This new theory for cartilaginous joint morphogenesis differentiates between static and dynamic loading conditions. Cartilage obtains its nutrients primarily through diffusion which increases with cyclic hydrostatic compression but not with static compression. Therefore in my new theory, static compressive loading inhibits cartilage growth while dynamic compressive loading promotes it. In proposing a mechanobiological theory for epiphyseal cartilage growth and adaptation, I offer a biomechanical understanding of the influence of mechanical loading on joint morphogenesis.

Moreover, by comparing the predicted joint shapes using both mechanoregulation algorithms, when the hinge motion was simulated, the growth law for endochondral ossification predicted the condylar outgrowth on the anterior side of the joint instead of on the posterior side where motion occurs as predicted by the new growth law specific for cartilage (Figure 4-8, A). When the ball & socket motion was simulated with hydrostatic compression inhibiting growth, the concave profile was predicted on the movable part (distal rudiment) and the convex profile on the non-movable part (proximal rudiment) (Figure 4-8, B). When I simulated the same type of motion with the new growth law the results showed opposite behaviours, the distal rudiment acquired a convex profile while the proximal rudiment a concave shape (Figure 4-8, B). This new shape is closer to any physiological ball and socket joints, such as the hip or the shoulder joint, where the distal and proximal rudiments acquire a convex and concave profile respectively. When rigid paralysis was simulated, in both cases the joints acquired similar shapes with the onset of a flat and non-interlocking shape at the joint region (Figure 4-8, C).

Material properties of inter-rudiment space and cartilage were assumed to be linear elastic, isotropic and homogeneous based on studies, and also tested by us (see Section 5.1), which showed that the fluid pressure in biphasic models is comparable to the hydrostatic stress in the single phase models when loaded at frequencies of 1 Hz (Carter and Wong, 2003; Shefelbine and Carter, 2004), which is close to the frequency of muscle contraction in utero (Hayat et al., 2011). However there are some limitations in this study. Muscles and ligaments were not explicitly modelled, motion was simulated through the use of a number of discrete steps, and simplified shapes were used. We are aware that a dynamic motion, the inclusion of ligaments and tendons, and the use of more realistic shapes would have made these models

more accurate. However, since these models are of generic joint shapes and configurations, and do not apply to one specific species (or even limb), this study was focussed on the joint motion likely to result from approximations of common movement sequences.

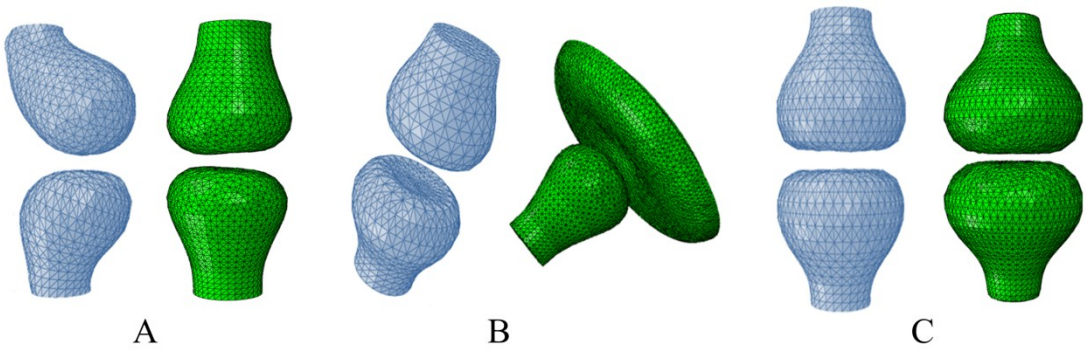

Figure 4-8 Comparison between the endochondral ossification algorithm (blue images), and the new mechanoregulation algorithm for cartilage growth (green images). A) Hinge motion; B) ball & socket motion; C) Rigid paralysis.

4.4 Summary

This study presents how stresses generated during static growth-related loading and dynamic post-cavitational movements can influence prenatal joint morphogenesis. This study predicts joint shape morphogenesis in 3D using a novel mechanobiology theory for cartilage growth. Our simulations predict a range of anatomically recognisable joint shapes based on the starting joint configuration and applied movement. The significance of this research is that it provides new and important insights into normal and abnormal joint development.

5 Sensitivity Analyses

There are many parameters in the model that play an important role in the resultant shapes. Therefore, in this section I will present the sensitivity analyses performed on the previously presented model. In particular, six points will be discussed: 1) why I choose linear elastic instead of poroelastic material properties; 2) the importance of having both static (pre-cavitation) and dynamic (post-cavitation) loading conditions; 3) the differences on the final joint shape between having or not having the inter-rudiment space; 4) the consequences of using different chondrocyte density curves (i.e., baseline growth rate); 5) the effects of applying an higher or lower biological contribution by varying the values of the constant k and, 6) how morphogenesis is influenced with an alternative initial alignment during immobilisation. This section aims to provide additional evidence for the choices made on our model.

5.1 Linear elastic versus Poroelastic

Although cartilage is a biphasic material, and the inter-rudiment space is also likely to be the same (Roddy et al., 2011a), I decided to model our materials as single phase and near incompressible (Poisson's ratio of 0.49 (Shefelbine and Carter, 2004)). This was based on previous studies which showed that the fluid pressure in biphasic models is comparable to the hydrostatic stress in the single phase models when loaded at frequencies of 1 Hz (Carter and Wong, 2003; Shefelbine and Carter, 2004), which is close to the frequency of muscle contraction (Vaal et al., 2000) in infants. At these frequencies the water does not have sufficient time to flow out of the cartilage making the fluid pressure and matrix shear stress being equivalent to the hydrostatic stress and octahedral shear stress of the single phase model (Shefelbine and Carter, 2004). However, I decided to model a 2D hinge joint with both linear elastic and poroelastic material properties in order to demonstrate, by varying the holding loading time and the value of cartilage permeability, that a linear elastic model was sufficient.

5.1.1 Abaqus Permeability

Abaqus calculates permeability as hydraulic conductivity. Permeability, usually represented as "k", is a property of soils that describes the ease of a fluid to move

through pore spaces. It depends on the intrinsic permeability $\hat{k}$ of the material, on the degree of saturation and on the density and viscosity of the fluid.

Abaqus calculates permeability as hydraulic conductivity using the following equation:

$$\bar{k} = \hat{k} * \frac{g}{v_k};$$

Where g is the gravitational acceleration and v_k the kinematic viscosity.

The intrinsic permeability $\hat{k}$ is given by:

$$\hat{k} = h_p * v_d;$$

Where h_p is the hydraulic permeability and v_d the dynamic viscosity.

Therefore, from now on I will refer to permeability as hydraulic conductivity.

5.1.2 Methods

The 2D version of the hinge model presented in Section 4.3.1, with same boundary and loading conditions (Figure 5-1) was used to study the differences between linear elastic and poroelastic material properties. The material properties used for both simulations are summarised in

Table 5-1. No motion was simulated. A total of 8 simulations were performed and the pore pressure was observed. Five of them were simulated with different holding loading time (1, 5, 10, 50 and 100 seconds) and constant hydraulic conductivity value ($6.573*10^{-8}\frac{m}{s}$) in order to confirm that for short time period the water does not have sufficient time to flow out of the cartilage. The remaining three simulations were performed with one second holding loading time but different hydraulic conductivity values ($6.573*10^{-7}\frac{m}{s}$, $6.573*10^{-8}\frac{m}{s}$, $6.573*10^{-9}\frac{m}{s}$), to understand cartilage behaviours when this value changes. Pore pressure and the von Mises stresses were then compared.

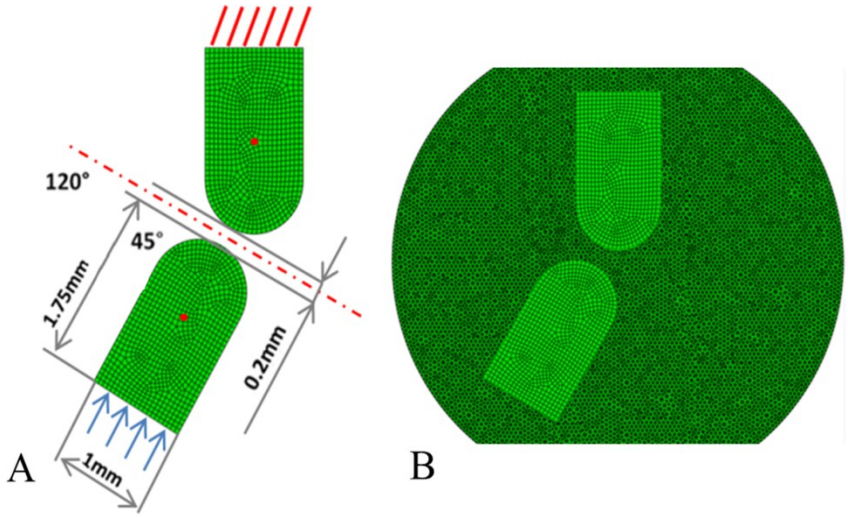

Figure 5-1 A) 2D model consisted of two opposing cartilage rudiment of the same dimension; the distal rudiment is at an initial angle of 45° to the vertical proximal rudiment; B) joint within the inter-rudiment space.

Table 5-1 Material properties for cartilage and inter-rudiment space from [1](Tanck et al., 2004), [2](Shefelbine and Carter, 2004), [3](Roddy et al., 2011a), [4](Tanck et al., 2000), [5](McCarty et al., 2011)

Linear elastic				**Poro-elastic**					
Rudiments		*Synovial*		*Rudiments*			*Synovial*		
E(Mpa)	υ	E(Mpa)	υ	E(Mpa)	υ	H_C[m/s]	E(Mpa)	υ	H_C[m/s]
1.1[1]	0.49[2]	0.287[3]	0.4[4]	1.1[1]	0.49[2]	6.573e-8[4]	0.287[3]	0.4[5]	6.573e-8[4]

5.1.3 Results

Two nodes, approximately at the center of each rudiment (Figure 5-1, A – red dots) were picked and used to compare the pore pressure and the von Mises stresses trends. When the holding loading time was varied up to 5 seconds with a value of hydraulic conductivity kept constant and equal to $6.573*10^{-8}\ \frac{m}{s}$ the results showed that the fluid did not have enough time to flow out of the cartilage. In both rudiments the pore pressure (blue line) and the von Mises stresses (red line) follow the same trend showing that the model with poroelastic material properties is behaving to all effects as a single phase model (Figure 5-2, Figure 5-3). However, different behaviours were seen when the model was loaded for 10 or more seconds (Figure 5-4, Figure 5-5, Figure 5-6). The fluid started to flow out significantly from the cartilage (blue line). 100 seconds were needed to reach equilibrium in the cartilaginous rudiments with no more fluid flow (Figure 5-6). When the value of cartilage's hydraulic conductivity was changed and the holding loading time was

kept constant (equal to 1 second), I observed that the lower the value of hydraulic conductivity, the higher the pore pressure in the cartilagineous rudiments (Figure 5-7). The pore pressure decreased with higher values of hydraulic conductivity (Figure 5-7, C - blue line) stopping the poroelastic model to behave as a single phase model.

Moreover, by comparing the hydrostatic stress distribution, I noticed a difference in stress magnitude between the poroelastic and the linear elastic model as shown in Figure 5-8, A, B. This difference in magnitude, as shown in Figure 5-8 C, was due to the fluid flowing from the inter-rudiment space to the rudiment, factor which is not present during the linear elastic simulations.

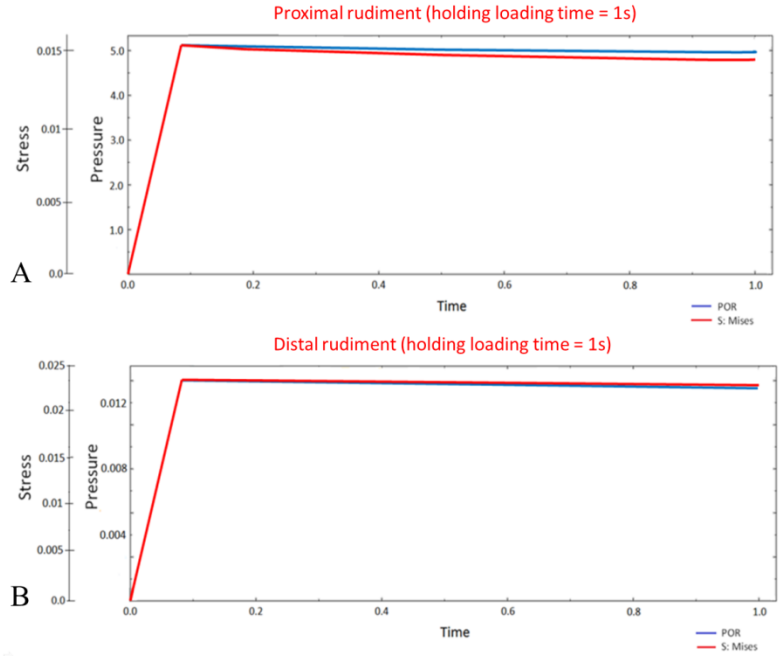

Figure 5-2 Pore pressure and Von Mises stresses on a node for the A) proximal and B) distal rudiment. The holding loading time is 1s and the hydraulic conductivity is equal to $6.573*10^{-8}\ \frac{\boldsymbol{m}}{\boldsymbol{s}}$.

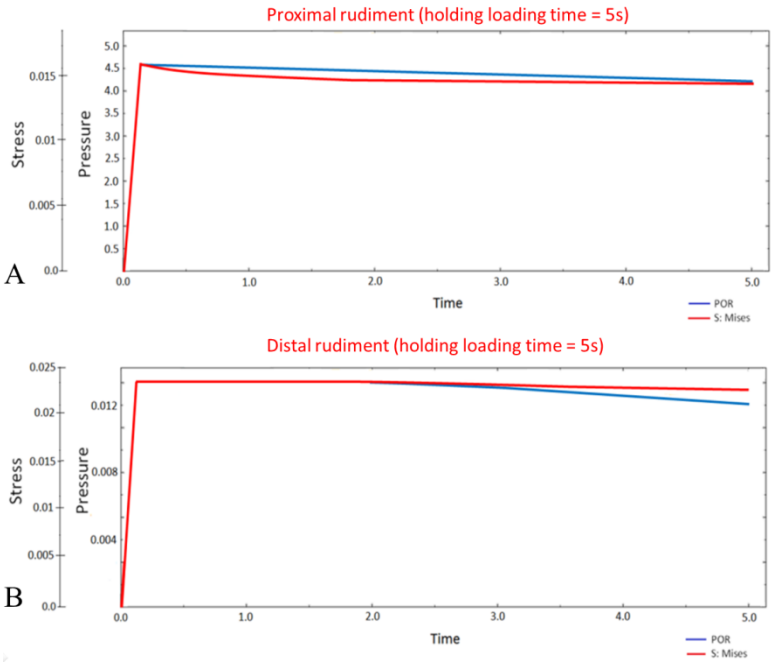

Figure 5-3 Pore pressure and Von Mises stresses on a node for the A) proximal and B) distal rudiment. The holding loading time is 5s and the hydraulic conductivity is equal to $6.573*10^{-8}\ \frac{m}{s}$.

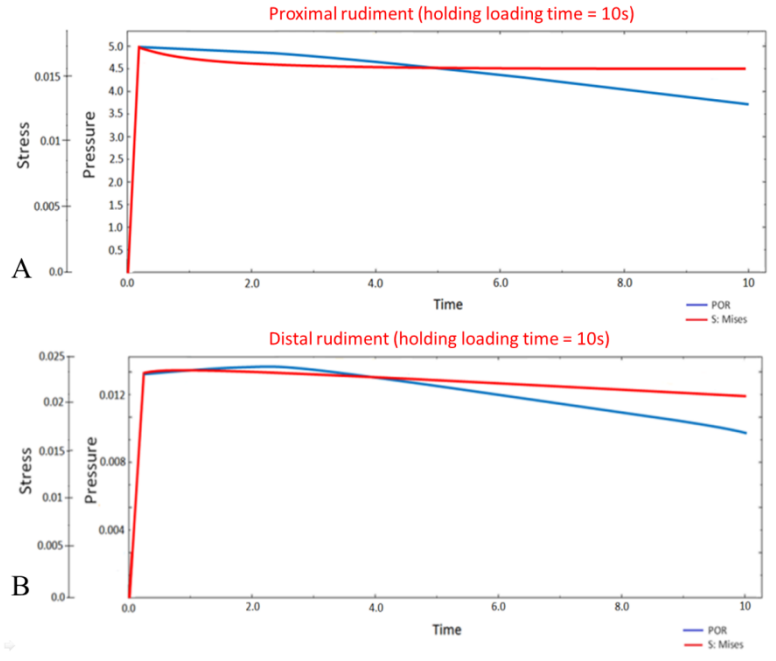

Figure 5-4 Pore pressure and Von Mises stresses on a node for the A) proximal and B) distal rudiment. The holding loading time is 10s and the hydraulic conductivity is equal to $6.573*10^{-8}\ \frac{m}{s}$.

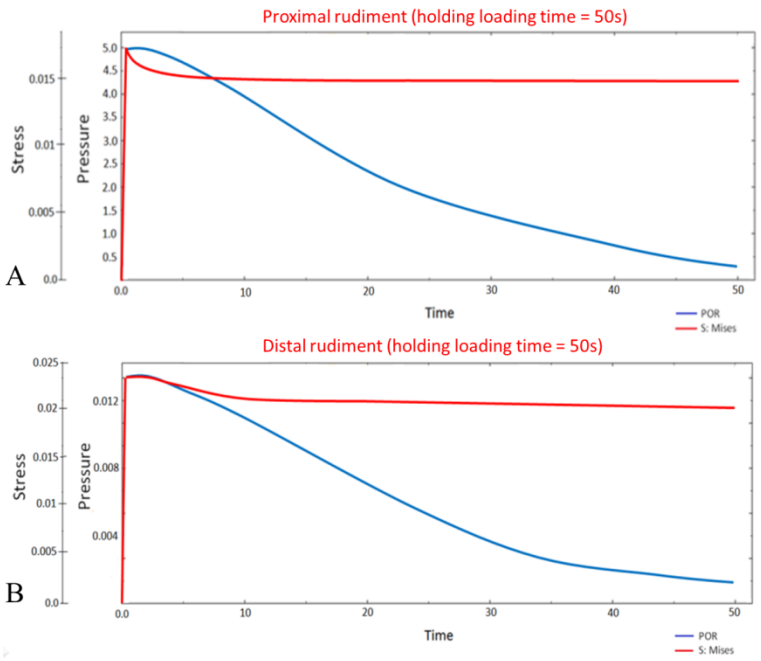

Figure 5-5 Pore pressure and Von Mises stresses on a node for the A) proximal and B) distal rudiment. The holding loading time is 50s and the hydraulic conductivity is equal to $6.573*10^{-8}\frac{m}{s}$.

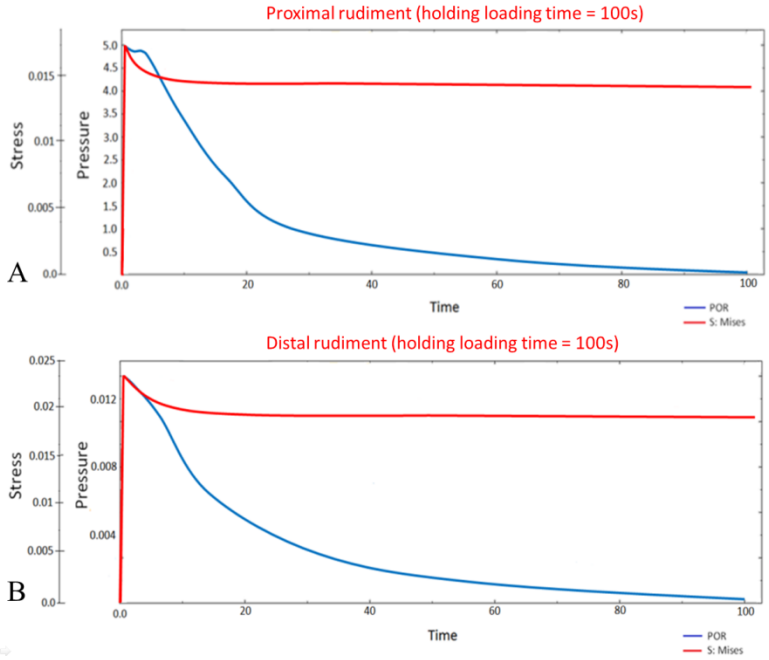

Figure 5-6 Pore pressure and Von Mises stresses on a node for the A) proximal and B) distal rudiment. The holding loading time is 100s and the hydraulic conductivity is equal to $6.573*10^{-8}\frac{m}{s}$.

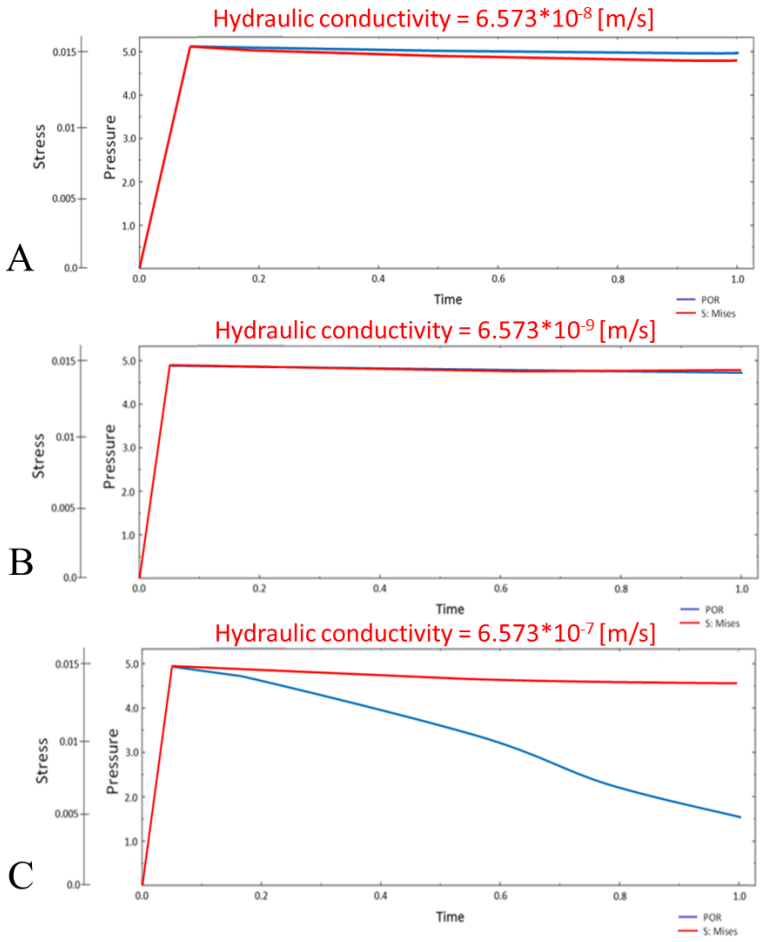

Figure 5-7 Pore pressure and Von Mises stresses on a node for the proximal rudiment. The holding loading time is kept constant and equal to 1s while the hydraulic conductivity varies. A) Hydraulic conductivity equal to $6.573*10^{-8}$ $\frac{m}{s}$; B) hydraulic conductivity equal to $6.573*10^{-9}$ $\frac{m}{s}$; C) hydraulic conductivity equal to $6.573*10^{-7}$ $\frac{m}{s}$.

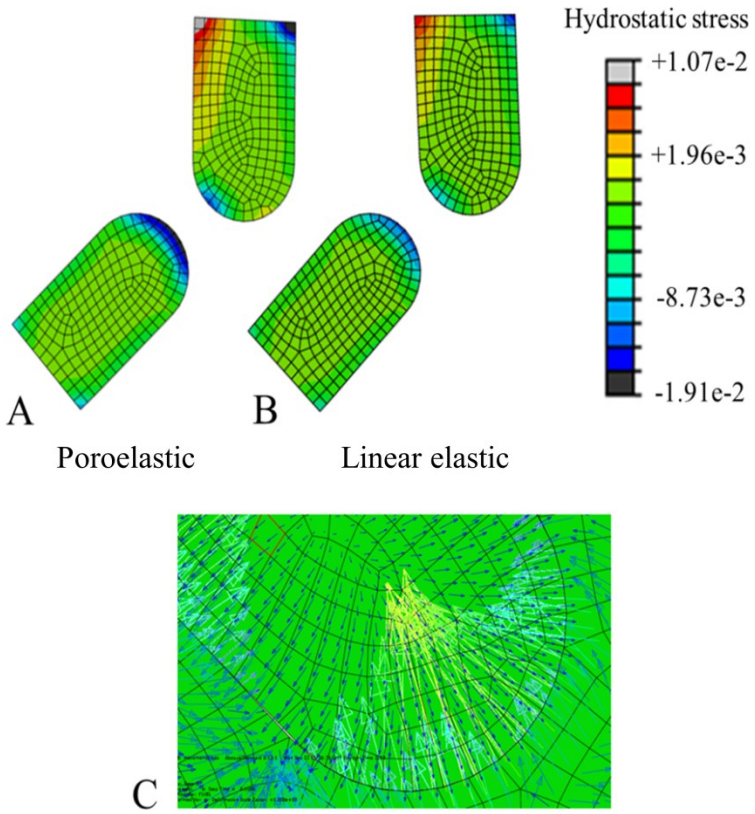

Figure 5-8 Hydrostatic stress distribution on the A) poroelastic and B) linear elastic model respectively; C) fluid direction, we assumed that the higher values of hydrostatic stresses for the poroelastic model are a consequence of the fluid flowing into the rudiment from the inter-rudiment space (long yellow arrows).

5.1.4 Conclusions

The results showed that, with a hydraulic conductivity of 6.573e-$^{8}\frac{m}{s}$, more than 5 seconds were needed for the fluid to start flowing out significantly from the cartilaginous rudiments. To see different behaviours between the two models, I had to increase the holding loading time to more than 5 seconds, or increase the hydraulic conductivity value. To conclude, these simulations confirmed that around frequencies of 1Hz, which is close to the frequency of muscle contraction (Vaal et al., 2000) in infants, the water does not have sufficient time to flow out of the cartilage making the fluid pressure and matrix shear stress being equivalent to the hydrostatic stress and octahedral shear stress of the single phase model. Because of the results achieved with this simulation, I was more confident about the use of linear elastic material properties to model cartilage morphogenesis.

5.2 Static and dynamic loadings

5.2.1 Introduction

During early prenatal development, the process of cavitation just started and not all joints are already fully cavitated (Scheuer and Black, 2004). Recent work has shown that the process of joint morphogenesis initiates prior to cavitation and continues after it (Nowlan and Sharpe, 2014). Since joints start to acquire their reciprocal shapes before cavitation, my model includes both a static phase (pre-cavitation), in which the joint morphogenesis initiates, and a dynamic phase of loading after cavitation has occurred. In this section, the importance of having both static and dynamic loading conditions will be explored.

5.2.2 Methods

The 2D version of the ball & socket and hinge models presented in Section 4.3.1, with same boundary conditions, loading conditions and material properties, were used to study the importance of having both static (pre-cavitation) and dynamic (post-cavitation) loading conditions. A total of four simulations were run to compare the final ball & socket and hinge joint shape with and in absence of the static loading.

5.2.3 Results

When morphogenesis of the ball and socket joint was simulated without the inclusion of the static load, and therefore assuming the joint was already cavitated, it developed a convex profile in the mid-line section of the acetabulum as shown in Figure 5-9, A. The typical ball & socket shape was missing and a non-interlocking profile can be seen (Figure 5-9, A). The inclusion of the static phase led to the acquisition of the physiological concave/convex profile before cavitation occurred (Figure 5-9, B). This shape was then maintained and emphasised during the dynamic loading phase (Figure 5-9, B). When the hinge joint was considered, during early development, to be already cavitated, and therefore without the inclusion of the static load, the joint morphogenesis was less affected as shown in Figure 5-10, A, B. However, the proximal rudiment showed a less rounded convex profile in both regions, posterior and anterior with a less pronounced growth posteriorly (Figure 5-10, A). The distal rudiment showed similar features with a less pronounced

rounded convex profile in its posterior region and the onset of a slight concave profile in the mid-line section was disappeared (Figure 5-10, A).

5.2.4 Conclusions

Separating the effects of static and dynamic loading conditions during prenatal joint morphogenesis showed that the pre-cavitational static loading phase was essential to some aspects of joint shape, such as for the acquisition of the convex/concave profile in a ball & socket joint. Therefore its inclusion was fundamental to achieve the results presented in Chapter 4.

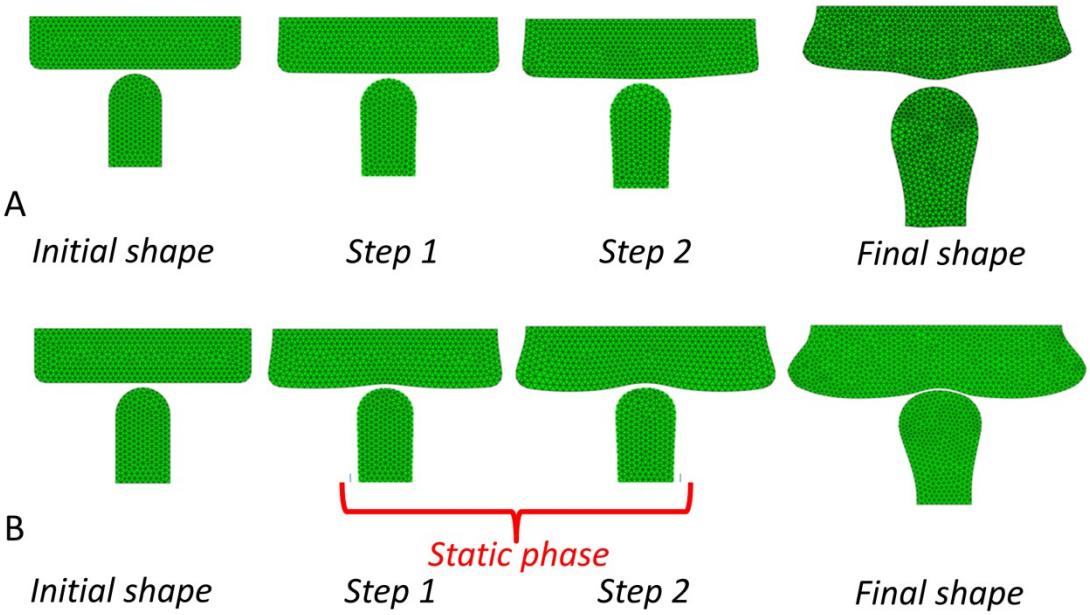

Figure 5-9 A) When only the dynamic phase was included in the simulation, a non-interlocking shape can be seen. B) When both static and dynamic phases were included in the simulation a convex/concave profile, typical of a ball & socket joint, can be seen.

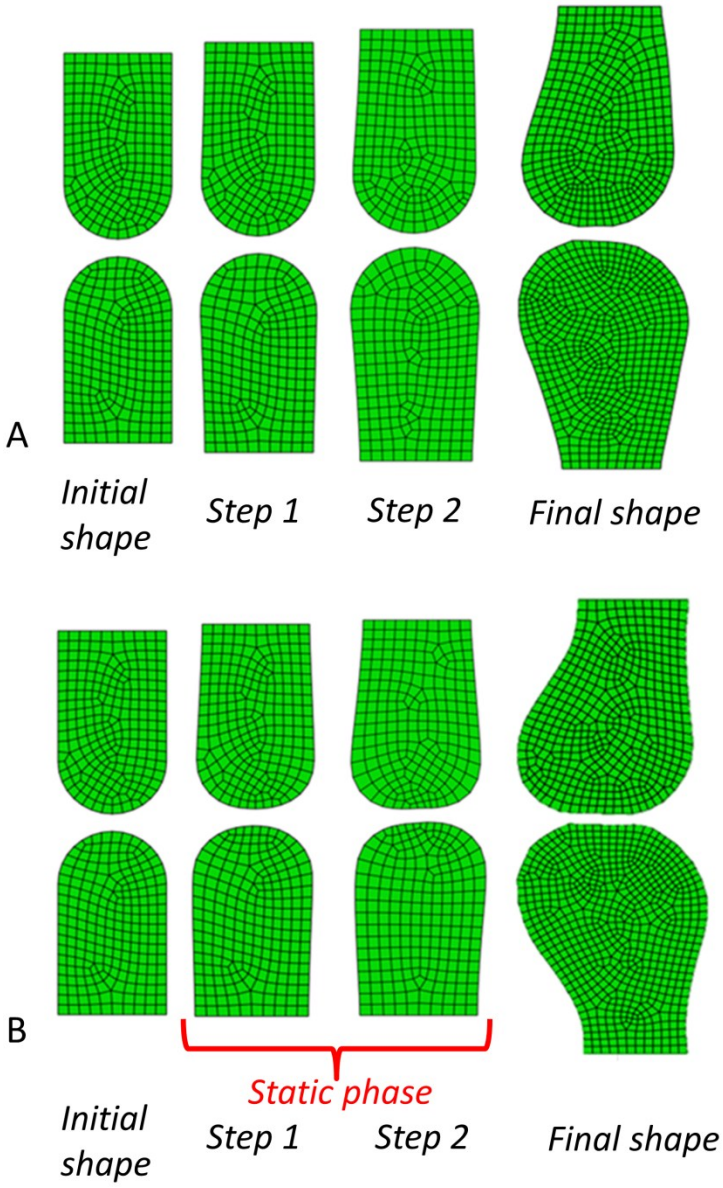

Figure 5-10 A) When only the dynamic phase was included in the simulation, both rudiments showed less rounded convex profiles. B) When both static and dynamic phases were included in the simulation, a hinge joint shape can be seen.

5.3 Effect of inter-rudiment space

5.3.1 Introduction

The inter-rudiment space was included in the simulations to avoid direct contact between the two rudiments, a function which is performed biologically by the interzone during early joint development and by the synovial fluid during later development. As already said (Section 3.2.9.1), mathematically it acts as a smoothing function to spread the loads. The goal of this section is to compare the effects on the final joint shape due to the inclusion or not of the inter-rudiment space.

5.3.2 Methods

Two models were used, one was the 2D version of the hinge model presented in Section 4.3.1, with same loading, boundary conditions and material properties. The second was a similar model where the inter-rudiment space was removed from the simulation and the two rudiments placed in contact. For both models the effects on stresses distribution and the predicted joint morphology after 2 static + 8 dynamic steps of growth were compared.

5.3.3 Results

When the simulation was run with the inter-rudiment space the stresses were evenly distributed across the joint and no areas of high stresses were present within the joint region (Figure 5-11, A). When the inter-rudiment space was removed, the direct contact between the two rudiments led to the generation of high stresses in small regions as shown in Figure 5-11, B. When morphogenesis after 10 steps of growth was simulated with the inter-rudiment space, the proximal rudiment showed more pronounced growth posteriorly (Figure 5-12, A). The distal rudiment showed similar features with a less pronounced rounded convex profile in its posterior region (Figure 5-12, A). When morphogenesis was predicted without the inter-rudiment space, the proximal rudiment showed similar trend with a more pronounced growth posteriorly (Figure 5-12, B). However, the distal rudiment showed a more pronounced growth anteriorly (Figure 5-12, B).

5.3.4 Conclusions

Even if the inclusion, or not of the inter-rudiment space led to slightly different features on the final joint shape, in both cases the final joint showed the generation of an interlocking shape. However, the tendency of the distal rudiment to grow more on its anterior side when the inter-rudiment space was removed, suggested that the inclusion of the inter-rudiment space could lead to more accurate results.

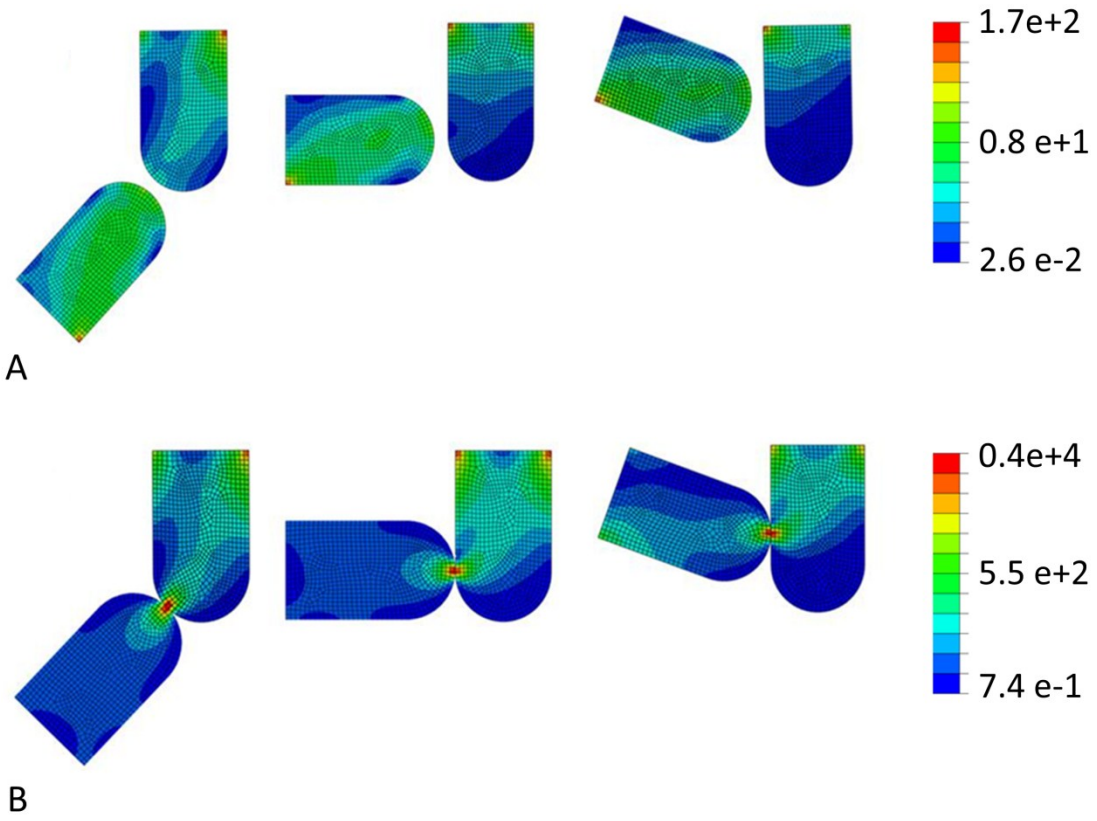

Figure 5-11 A) von Mises stress distribution when the inter-rudiment space was included in the model. B) von Mises stress distribution when the inter-rudiment space was removed from the simulation.

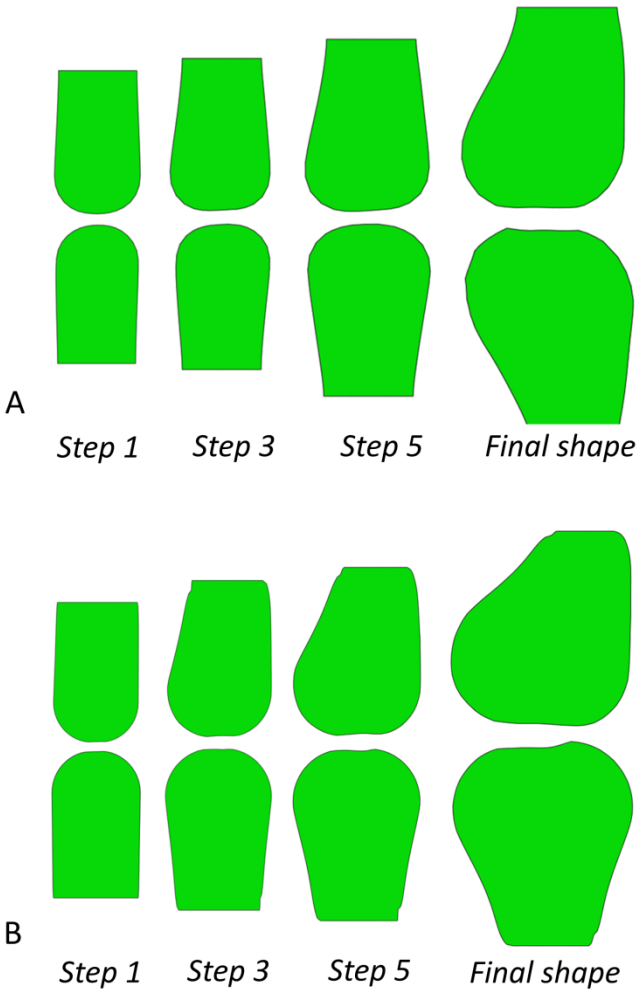

Figure 5-12 A) Predicted joint morphology over time when the inter-rudiment space was included in the simulation; B) predicted joint morphology over time when the inter-rudiment space was removed from the simulation.

5.4 Chondrocyte density curves

5.4.1 Introduction

As described in Section 3.2.6 the biological contribution to growth (i.e. the intrinsic growth due to hormones, genes and nutrients), was assumed to be proportional to the chondrocyte density (C_d). C_d was estimated by Heegaard study (1999) by measuring the grey level distribution of cell density on a sagittal section micrograph of a prenatal joint and the numerical coefficients were taken directly from their study (Chapter 3, Section 3.2.6):

$$C_d = k * (0.14 - 0.87\xi + 4.40\xi^2 - 2.66\xi^3)$$

In this section the consequences of using different chondrocyte density curves were explored in order to understand their effect on the final joint shape.

5.4.2 Methods

The 2D version of the hinge model presented in Chapter 4, was used to perform a sensitivity analysis with alternative linear curves for the chondrocyte density (namely a linear estimation of the polynomial curve, a line with a higher slope, and a line with a lower slope) as shown in Figure 5-13. The joint shapes obtained for each curve, after 2 static + 8 dynamic steps of growth, were then compared with the result obtained with the curve proposed by Heegaard et al. (1999).

5.4.3 Results

When a linear approximation of the polynomial curve was used, the shapes were almost identical (Figure 5-14). The proximal rudiment showed a rounded convex profile in both posterior and anterior regions, with more pronounced growth posteriorly, and the distal rudiment showed a less pronounced rounded convex profile posteriorly and the acquisition of a slight concave profile in the mid-line section. When the "higher slope" curve for the chondrocyte density was used, there was more pronounced growth at the epiphysis, while the opposite was true of the "lower slope" curve (Figure 5-14).

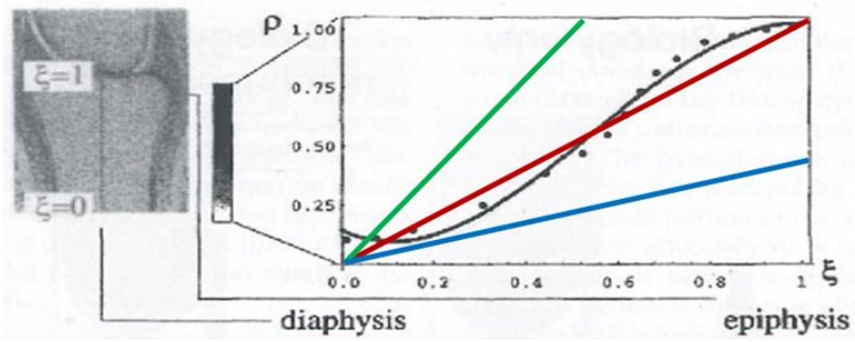

Figure 5-13 The chondrocyte density curves used during the simulations: original cubic curve (black), the best fitted linear curve (red), the linear curve with higher degree of slope (green) and the linear curve with lower degree of slope (blue).

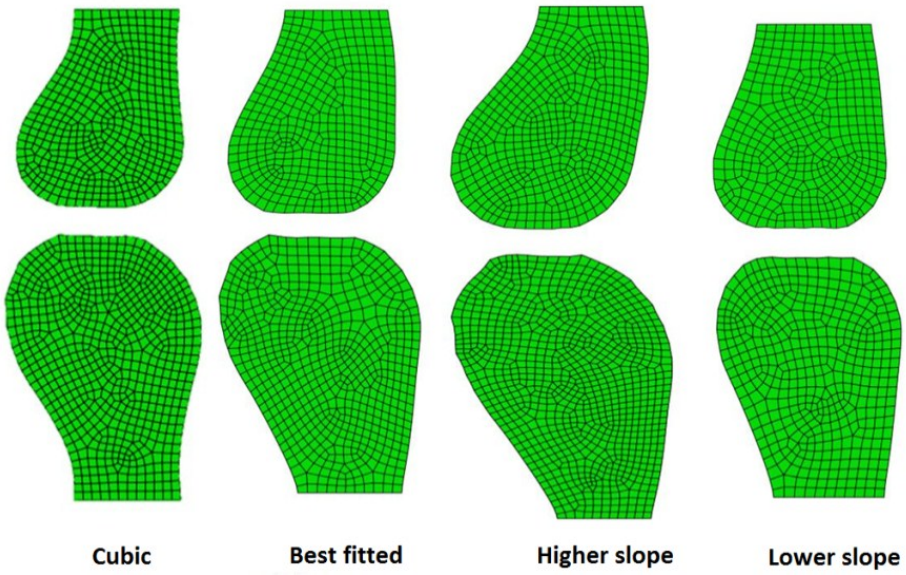

Figure 5-14 Joint morphogenesis obtained after 10 steps of growth using a different chondrocyte density curve

5.4.4 Conclusions

The use of different chondrocyte density curves to simulate the biological contribution to growth did not particularly affected the final joint shape which always showed the same primary shape features, with the proximal rudiment showing a rounded convex profile in its posterior, and the distal rudiment showing a less pronounced rounded convex profile posteriorly with the acquisition of a slight concave profile in the mid-line section, as shown in Figure 5-14. Therefore, the polynomial curve used to simulate the biological contribution was a reasonable choice.

5.5 The constant k

5.5.1 Introduction

The constant k determines the amount of biological growth (Chapter 3, Section 3.2.5). A value of $11*10^3$ was chosen in order to maintain the biological growth in the range of 75-85% of the total growth as explained in section 3.2.6. The mechanics modulate growth at the local level. In this section we explore the effects of applying a higher or lower biological contribution by varying the values of the constant k.

5.5.2 Methods

The 2D version of the hinge model presented in Chapter 4, with same boundary conditions, loading conditions and material properties, was used. Two different values of *k* were used for the sensitivity analysis and joint morphology was predicted with a higher (85-95% of the total growth) or a lower influence (55-65% of the total growth) due to the biological contribution. The final joint shapes were then compared with the original simulation (75-85% of the total growth).

5.5.3 Results

When the contribution of the biological growth range was increased, the mechanobiological contribution was too low to have an influence on the total growth and joint morphology, as shown for the simplified shape in Figure 5-15. When instead the *k* value was decreased (55-65% of the total growth), the effects of the mechanobiological stimulus were more evident, with more extreme changes at the epiphyses and decreased growth overall, as shown in Figure 5-15.

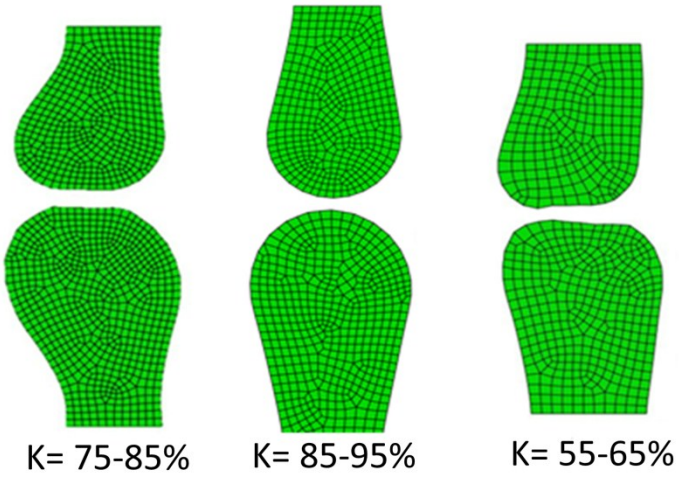

Figure 5-15 Joint morphogenesis with different biological contribution. From left to right: 1) shape obtained with the original amount of biological contribution. 2) shape obtained with a higher biological contribution; 3) shape obtained with a lower biological contribution.

5.5.4 Conclusions

The use of different amount of biological contribution to growth showed the importance of having a well-balanced simulation in terms of its biological and mechanobiological contributions. A biological contribution between 75-85% of the total growth allowed the appreciation of the changes in shape due to the mechanobiological contribution maintaining at the same time a nicely smoothed joint profile.

5.6 Different alignment during immobilisation

5.6.1 Introduction

This section presents how morphogenesis is influenced with an alternative initial alignment during immobilisation. When immobilisation was initially simulated (Chapter 4, Section 4.3.1) the two rudiments were assumed to be aligned along their vertical axis. Therefore, the effect of having the distal rudiment at a different angle, condition that can happen with contractures that accompany immobilisation, was explored.

5.6.2 Methods

A modified 2D version of the immobilised model presented in Chapter 4, with the distal rudiment positioned at an angle of -60° respect to the vertical proximal rudiment was developed (Figure 5-16, A). Boundary conditions, loading conditions and material properties remained unchanged (Section 4.3.1).

5.6.3 Results

When morphogenesis was simulated, the proximal rudiment slightly bended on the direction of the applied load and its anterior region acquired a flat shape (Figure 5-16, B). The distal rudiment showed the onset of a flat shape on its top region (Figure 5-16, B). The overall shape showed the loss of an interlocking joint.

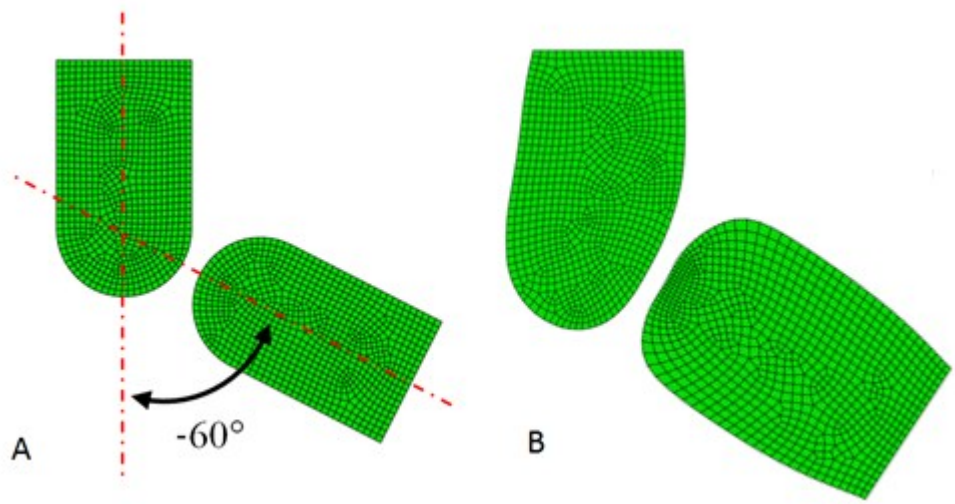

Figure 5-16 A) Initial alignment of the joint during immobilisation growth simulation with the distal rudiment positioned at an angle of -60° respect to the vertical proximal rudiment, and B) resulting predicted morphogenesis.

5.6.4 Conclusions

Exploring the effect of an alternative initial alignment during immobilisation showed consistency of the developed algorithm by predicting a non-interlocking shape no matter the joint's angle.

5.7 Summary

In this chapter I presented the sensitivity analyses performed on the model presented in Chapter 4. There are many parameters in the developed model that could have played an important role in the resultant shape. As the models used in this section were the same as that used in Chapter 4, all the limitations listed in Section 4.3.3 can also be applied with these simulations. An additional limitation relates to Section 5.1 where the linear elastic and poroelastic model versions were compared. The von Mises stresses were analysed and compared with the pore pressure. We are aware that the hydrostatic pressure would have been a better stimulus for this comparison; however this section was replicating already existing studies which showed that single and bi-phasic models are comparable when loaded at low frequencies (Carter and Wong, 2003; Shefelbine and Carter, 2004). Therefore, the aim of this section was solely focused on corroborating these studies as efficiently as possible.

However, the goal of this section was to provide further details for the assumptions made on our model and in the same time clarify any possible doubts on the choices made.

6 Effect of Normal and Abnormal Loading on Morphogenesis of the Prenatal Hip Joint: Application to Hip Dysplasia

Following the previous model (Chapter 4), where predictions of a range of anatomically recognisable joint shapes was achieved, in this chapter a dynamic mechanobiological simulation of the prenatal hip joint is use to explore the effects of normal, reduced and asymmetric fetal movements on hip joint growth and morphogenesis. Despite the clinical importance of the process of morphogenesis for postnatal skeletal malformations such DDH, there has been little research on how the hip joint shape forms in the developing embryo. With the developed simulations, for the first time, a successful prediction of the physiological trends of decreasing sphericity and acetabular coverage of the femoral head during fetal development was achieved. This study demonstrates how a full range of symmetric movements helps to maintain some of the acetabular depth and femoral head sphericity, while reduced or absent movements can lead to decreased sphericity and acetabular coverage of the femoral head. Moreover, when an abnormal movement pattern is applied, a deformed joint shape was predicted, with an opened asymmetric acetabulum and the onset of a malformed femoral head. This research provides evidence for the importance of fetal movements in promoting normal hip joint morphogenesis, particularly joint coverage, and an explanation of how abnormal movements may lead to joint instability and DDH in the infantile hip. This chapter presents an adapted version of the work submitted at the Journal of Biomechanics (Giorgi et al., 2015a; Giorgi et al., 2015b) (see Appendix 10).

6.1 Introduction

As described in section 2.4, at around gestational week 11 a globular femoral head is almost completely enclosed by a deep-set acetabulum (Figure 2-7, Chapter 2.4). From that time until birth, the acetabulum becomes shallower and the femoral head loses substantial sphericity, becoming more hemi-spherical (Ráliš and McKibbin, 1973). The coverage of the femoral head is never as low as it is around the time of

birth (Ráliš and McKibbin, 1973) (Figure 2-8, Chapter 2.4), which most likely means that the hip joint is at its most unstable shape at this time. DDH occurs when the hip joint is malformed, unstable or dislocated, and occurs in 1.3 per 1000 births (Leck, 2000). As already said (Section 1.1), two types of dislocation have been defined (American Academy of Pediatrics, 2000): 1) teratologic dislocations and 2) typical dislocations. In the most severe cases of DDH, the femoral head is completely dislocated from the acetabulum, while in less severe manifestations, the femoral head is partially dislocated or easily dislocatable from the acetabulum (Ponseti, 1978). DDH is the most common congenital abnormality of the hip joint which is thought to be strongly linked to abnormal fetal movement (Section 2.4.2). Despite the acknowledged influence of fetal movements on hip joint formation, the mechanism by which these movements affect joint morphogenesis is still unknown. In this study, I develop a mechanobiological simulation of prenatal hip joint morphogenesis, in order to propose and test hypotheses on how fetal movements and position could impact upon the shape of the developing hip joint. The research builds upon the previously developed model (Chapter 4). In the current study, growth and shape change of an idealised hip joint were predicted by applying dynamic joint movements to the centre of the femoral head. The predictions of growth were then correlated with published human hip joint shape data. I also investigate the effects of reduced, or asymmetric, movement at various stages of fetal development. I hypothesise that reduced movements due to sub-optimal intra-uterine conditions, or asymmetric loading on the acetabulum due to fetal breech position or increased joint laxity, may negatively influence hip joint shape at birth. Moreover, we explore the influences of growth related stresses and strain to hip joint morphogenesis. Through use of a dynamic mechanobiological simulation of a simplified hip joint, we aim to provide new insights into the normal physiology of joint morphogenesis and into the etiology of DDH.

6.2 Material and Methods

6.2.1 Model geometry and material properties

An idealised 2D geometry of a simplified hip joint was created in Abaqus. Due to the lack of access to fetal realistic hip joint shapes, minimal additional insights on the effects of joint motion on shape would be gained by using 3D simulations. The joint

consisted of two opposing cartilage rudiments: the proximal femur and the pelvis, which included a concave acetabular region (Figure 6-1, A). The interlocking shape was generated with the same proportions of a human hip joint at gestational week (GW) 11 of development (Ráliš and McKibbin, 1973), while the initial dimensions were arbitrary (Figure 6-1, A). The initial depth-to-diameter ratio of the acetabulum was approximately 75%, and the femoral head perfectly matched the acetabular shape with a height-to-diameter ratio of approximately 85%. A similar model which included the inter-rudiment space (Figure 6-1, B) was also used to study its effectiveness with the current simulation. Therefore, models with and without a capsule were run to test if a congruent shape (Figure 6-1, A) was enough to evenly spread the loads within the joint region. The secondary ossification centre of the proximal femur does not normally form until after birth (Scheuer and Black, 2004) and the acetabulum is still cartilaginous (Portinaro et al., 1994; Scheuer and Black, 2004). Therefore, the models were entirely cartilaginous for the duration of the simulations. The material properties used are the same used for the previously described models (Chapter 4, Section 4.3.1) and the meshes were generated by using linear plane stress triangle elements (CPS3). The stresses were calculated at the integration points.

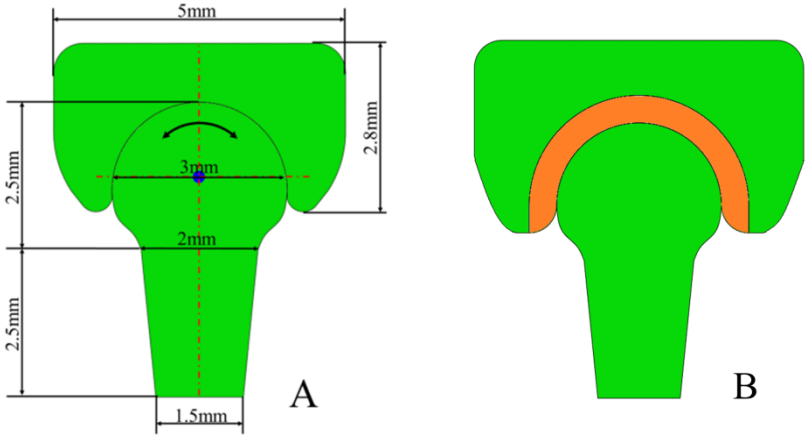

Figure 6-1 A) Initial model of the concave pelvis and spherical femoral head. B) Same model with inclusion of the inter-rudiment space.

6.2.2 Movements and boundary conditions

The pelvis was fixed for all translations and rotations at its proximal end and at its sides. In the case of normal (symmetric) movement, the shaft of the femur was initially aligned with the vertical axis of the pelvis in order to obtain a perfect match between the femoral head and the acetabulum (Figure 6-1, A). The explicit module

of Abaqus was used to simulate dynamic joint movements by applying a rotation to the centre of the femoral head. A complete cycle of motion included four different phases, a pre-load phase followed by three rotations of the femoral head around its centre. During the pre-load phase, an axial displacement of 1μm was applied on the distal rudiment towards the proximal rudiment, and this displacement was maintained through the entire motion to generate contact between the two rudiments. The three rotations were as follows: 1) anticlockwise rotation of the femoral head, from the midline position to the extreme left position; 2) clockwise rotation, from the extreme left to the extreme right; 3) anticlockwise rotation of the femoral head to the initial midline position. Compared with the previous model (Chapter 4), where joint loads were represented by a number of discrete steps, with these dynamic movements, stresses can be observed during the entire joint motion, allowing a more accurate picture of their patterns. Frictionless, impenetrable contact was modelled between the two components of the model.

Growth and morphogenesis of the hip joint from GW 11 to birth were modelled, with 28 cycles used, where one cycle was equivalent to approximately one week. Two variables were identified as decreasing over the course of development, namely the rate of fetal growth (and therefore the rate of *rudiment expansion*) and the *range of hip motion*. By plotting the fetal weight change (Doubilet et al., 1997) on a logarithmic scale, we identified three stages during which the fetus grows at different rates (Figure 6-2): 1) early stage, from GW 11 to 18; 2) middle stage, from GW 19 to 34; 3) late stage, from GW 35 to birth. The rate of *rudiment expansion* in the model was adapted according to the rate of fetal growth (Figure 6-2) and was implemented by varying the orthonormal thermal expansion capabilities of the finite element solver. A value equal to 1 was chosen to simulate the maximum expansion within a constrained volume during the early stage of development and then reduced according with the relative decrease in the slope of the middle and late stage of development.

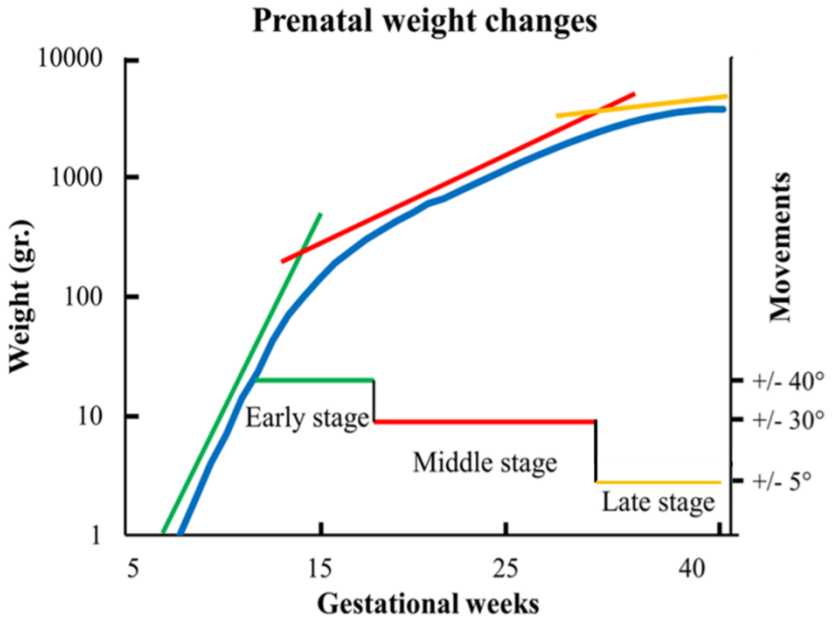

Figure 6-2 Changes in fetal weight on a logarithmic scale (extracted from data from (Doubilet et al., 1997) taken as a measure of the rate of fetal growth. Three stages of fetal growth were identified; the movements applied for each stage are superimposed.

6.2.3 Fetal Movements

There is very little information on the range of motion of the prenatal hip joint. However, fetal cine-MRI can now be used for viewing and assessing fetal movements (Hayat et al., 2011). Using fetal cine-MRI data obtained from our collaborators (Profs Hajnal and Rutherford, King's College London, UK), I was able to make a realistic estimate of the range of motion at the hip over gestation. Five MR image sequences were analysed and the maximum range of hip motion over the 1.5 minute average time frame of the scan was calculated. The angle generated by the intersection of the spine line and the longitudinal axis of the femur was used to quantify the hip motion as shown in Figure 6-3, A, B. All the image sequences belonged to the middle stage of development: three in the early-middle (GW: 21- 22) and two in the late-middle (GW: 29, 34) stages. The first set showed a maximum range of motion of 90° with an average value over the three sequences of 52°. The second set showed a maximum range of motion of 15° with an average value of 12.5°. Because all the scans belonged to the middle stage, I assumed higher and lower range of motion for the early and late stages, with an intermediate value for the middle stage. Therefore, symmetrical movements from +/- 40° in the early stage, +/- 30° in the middle stage, and +/- 5° in the late stage were used to simulate physiological prenatal hip motion over the course of development.

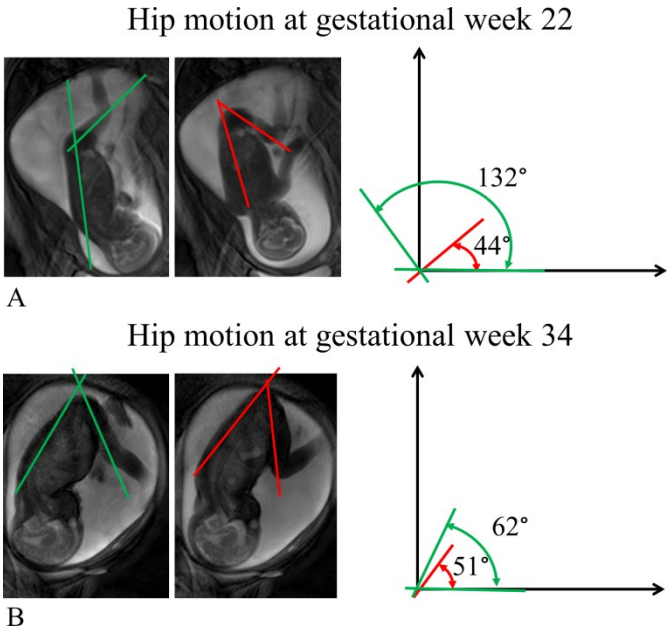

Figure 6-3 A) Two timeframes from a fetal cine-MRI at 22 gestational weeks showing a hip flexion-extension range of 88°. B) Timeframes from a fetal cine-MRI at 34 gestational weeks showing a hip flexion-extension of 11°. Fetal cine-MR images courtesy of Professors Hajnal and Rutherford, Kings College London, UK.

6.2.4 Growth-generated biophysical stimuli

During early embryonic morphogenesis, developing cells receive extrinsic signal that lead to particular changes in cell behaviour, such as differentiation, migration or proliferation. In addition, morphogenesis is regulated by inductive signals transmitted within cells through direct contact, diffusible molecules, and gap junction (Henderson and Carter, 2002) (Chapter 2, Section 2.5.3). During development, different tissues form and begin to grow at different rates and growth-generated strain and pressures are used to refer to the local deformation and corresponding forces generated by this differential growth. It has been proposed that the acetabulum is moulded by the femoral head (Ponseti, 1978) and therefore, the use of congruent shapes (Figure 6-1, A) may play a role during growth due to the direct interaction between the acetabular and femoral part. Therefore, in this section, the hypothesis that growth-generated strains and pressures may influence the process of morphogenesis by modulating growth rates was explored.

To test the effects of the growth-generated strains and pressures, simulations composed of six different steps where: 1) an explicit simulation of the joint motion

was run; 2) the resulting hydrostatic stresses of step one were used to calculate a value of growth for each node as described in section 3.2.5; 3) morphogenesis was simulated using the thermal expansion solver of Abaqus (Chapter 3.2.5); 4) the growth-generated hydrostatic pressures were used to calculate a new value of growth; 5) the growth values calculated at step 2 (contribution from stresses induced by movement) were then summed with the values calculated in step 5 (contribution from stresses induced by expansion and therefore, resulting by the interaction of the tissues) ; 6) a new step of morphogenesis was simulated by applying the new values of growth (contribution from stresses induced by movement + growth-generated stresses) to the initial joint shape (step 1). This entire process is graphically shown in Figure 6-4.

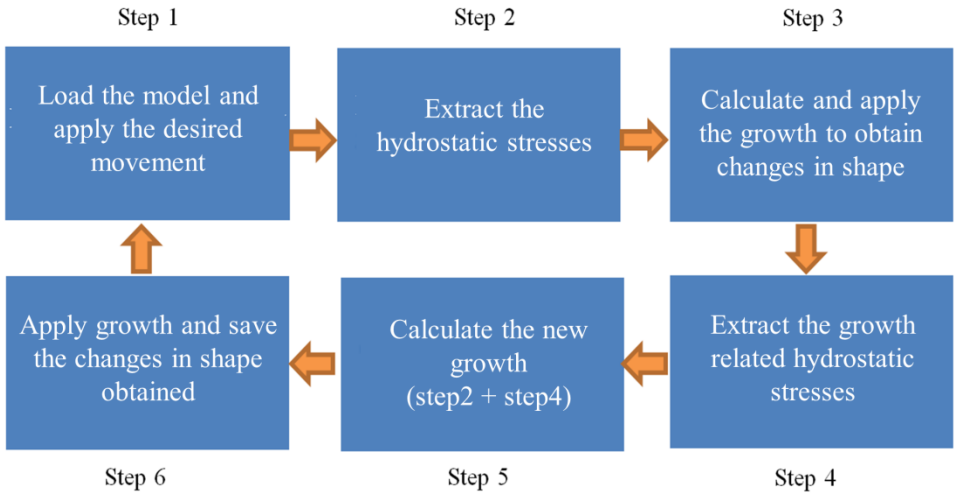

Figure 6-4 Diagram showing the steps involved to calculates the growth-generated strain and pressure and how to obtain changes in shape.

6.2.5 Altered movement patterns

As explained in section 2.4.2, the risk of DDH increases with abnormal movements or intrauterine conditions which reduce or restrict the movements *in utero*. Therefore, in addition to physiological loading conditions (symmetric movements), we explored the effects of altering movement patterns. Reduced movements were simulated by decreasing joint motion by approximately 80% at each of the three stages of development, as described in Table 6-1. Absent movements were simulated by retaining the femoral head in its initial position for the entire simulation without any rotation applied (but still maintaining the pre-load compression).The effects of

asymmetric movements were also simulated. Asymmetric movements differed from symmetric movements only for the initial configuration, where the longitudinal axis of the femoral head was rotated by 20° to the right of the vertical axis of the acetabulum (Figure 6-5). Rotations occurred about this new offset axis instead of the vertical axis. This new setup was also used to explore the effect of reduced asymmetric movements at each of the three stages of development as described in Table 6-1. Finally, simulations with a constant rate of rudiment expansion were run in order to separate out the influences of growth rate and range of movements on the resulting joint shape.

Table 6-1 Ranges of motion, in degrees, used to simulates physiological and reduced symmetric movements at each stage of development.

Type of movements	**Early 11^{th}-18^{th} Weeks**	**Middle 19^{th}-34^{th} Weeks**	**Late 35^{th}-birth**
Symmetric movements [°]			
Physiological	+/- 40	+/- 30	+/- 5
Early reduction	+/- 10	+/- 30	+/- 5
Middle reduction	+/- 40	+/- 8	+/- 5
Late reduction	+/- 40	+/- 30	+/- 1
No movements	0	0	0

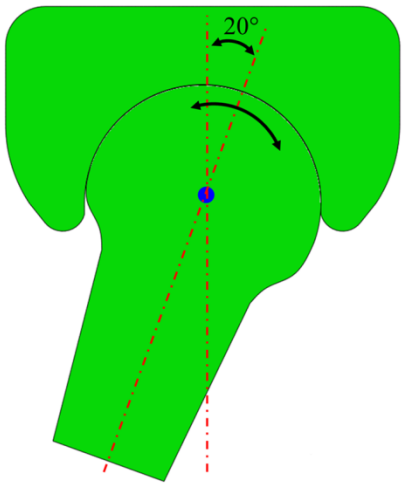

Figure 6-5 Initial configuration used for the abnormal (asymmetric) movement; the femoral head is rotated 20° to the right of the vertical axis of the acetabulum.

6.2.6 Growth & Morphogenesis

As described in Chapter 3, growth and morphogenesis of the rudiments were controlled by biological and mechanobiological growth rates. The biological contribution was considered to be proportional to the chondrocyte density (Heegaard et al., 1999). For the femoral head, the chondrocyte density was greatest at the proximal epiphysis of the rudiment (Heegaard et al., 1999), while for the pelvic rudiment, the chondrocyte density was greatest at the acetabulum, as shown in Figure 6-6, A. Radial growth of the immature acetabulum occurs mainly by expansion at the triradiate cartilage (Portinaro et al., 1994; Scheuer and Black, 2004), which is formed by the junction of the cartilaginous ends of the ilium, ischium and pubis (Portinaro et al., 1994). I am unaware of any study quantifying the rate of expansion at the triradiate cartilage. However, by comparing the rates of growth of the murine long bones (Hansson et al., 1972) and the pelvis (Harrison, 1958), I calculated that during very early postnatal development, the pelvis grows at a rate which is close to the half that of the femur in the mouse (Figure 6-6, B). Therefore, I implemented our model so that the maximum value for the biological contribution at the acetabulum was the half of the femur. For sensitivity analysis purposes some simulations were also run with the same biological growth between pelvis and femur. The results of these simulations will be discussed later in this chapter.

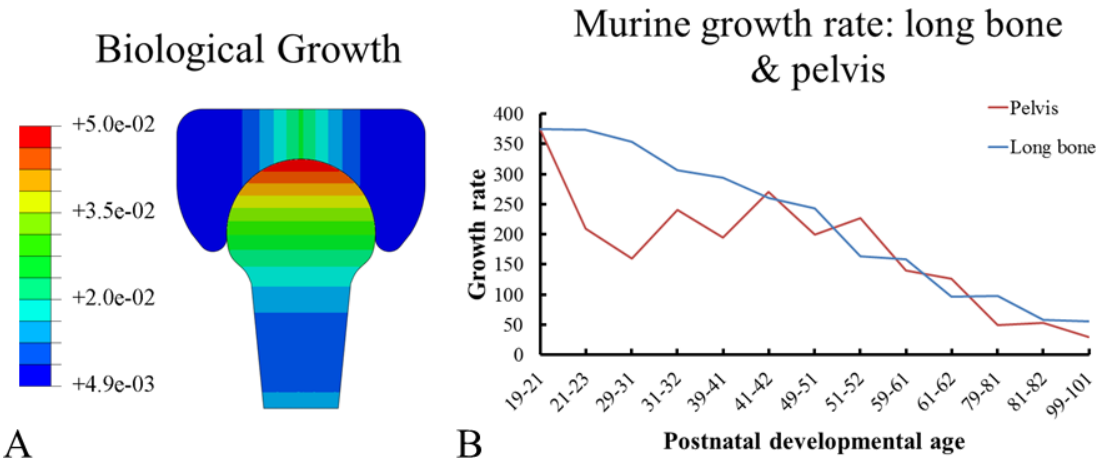

Figure 6-6 A) Biological growth distribution for long bone and pelvis; the colour plot shows that maximum value for the biological contribution at the acetabulum was the half of the femur. B) comparison of the rates of growth of the murine long bones and the pelvis; data were extracted from (Hansson et al., 1972; Harrison, 1958).

As already described in Section 4.2, the mechanobiological growth rate was proportional to the dynamic compressive hydrostatic stress generated by the movements. The overall mechanobiological contribution to growth was calculated at each node of the model as the average stresses throughout a full joint motion and was also weighted by the chondrocyte density, based on the assumption that the greater the number of cells, the greater the potential to respond to mechanical loading (by secreting matrix and proliferating). The total growth was the sum of the biological and mechanobiological contributions as shown by the equations below:

$$\frac{d\varepsilon}{dt} = \frac{d(\varepsilon_b)}{dt} + \frac{d(\varepsilon_m)}{dt}$$

where:

$$\frac{d(\varepsilon_b)}{dt} = \dot{\varepsilon}_b = C_d = (0.14 - 0.87\,\xi + 4.40\,\xi^2 - 2.66\,\xi^3)$$

$$\frac{d(\varepsilon_m)}{dt} = \dot{\varepsilon}_m = -C_d * \left(\frac{\sum_{i=1}^{N} \sigma_{hi}}{N} \right)$$

where $\dot{\varepsilon}_b$ and $\dot{\varepsilon}_m$ are the biological and mechanobiological contribution to growth respectively (Shefelbine and Carter, 2004), C_d the chondrocyte density, σ_h the compressive hydrostatic stress, and N the number of movements per step.

Morphological changes due to growth or adaptation were analysed relative to the initial shape of the joint. The changes in shape were assessed over time by looking at two parameters, the "acetabular ratio" and the "femoral head ratio". These parameters are derived from the measurements proposed by Ralis & McKibbin (1973) where the acetabular shape was assessed by the ratio between the deepest height (a_2) to the greatest width (a_1) of the acetabular cavity (Figure 6-7, A), and the femoral head shape was assessed as the ratio of the greatest height (h_2) of the femoral head to the greatest diameter (h_1) as measured perpendicularly to the greatest diameter (Figure 6-7, A). The congruence of the joint over the developmental period was assessed as the degree of joint coverage, which was measured as the length of the edges in common between the acetabulum and the femoral head. As a measure of asymmetry, I calculated the acetabular and femoral head skew factors (Figure 6-7, B). A reference point was identified using the centre of the initial acetabular cavity, which was calculated as the crossing point between its vertical and horizontal axes (Figure 6-7, A). This reference point was then kept constant over development, and the skew factor was calculated as the distance between this point and its most left and right extremities (Figure 6-7, B). The same technique was used for the femoral head, where the distance between the reference point, which was its rotational centre, and its left and right extremities lie on the horizontal line passing through the reference point, were used to calculate the skew factor (Figure 6-7, B). A graphical representation of the entire process is shown in Figure 6-8.

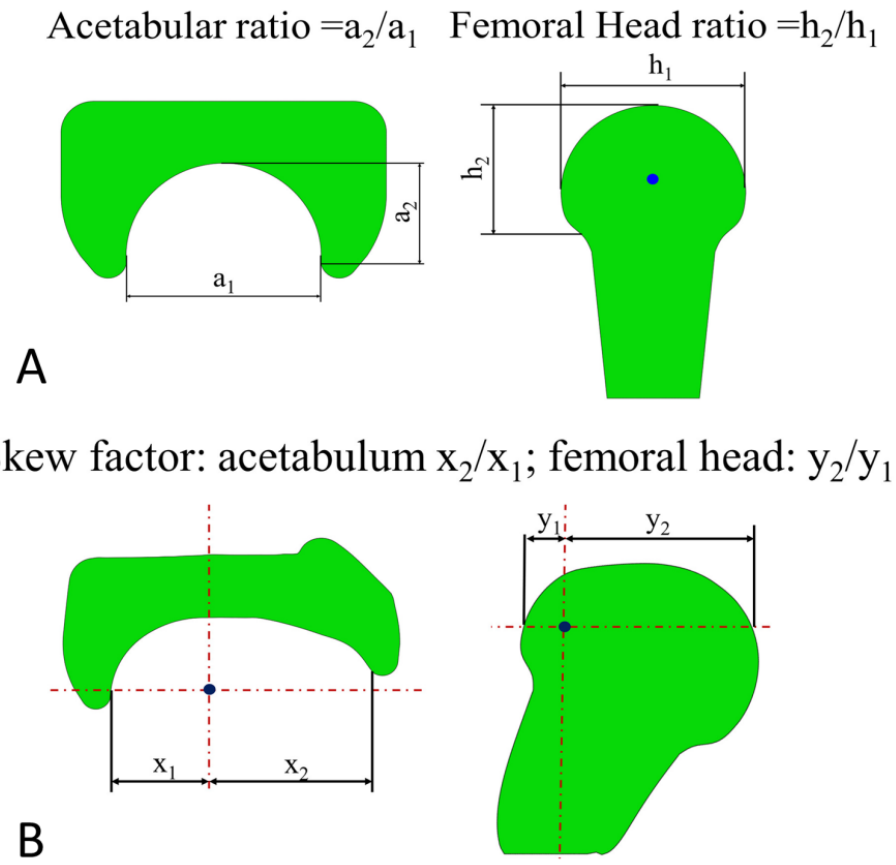

Figure 6-7 Method used to calculate the acetabular and femoral head skew factors.

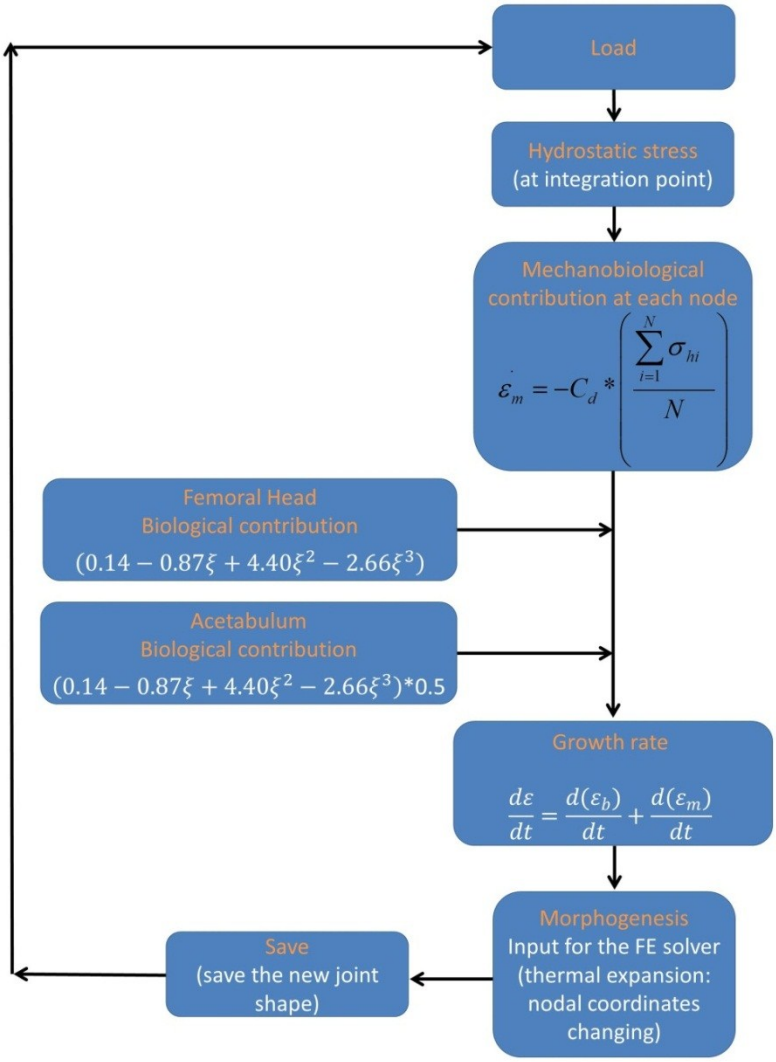

Figure 6-8 Graphical representation of the process used to simulate prenatal hip joint development.

6.3 Results

6.3.1 Inclusion of the inter-rudiment space

Models with and without the inter-rudiment space were run to test if a congruent shape (Figure 6-1, A) was enough to emulate the role of smoothing function performed by the inter-rudiment space in the previously presented model (Chapter 4).

When 10 cycles of growth were simulated with both models, the decreasing trend in the *acetabular ratio* and *femoral head ratio* were almost the same (Figure 6-9). In absence of the inter-rudiment space, the perfect match/congruence between the two

components of the joint (Figure 6-1, A) was enough to evenly spread the stresses during motion and, this third component (the inter-rudiment space) which in the previously presented model acted as a smoothing function to spread the loads (Chapter 3, Section 3.2.9.1), was not needed. Therefore, all the results discussed from here on are based on the model shown in Figure 6-1 , A which does not include the inter-rudiment space.

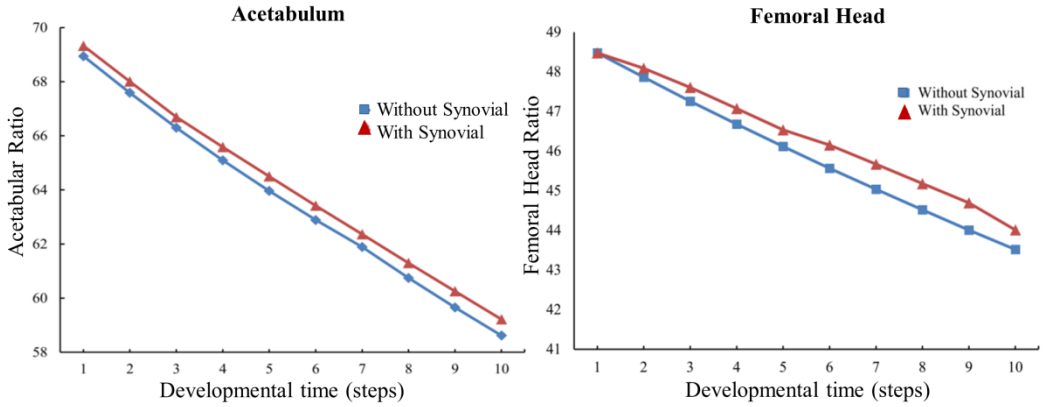

Figure 6-9 Acetabular and femoral head ratio. The graphs show the differences between having or not the inter-rudiment space included within the model. Both ratios show similar behaviours.

6.3.2 Growth related pressure

When one cycle of motion was simulated using the shape shown in Figure 6-1, A, the hydrostatic stresses generated by the movements and the ones obtained during growth were compared. The magnitude of the growth related hydrostatic pressure was much smaller, as indicated by the legend in Figure 6-10 B, compared with the hydrostatic pressure due to movements as shown in Figure 6-10 A.

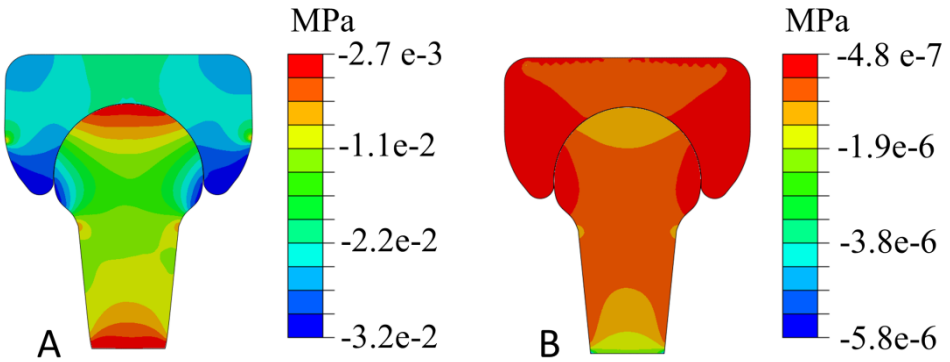

Figure 6-10 A) hydrostatic stress distribution generated by the movements; B) hydrostatic growth related stresses.

Therefore, the growth related pressure as stimuli for joint shape development were not included in further simulations.

6.3.3 Same biological growth for acetabulum and femoral head

For sensitivity analysis purposes, some simulations were also run with same biological contribution between pelvis and femur (Figure 6-11, A). The shape obtained after 10 cycles of growth predicted a progressive opening of the acetabulum and a decrease in roundness of the femoral head. However, the final joint shape showed the onset of a concave shape on the femoral part (red arrow) and the generation of a bump within the acetabular region (black arrow) (Figure 6-11, B).The generation of the bump (black arrow) was due to the high values of growth concentrated in that region, condition which is not physiological. The joint became non-interlocking.

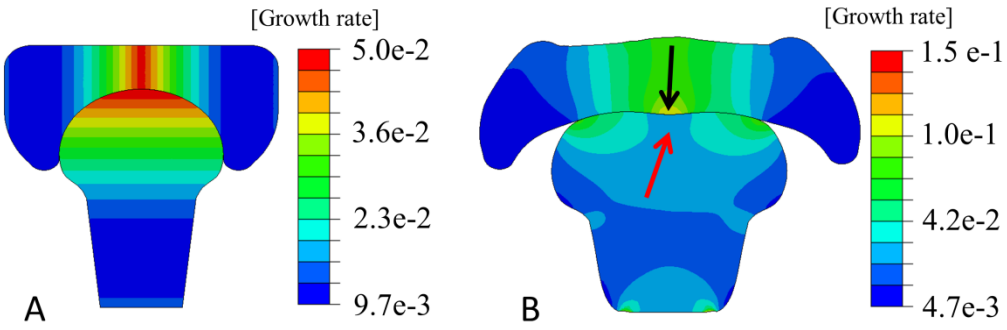

Figure 6-11 A) Initial joint shape showing the distribution of the biological contribution. B) joint shape obtained after 10 loading cycles when the biological contribution between the pelvis and femur was kept equal.

6.3.4 Hydrostatic stress distribution

The hydrostatic stresses of an entire cycle of physiological movements were always compressive, as shown by Figure 6-12, A, due to the two rudiments being constantly in contact. Stresses due to physiological movements, when applied to the initial geometry, were higher in the acetabulum (especially in its rim) and along the distal curvature of the femoral head. When combined with the biological growth rates (Figure 6-12, B), the stresses generated by one full cycle of physiological motion showed higher values of growth at the most proximal part of the femoral head and at the middle of the acetabulum (as shown in Figure 6-12, C).

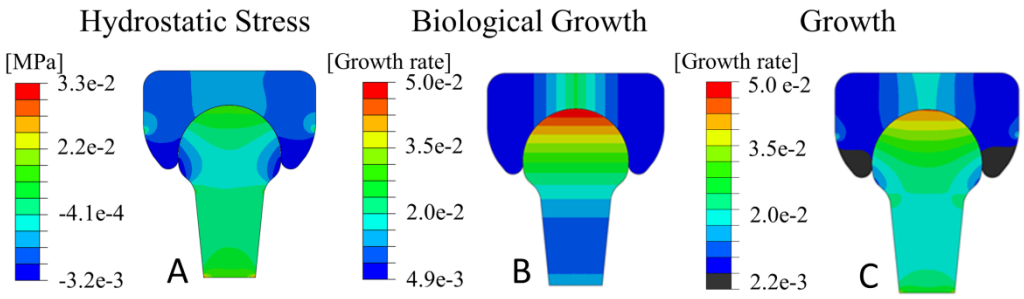

Figure 6-12 A) Resulting hydrostatic stresses, averaged over the first full cycle of physiological motion; B) biological contribution to growth; C) stresses generated by the combination of biological and hydrostatic stresses.

6.3.5 Morphogenesis

When growth due to physiological symmetric movements was simulated, the model predicted a progressive opening of the acetabulum, making it increasingly shallow up to birth, and a gradual decrease in roundness of the femoral head showing the onset of a flatter surface at its most proximal region (Figure 6-13, A, B). The predicted joint at birth showed an approximate 50% decrease in acetabular coverage of femoral head compared with the initial shape, but maintained a clear interlocking shape (Figure 6-13, A). The predicted trends showed a striking similarity with the experimental data (Ráliš and McKibbin, 1973), as shown in Figure 6-13, B, C. The predicted decrease in the acetabular ratio over the course of the simulation is almost identical (although slightly shifted) compared to the experimental curve, while our model predicts a faster decrease in femoral head roundness in the early phase of gestation than for the experimental data.

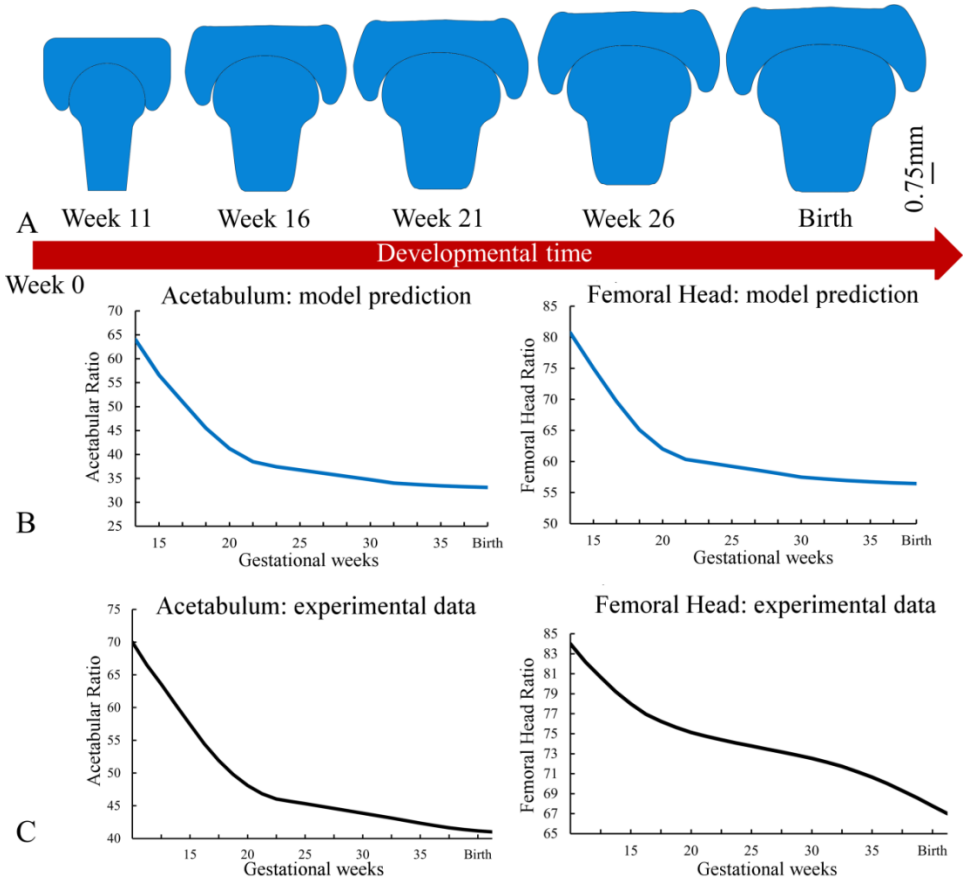

Figure 6-13 A) Predicted hip joint morphogenesis under physiological symmetric movements; a progressive opening of the acetabulum and a gradual decrease in roundness of the femoral head were predicted. B) Quantification of the changes in shape based on the acetabular shape and femoral head roundness parameters. C) Changes in human hip joint shape over development measured experimentally by Ralis & McKibbin (1973).

When reduced movements at the early stage were simulated, such as could occur due to neuromuscular disorder (Aronsson et al., 1994), the femoral head roundness decreased further and the acetabulum became shallower compared to the physiological predictions (Figure 6-14, A, B), resulting in a 60% decrease in acetabular coverage of the femoral head (as compared with the initial joint shape), and therefore potentially a less stable joint at birth. In contrast, reduced movements at the middle or late stage of development resulted in minimal joint shape changes from the physiological joint prediction (Figure 6-14, A). When absent movements were simulated the acetabulum became even shallower and the femoral head ratio decreased even further compared with the predicted shape for early reduced movements (Figure 6-14, A). Therefore, the presence of movements at the early stage were most critical in maintaining acetabular coverage of the femoral head, with

reduced or absent movements in the early stage contributing to decreased coverage of the femoral head, and a likely reduction in joint stability.

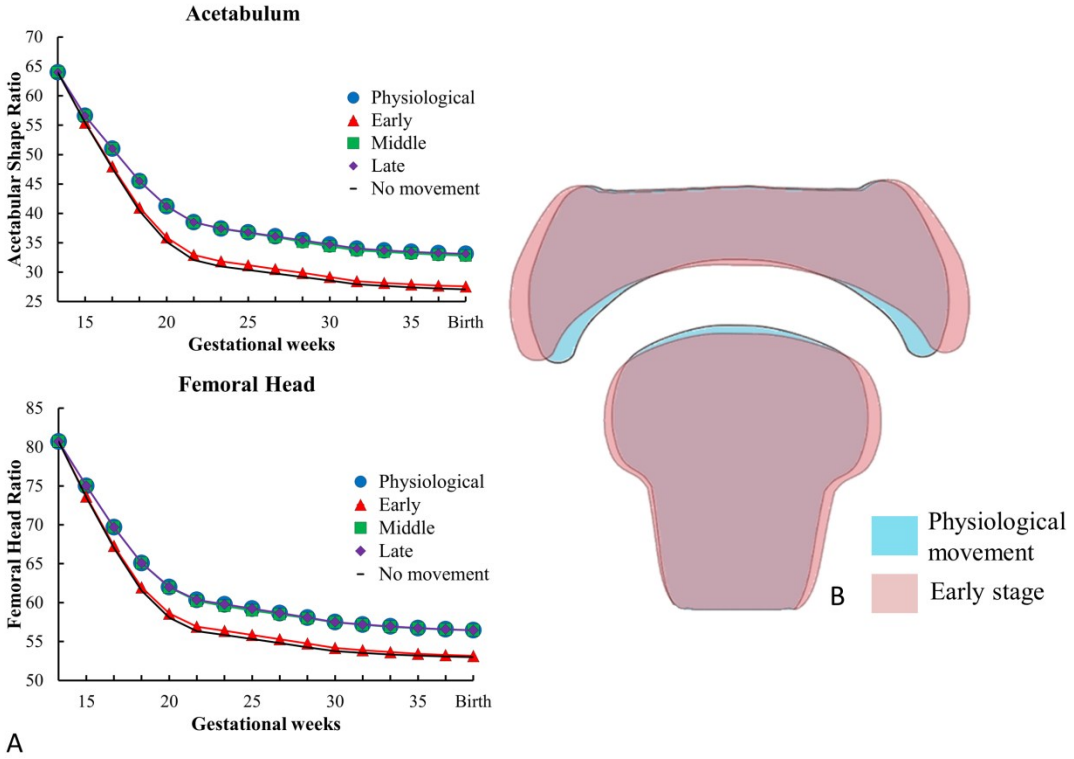

Figure 6-14 A) The effects on acetabular and femoral head shape of reduced movements at each stage of development (early, middle and late) and of a complete absence of movements. B) Predicted shapes under physiological movements (blue) and early reduction of movements (red).

When a constant rate of *rudiment expansion* was implemented, in order to separate out the influences of growth rate and range of movements on the resulting joint shape, the results showed that the rates at which the acetabular ratio and the femoral head ratio decreased were inversely proportional to the ranges of movement (Figure 6-15). Physiologically the largest range of motion is experienced during the early stage of development. This phase also coincides with the highest rate of fetal growth. Therefore the reduction of joint motion during this phase is having the most impact of the final joint shape.

When an asymmetric movement pattern was applied, the acetabulum became increasingly open in the direction of the applied loads (Figure 6-16, A), leading to development of an asymmetric shape. The shape of the femoral head was also affected showing a loss of head roundness and the onset of a malformed overall shape (Figure 6-16, A). The predicted shape is similar to the deformed shape typical

of a dysplastic hip joint as shown in Figure 6-16, B, where the interlocking shape is lost, increasing the risk of subluxation or dislocation of the hip. This configuration was implemented following Sandell et al. (2012), who showed that the presence of a maloriented articular surface may lead to excessive and eccentric loading on the acetabular rim and therefore increasing the risk of DDH. Moreover, in line with this study, Portinaro et al. (1994) hypothesised that ligamentous laxity or malpositioning in utero (breech position) may leads to abnormal loading allowing the femoral head to displace and encourage deformity.

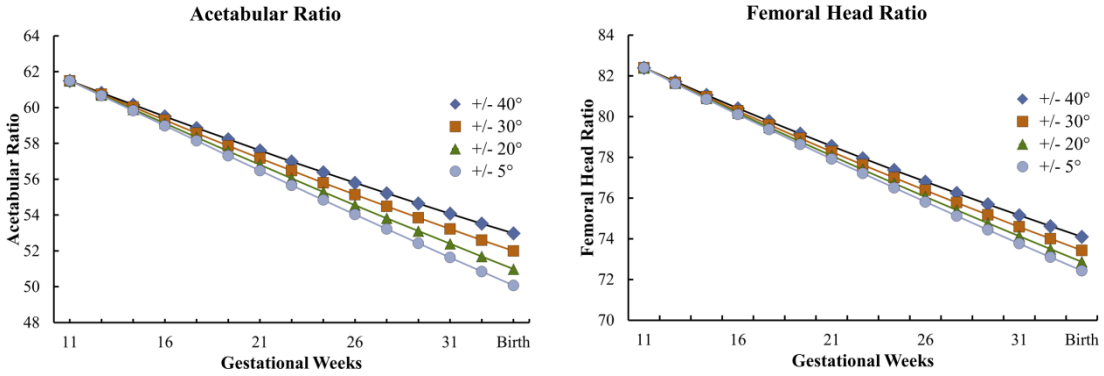

Figure 6-15 Acetabular and femoral head ratios when a constant rate of rudiment expansion was implemented; the rates at which both ratios decreased were inversely proportional to the range of movement.

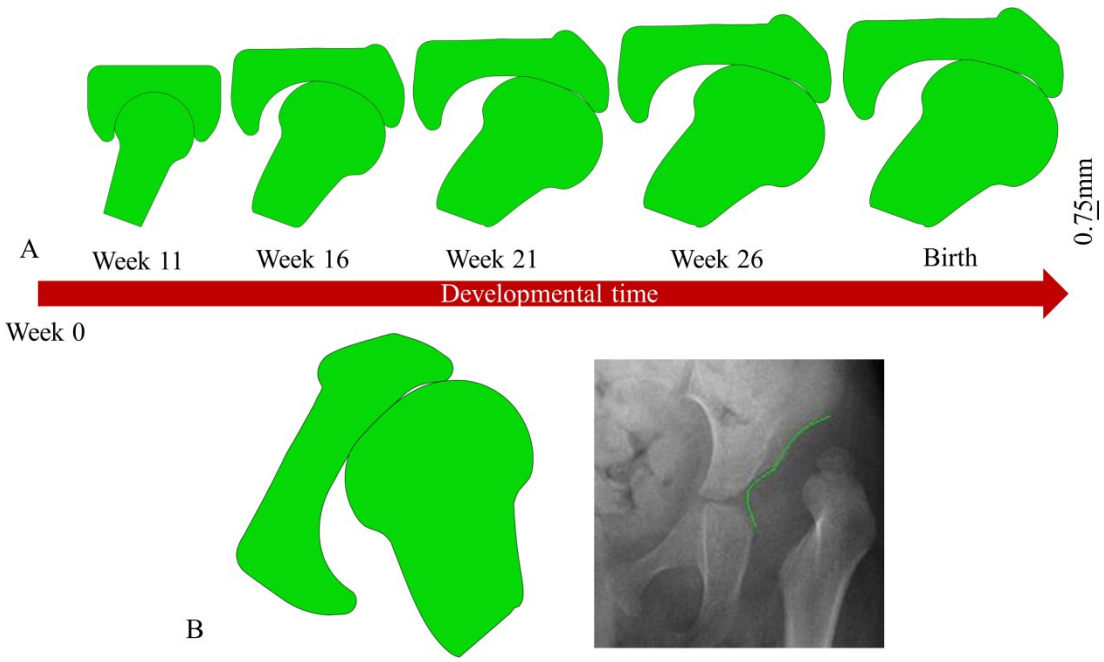

Figure 6-16 A) Predicted joint morphogenesis under asymmetric movements. B) The predicted hip joint shape at birth when asymmetric loading occurs is similar to the hip joint of a 30 month old infant affected by DDH. Image adapted with permission from Dr Frank Gaillard from website www.radiopaedia.org.

When asymmetric movements were reduced at the early, middle or late stages, or absent completely, our models predicted that early reduced movements, or absent movements, actually led to a deeper acetabulum than simulations with a full range of asymmetric movements, or reduced movements in the middle or late stages (Figure 6-17, A). The model in which no movements were applied in the asymmetric configuration was found to be the best in acetabular shape retention compared to all other asymmetric movement simulations. By measuring the acetabular skew factor (Figure 6-7, B), we observed that the simulations with a full range of asymmetric movement throughout, or full asymmetric movement at the early stage, predicted a more asymmetric acetabular shape compared with other asymmetric simulations (Figure 6-17, B). This suggests that in case of asymmetric loading, the higher the range of movement, the higher the likelihood of a skewed, shallower acetabulum. Therefore, asymmetric movements have the opposite effect on acetabular shape than symmetric movements. While a full range of symmetric motion in the early stage lead to maintenance of a deeper acetabulum (Figure 6-14, A), a full range of asymmetric motion in the early stage has a detrimental effect on acetabular shape (Figure 6-17, B).

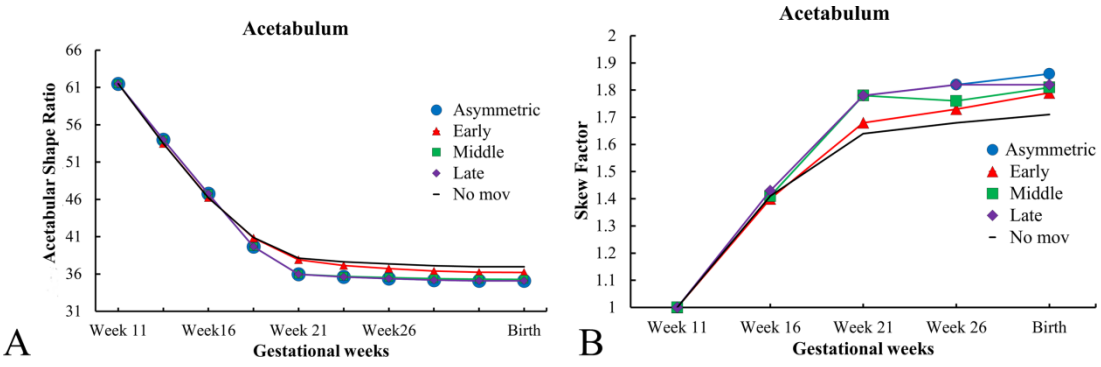

Figure 6-17 A) The effects of reduced asymmetric movements on acetabular shape and B) skew factor at each stage of development (early, middle and late) and under a complete absence of movements.

No influence of reduced or absent asymmetric movements, as compared to a full range of asymmetric movements, was found for the femoral head roundness or skew factor (Figure 6-18), which always exhibited the asymmetric profile shown in Figure 6-16.

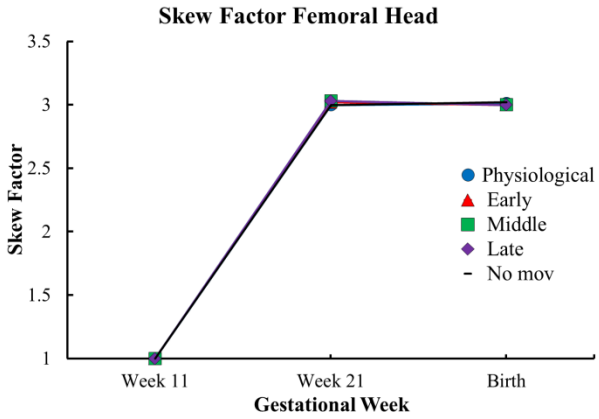

Figure 6-18 Skew factor at different stage of development (early, middle and late) and under a complete absence of movements. No influence of reduced or absent asymmetric movements, as compared to a full range of asymmetric movements, was found for the femoral head.

6.4 Discussion

In this study I describe a dynamic mechanobiological simulation of the prenatal hip joint with which I explore the effects of normal, reduced and asymmetric fetal movements on hip joint growth and morphogenesis, providing insights into the normal physiology of the hip joint and the etiology of DDH. The predicted joint shapes when physiological, symmetric movements were applied well approximated the anatomical changes in shape reported in the literature for fetal human hip joint development (Ráliš and McKibbin, 1973). In my predictions, the acetabulum progressively opened and the femoral head showed the onset of a flatter surface at its proximal end over development (Figure 6-13, A, B). The overall joint shape changes replicated the trends of human hip joint development, where its natural growth and development leads to a decrease in coverage of the femoral head while maintaining its interlocking shape (Figure 6-13, A, B, C).

When reduced symmetric movements at the early stage of development were simulated, the joint maintained its interlocking shape at birth but the femoral head roundness decreased and the acetabulum became shallower (Figure 6-14, A, B). The predicted shape under early reduced movements would likely be less stable at birth than the shape predicted under normal physiological conditions due to the loss of joint coverage, which would increase the risk of subluxation or dislocation of the hip. When reduced movements at the middle or late stage of development were simulated, minimal changes in joint shape compared to growth under physiological

movement were observed (Figure 6-14, A), suggesting that movement in the early stage of development is the most critical for joint shape. This may explain why the hip joint is so severely affected in cases of paralytic dislocations, where movement may have been reduced or absent from an early stage of development. These results suggest that movements during development tend to minimise the natural trend of decreasing stability (Figure 6-14, A). When, for sensitivity analysis, symmetric movements with a constant growth rate (*rudiment expansion*) were simulated, the rates at which the acetabular ratio and the femoral head ratio decreased were inversely proportional to the ranges of movement (Figure 6-15). This indicates that, with a constant growth rate, the larger the range of movement, the greater the acetabular depth and femoral head roundness. Physiologically, the largest range of motion is experienced during the early stage of development.

When an asymmetric movement pattern was simulated, the predicted joint shape was abnormal: the acetabulum opened in the same direction as the applied loads and the femoral head lost its roundness, showing an overall deformed shape of the joint typical of hip dysplasia as shown in Figure 6-16, B. Acetabular depth and skew were exacerbated with greater asymmetric movement ranges (Figure 6-17, B), suggesting that increased movements in the case of mal-positioning or joint laxity in utero may actually increase the risk of DDH. In contrast to the acetabulum, the shape of the femoral head was always acquired the same malformed shape with asymmetric positioning, regardless of when or whether asymmetric movements were reduced. While, with symmetric movements the predicted decrease in the acetabular ratio was almost identical (although slightly shifted), the decrease in femoral head ratio was faster, especially in the early phase of gestation, compared to the experimental curve (Figure 6-13, B, C). While the simplified profile used for the acetabulum is similar to its physiological deep cup shape, the simplified shape used for the femoral head may not adequately represent the complex profile which it acquires during development. If a more realistic femoral head shape was included in the model, it could potentially lead to more accurate results from our simulations. For this study, the maximum range of hip motion at different stages was gathered by analysing different MR imaging sequences of the developing fetus. Even if the actual range of motion used may not perfectly match with the real physiological motion, the reduced trend of physiological symmetric movements over time reflect the finding of Hayat et al.

(2011). In this study, I assumed that during normal development the movement at the fetal hip joint is symmetric, based on previous observations that at the very early prenatal age the femoral head is almost fully covered by the acetabular cavity (Ráliš and McKibbin, 1973) minimising all translations. Conditions such as fetal breech position or joint laxity (Luterkort et al., 1986; Muller and Seddon, 1953; Portinaro et al., 1994) which are risk factors for DDH (Ponseti, 1978; Portinaro et al., 1994), were assumed to lead to asymmetric movements at the hip, due to the loss of the distributed pressure patterns that these conditions may generate.

6.5 Summary

This research demonstrated that normal fetal movements are important for the emergence of hip joint shape and coverage. The natural tendency of the developing hip joint is to decrease in sphericity and acetabular coverage of the femoral head between 11 gestational weeks and birth (Ráliš and McKibbin, 1973) and this model predicted these physiological trends. It showed that physiological, symmetric movements help to maintain some of the acetabular depth and femoral head sphericity while reduced movements at an early stage of development or completely absent movements, such as could occur from a neuromuscular disorder, lead to decreased sphericity and acetabular coverage of the femoral head, increasing the risk of subluxation or dislocation of the hip. It also showed that asymmetric movements, which were hypothesised to result from fetal breech position or increased joint laxity, lead to an abnormal hip joint shape with characteristics of DDH such as a malformed femoral head and an asymmetric shallower acetabulum which increase the likelihood for the femoral head to dislocate (Larsson et al., 1991; Ziegler et al., 2008).

There are some limitations in this study. The mechanoregulation algorithm developed and used was based on a number of studies which showed that cartilage synthesis was inhibited by static loading and it was stimulated by dynamic loading. However, if researchers agree on the inhibitory effects of static compression on the synthesis of cartilage, contradictory results can be found in literature regarding the effects on biosynthesis due to dynamic compression leaving space for further research in both experimental and computational fields. The shapes used in this

study are theoretical shapes representative of a human hip joint. While the simplified profile used for the acetabulum is similar to its physiological deep cup shape, the simplified shape used for the femoral head may not adequately represent the complex profile which it acquires during development. If a more realistic femoral head shape was included in the model, it could have potentially lead to more accurate results from our simulations. Unfortunately we did not have access to realistic human's prenatal hip joint shapes. For this study, the maximum range of hip motion at different stages was gathered by analysing different MR imaging sequences of the developing fetus. Even if the actual range of motion used may not perfectly match with the real physiological motion, the reduced trend of physiological symmetric movements over time reflect the finding of Hayat et al. (2011). However, further improvement may be achieved by using novel cine-MRI techniques to automatically track hip joint displacement during fetal kick. Moreover, in this study, due to a lack of information in literature, it was assumed that during normal development the movement at the fetal hip joint was symmetric while conditions such as fetal breech position or joint laxity were assumed to lead to asymmetric movements at the hip due to the loss of the distributed pressure patterns that these conditions may generate.

To conclude, this study provides the first computational model able to predict the early onset of teratologic DDH. It successfully predicted, when immobilisation or reduced movement were simulated, the loss of joint congruency typical of this type of hip dislocation (Aronsson et al., 1994; Nowlan et al., 2014). The effects of breech position or oligohydramnios, usual factors for the so-called typical dislocation (Aronsson et al., 1994; Nowlan et al., 2014), also led to an abnormal hip joint shape with characteristics of DDH. Understanding the factors driving hip joint morphogenesis during prenatal development is critical for developing strategies for early diagnosis and preventative treatments for congenital musculoskeletal abnormalities, such as developmental dysplasia of the hip. Therefore, this research provides evidence for the importance of fetal movements in promoting normal hip joint morphogenesis, particularly joint coverage, and an explanation how abnormal movements could lead to joint instability and DDH in the infantile hip.

7 Outcomes, Contributions and Future Works

This chapter summarises the main outcomes of this thesis, drawing together the insights obtained from the two main simulations presented in order to provide a greater understanding of the process of prenatal joint morphogenesis and its importance to postnatal skeletal malformations such as DDH. Recommendations for further work in the field of computational development of prenatal joint are discussed and concluding remarks are provided.

7.1 Outcomes and Contributions to the field of developmental mechanobiology

This research has advanced the basic understanding of prenatal joint shape development and the implication that different mechanical environments within the joint region, might have on developmental skeletal diseases such as DDH. Advances were made by: 1) proposing a novel mechanobiological simulation of prenatal joint morphogenesis and, 2) proposing and testing hypotheses on how fetal movements impact upon the shape of the developing hip joint.

This section highlights the key outcomes of the main chapters of this thesis and their significance for the field of developmental biomechanics.

7.1.1 Simulation of prenatal joint development

Despite the clinical importance of the process of morphogenesis, there is very little understanding about factors that drive this process (Pacifici et al., 2005). The consequences of incomplete or abnormal morphogenesis can be debilitating (Leck, 2000) and it is clear that lack of motion affects joint shape morphogenesis (Kahn et al., 2009; Mikic et al., 2000; Nowlan et al., 2010a; Osborne et al., 2002; Roddy et al., 2011a; Roddy et al., 2011b). Few studies have explored the role of motion, or loading, on joint shape in depth (Heegaard et al., 1999; Sarin and Carter, 2000; Shefelbine and Carter, 2004).

In this study the evolution of the algorithms used to model joint morphogenesis was discussed (Chapter 3). Starting with a model very similar to that of Heegard et al. (1999), their achievements and limitations were described and discussed. Through the use of three different simulations (Chapter 3, Section 3.2), the effectiveness of

the endochondral ossification law proposed by Carter et al. (1987) as algorithm to predict prenatal joint development was explored. From these studies it was concluded that a new mechanobiology theory specific for cartilage growth and morphogenesis was needed.

A novel mechanoregulation algorithm specific for cartilage growth was developed (Chapter 4, Section 4.2) and a 3D mechanobiological simulation of joint morphogenesis in which the effects of a range of movements and different initial joint shapes was proposed. It used idealised shapes to represent a generic ball and socket joint and a generic hinge joint on which applied movement patterns typical for these joints in order to predict the effects on shape development. Both pre- and post-cavitational phases of joint development were simulated. It also examined the effect of rigid paralysis on joint shape by growing a joint when no movement was applied. Moreover, due to the many parameters that might play an important role in the resultant shapes, a sensitivity analysis was performed on the previously presented model (Chapter 5).

This study concluded that the starting joint configuration and applied movement were fundamental for the development of specific and anatomically recognisable joint shapes. Furthermore, the stresses generated during static pre-cavitational loading and dynamic post-cavitational movements differentially affected the process of prenatal joint morphogenesis. It provides new and important insights into normal and abnormal joint development and it helps us to understand the factors driving joint morphogenesis at a very early stage. Increasing knowledge about these factors is critical for developing strategies for early diagnosis and preventive treatments for congenital musculoskeletal abnormalities, such as developmental dysplasia of the hip.

7.1.2 Effects of normal and abnormal loading conditions on morphogenesis of the prenatal hip joint: application to hip dysplasia

Human hip joint morphogenesis has been described by Ralis and McKibbin (1973). At around gestational week 11, a globular femoral head is almost completely enclosed by a deep-set acetabulum. The coverage of the femoral head is never as low as it is around the time of birth (Ráliš and McKibbin, 1973), which most likely

means that the hip joint is at its most unstable at this time. Despite the acknowledged influence of fetal movements on hip joint formation, the mechanism by which these movements affect joint morphogenesis is still unknown.

This study proposed a mechanobiological simulation of prenatal hip joint morphogenesis, in order to propose and test hypotheses on how fetal movements and position could impact upon the shape of the developing hip joint. This study predicted growth and shape change of an idealised hip joint, and correlated it with published human hip joint shape data. It also investigated the effects of reduced, or asymmetric, movement at various stages of fetal development.

This study concluded that normal fetal movements are important for the emergence of a physiological hip joint shape and that movements during development tend to minimise the natural trend of decreasing stability. It also showed that physiological, symmetric movements help to maintain some of the acetabular depth and femoral head sphericity while reduced movements at an early stage of development or completely absent movements, lead to decreased sphericity and acetabular coverage of the femoral head, increasing the risk of subluxation or dislocation of the hip. Moreover, it shows that, in the case of mal-positioning (i.e. fetal breech position) or joint laxity in utero, movements may actually lead to an abnormal hip joint shape with characteristics of DDH such as a malformed femoral head and an asymmetric shallower acetabulum which increase the risk for the femoral head to dislocate (Larsson et al., 1991; Ziegler et al., 2008).

Chapter 5 provides evidence for the importance of fetal movements in promoting normal hip joint morphogenesis, particularly joint coverage, and an explanation how abnormal movements could lead to joint instability and DDH in the infantile hip.

7.2 Future Perspectives

The studies conducted throughout this thesis open new questions and possibilities for future research. This section suggests some of the areas that could be investigated to deepen the current understanding of prenatal joint morphogenesis using computational methods.

7.2.1 Improvements on the mechanoregulation algorithm for cartilage growth

Initially, the endochondral ossification growth theory (Carter et al., 1987) was used to predict cartilage growth under different mechanical loadings (Chapter 3). This theory, proposed in 1987, derived from a study where the influence of cyclic and multi-axial loads on bone growth and ossification were explored. By looking at the principal stresses generated within a bone, as a reaction to an applied external force on it, researchers proposed that cyclic hydrostatic compressive stress inhibits bone growth and ossification, while cyclic octahedral shear stress promotes them.

A different theory, specific for this project, was made by looking at how cartilage responds to different loading conditions. In vitro studies indicated that static compressive loading inhibits cartilage growth (Burton-Wurster et al., 1993; Guilak et al., 1994) while cyclic compressive loading promotes growth (Kim et al., 1994; Korver et al., 1992; Parkkinen et al., 1992). Therefore, in this novel theory for cartilage growth, cyclic hydrostatic compression promotes growth and static hydrostatic compression inhibits growth. However, even if the current mechanoregulation algorithm for cartilage growth successfully predicted the process of prenatal joint morphogenesis, further improvements can be done.

7.2.1.1 Biological and mechanobiological improvements

As explained in Section 3.2.6 growth and morphogenesis are controlled by biological and mechanobiological growth rates.

Further advances on the biological contribution to growth can be gained by comparing histological analysis of controlled and immobilised chick models at different time frames. This technique would make possible to separate the contribution to growth due to biological and mechanobiological factors. By exploring the effects of flaccid paralysis (unloaded joint) and by looking at cell proliferation and apoptosis in both conditions controlled and immobilised, important insights on the biology involved during growth and shape might be gained. Understanding the growth of the unloaded joint, and therefore the growth due to the biological contribution, would allow the development of an algorithm that can be used as input for computational models. With this method the changes in shapes due to the biological growth will be prescribed rather than predicted.

Further advances on the mechanobiological factor to growth can be also gained by looking at different time frames of developing joints under a variety of mechanical loading. Through the use of Optical Projection Tomography (OPT) (Sharpe et al., 2002), high resolution 3D representation of fetal joints can be obtained. By comparing the joint shapes at different developmental time and knowing the mechanical loads experienced by the joint during development, computational models can be used to explore the different type of stresses and strains that led to specific changes in shape. This research will help, by looking at, for example, hydrostatic stresses and pressures, deviatoric strain, shear stresses, fluid velocity, von Mises stresses, to find the best weighted combination of these stimuli during the process of joint morphogenesis. This approach will help to better understand which stimuli are significantly involved during the process of morphogenesis, therefore helping to develop more accurate mechanoregulation algorithm for cartilage growth.

7.2.2 Moving towards physiological models

Due to the assumptions made through the study, such as the use of simplified shapes and movements, a quantitative comparison between the results achieved and real joints could not be done. To move towards to more physiological models two improvements will be suggested in this section: 1) the use of real joint shapes, and 2) a better estimation of the biomechanics of the fetal movements.

7.2.2.1 The uses of real joint shapes to predict prenatal joint growth and morphogenesis

In this research, theoretical shapes, representing prenatal synovial joints, were used to predict joint morphogenesis. Even if the results achieved resembled realistic joint shapes (Chapter 4, Section 4.3.2) and, they replicated the trends of human hip joint development (Chapter 0, Section 6.3), a further and interesting advance of the current model will be achieved by using realistic shapes from animal models such as chicks or mice or, even more from human fetal images. Optical Projection Tomography (OPT) (Sharpe et al., 2002) or image segmentation software can be used to create 3D representation of fetal joints. These 3D realistic joint models can be imported in software for finite element analysis and used to explore the effects of different mechanical environments within more complex and realistic geometries.

Two examples of 3D representation of a lower and upper limb of a mice of 14.5 embryonic days old scanned with OPT are shown in Figure 7-1, A, B.

The use of realistic joint will advance the current computational leading therefore, to a more accurate picture of the mechanics involved during joint motion.

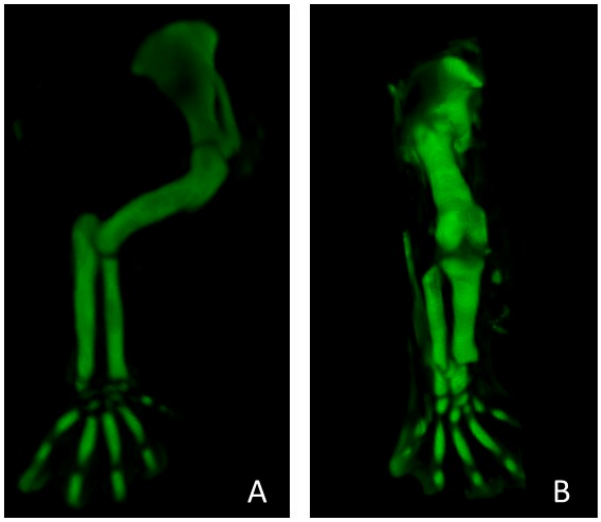

Figure 7-1 A) 3D representation of the right upper limb of a mice of 14.5 embryonic days obtained using OPT scans. B) 3D representation of the right lower limb of a mice of 14.5 embryonic days obtained using OPT scans. Images from Lisa Abela (unpublished work).

7.2.2.2 Biomechanics of fetal movements: a tracking software

In this thesis the maximum range of hip motion was calculated by looking at the angle generated by the intersection of the spine line and the longitudinal axis of the femur (Chapter 0, Section 6.2.3). With this method I was able to make realistic estimation of the hip motion over development (Section 6.2.3). However, a deeper research focused to develop better techniques to monitoring fetal movements, will provide essential information to develop more accurate computational models.

A current study in the Nowlan group, focus to capture fetal movement in utero by using novel cine-MRI techniques (Hayat et al., 2011), is aimed to develop a method to automatically track hip joint displacement during fetal kicking (Figure 7-2, A). Realistic hip joint motions can be used as input for computational models and, together with realistic joint shapes (Section 7.2.2.1), will provide a more physiological environment (Giorgi et al., 2011) where to study the importance of movements during prenatal development.

Moreover, musculoskeletal models can also be used to predict the mechanical environments generated by specific motion within the joint region (Figure 7-2, B). This will provide additional information regarding the developing joint and therefore increasing the chances, using computational models, to identify mechanical environments which increase the risk of joint deformities such as DDH. Being able to capture fetal movement and specific mechanical environments in utero will provide fundamental information which will help to develop more realistic and reliable computational models.

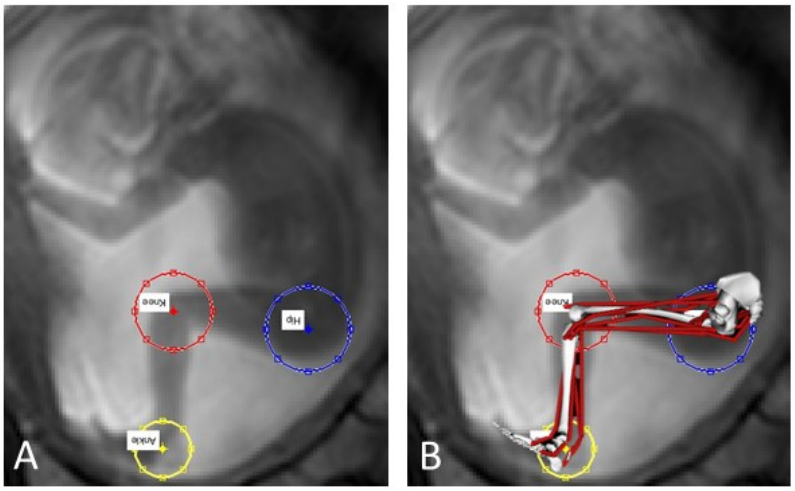

Figure 7-2 A) Example of the tracking system used to capture fetal movement in utero. B) Example of a musculoskeletal models used to investigate the forces in the joints due to fetal movements. Images from Stefaan Verbruggen (unpublished work).

7.2.3 Ex-vivo culture of embryonic limbs: an optimal method to validate computational models

Numerous publications have presented results of reduced skeletal growth and joint development in embryonic animal models where the mechanical environment has been supressed (Drachman, 1966; Osborne et al., 2002; Roddy et al., 2011b). The influence of mechanical stimulation during this developmental time period is further highlighted by clinical conditions, such as developmental dysplasia of the hip (DDH), which occur when fetal movements are restricted (Muller and Seddon, 1953; Portinaro et al., 1994; Shefelbine and Carter, 2004). Even if, there is a clear relationship between mechanical stimulation and pre-natal joint formation, it has never been characterised. A preliminary work in our lab has managed to culture

whole embryonic chick hind limb explants under compressive cyclic loading. A customised arrangement during *in vitro* cultivation allows for flexion and extension of the knee joint under loading. The developing joints can be cultured under a controlled biomechanical environment, where parameters such as the magnitude, frequency and duration of compressive loading can be adjusted. The system has been tested under static and dynamic conditions in a pilot study. Embryonic chick hind limbs were harvested at 7 days of incubation for 3 experimental groups (A – Uncultured; B - Static, unloaded; C – Dynamic). Outlines of the knee joint shapes from the 3 groups are shown in Figure 7-3.

The results achieved by ex-vivo experiments can be then scanned through OPT and, the 3D reconstruction on the joint can be compared with the predicted shape from computational simulations. Joint size and specific anatomical features can be then compared. By exploring how, variations in mode, magnitude and frequency of experienced mechanical stimuli alter the joint shape morphology ex-vivo, in addition to significantly increases knowledge on the effects of mechanical stimuli on distribution of growth, cavitation and shaping of synovial joints, will provide an optimal method to validate the reliability of computational models in predicting prenatal joint morphogenesis.

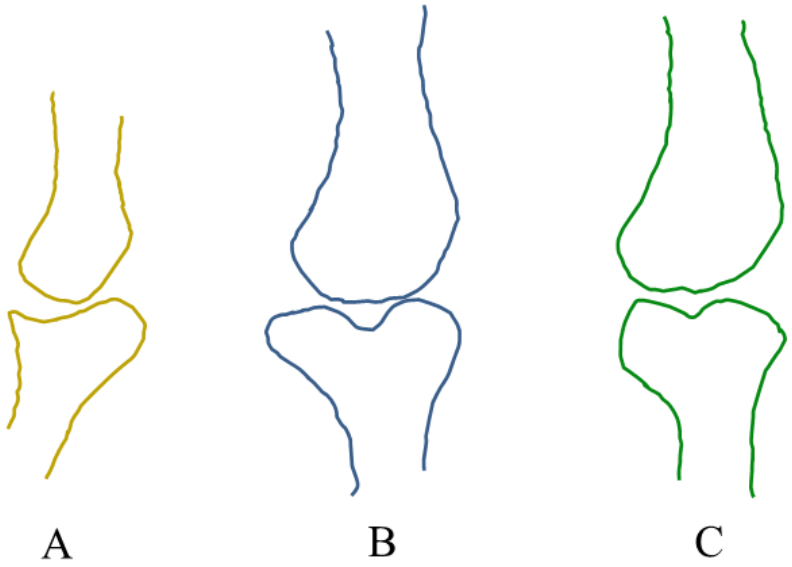

Figure 7-3 Figure shows the outlines of the knee joint shape obtained from the initial pilot study in the sagittal plane. The shapes indicate the cultured system used allowed for growth and development of the developing joint *in vitro* under both static and dynamic stimulation. (A – Uncultured; B – Static, unloaded; C – Dynamic). Images from Vikesh Chandaria (unpublished work).

7.2.4 Conclusions

Deepening our knowledge on the importance of fetal movements for the emergence of physiological joint shapes is crucial to develop strategies for early diagnosis and preventative treatments for congenital musculoskeletal abnormalities. Being able to quantify the forces generated due to fetal movements and understand their role in joint morphogenesis will enable clinicians to identify environments which increase the risk of joint malformations. This research provides new and important insights into the factors driving joint morphogenesis and for the importance of fetal movements during hip joint development. It shows that computational models can be used to study the early onset of teratologic and typical DDH and therefore, inform future preventative measures for such conditions.

8 Bibliography

American Academy of Pediatrics, 2000. Committee on Quality Improvement, Subcommittee on Developmental Dysplasia of the Hip. Clinical practice guideline: early detection of developmental dysplasia of the hip. Pediatrics 105, 896-905.

Archer, C.W., Dowthwaite, G.P., Francis-West, P., 2003. Development of synovial joints. Birth Defects Research Part C: Embryo Today: Reviews 69, 144-155.

Ares, O., Conesa, X., Seijas, R., Carrera, L., 2009. Proximal tibiofibular dislocation associated with fracture of the tibia: a case report. Cases Journal 2, 196.

Armstrong, C., Lai, W., Mow, V., 1984. An analysis of the unconfined compression of articular cartilage. Journal of biomechanical engineering 106, 165-173.

Aronsson, D.D., Goldberg, M.J., Kling, T.F., Roy, D.R., 1994. Developmental dysplasia of the hip. Pediatrics 94, 201-208.

Asanbaeva, A., Tam, J., Schumacher, B.L., Klisch, S.M., Masuda, K., Sah, R.L., 2008. Articular cartilage tensile integrity: modulation by matrix depletion is maturation-dependent. Archives of Biochemistry and Biophysics 474, 175-182.

Bagnall, K., Harris, P., Jones, P., 1982. A radiographic study of the longitudinal growth of primary ossification centers in limb long bones of the human fetus. The Anatomical Record 203, 293-299.

Bamshad, M., Van Heest, A.E., Pleasure, D., 2009. Arthrogryposis: a review and update. The Journal of Bone & Joint Surgery 91, 40-46.

Bardeen, C.R., Lewis, W.H., 1901. Development of the limbs, body-wall and back in man. American Journal of Anatomy 1, 1-35.

Beaupré, G.S., Stevens, S.S., Carter, D.R., 2000. Mechanobiology in the development, maintenance, and degeneration of articular cartilage. Journal of rehabilitation research and development 37, 145-152.

Bellairs, R., Osmond, M., 2005. Atlas of chick development. Academic Press.

Bialik, V., Bialik, G.M., Blazer, S., Sujov, P., Wiener, F., Berant, M., 1999. Developmental Dysplasia of the Hip: A New Approach to Incidence. Pediatrics 103, 93-99.

Burton-Wurster, N., Vernier-Singer, M., Farquhar, T., Lust, G., 1993. Effect of compressive loading and unloading on the synthesis of total protein, proteoglycan, and fibronectin by canine cartilage explants. J Orthop Res. 11, 717-729.

Carter, D., Beaupre, G., 1999. Linear elastic and poroelastic models of cartilage can produce comparable stress results: a comment on Tanck et al.(J Biomech 32: 153-161, 1999). Journal of Biomechanics 32, 1255-1257.

Carter, D., Orr, T., Fyhrie, D., Schurman, D., 1987. Influences of mechanical stress on prenatal and postnatal skeletal development. Clin. Orthop. Relat. 15, 237-250.

Carter, D., Wong, M., 1988a. The role of mechanical loading histories in the development of diarthrodial joints. J Orthop Res 6, 804-8016.

Carter, D., Wong, M., 2003. Modelling cartilage mechanobiology. The royal society 358, 1461-1471.

Carter, D.R., Beaupré, G.S., Giori, N.J., Helms, J.A., 1998a. Mechanobiology of Skeletal Regeneration. Clinical Orthopaedics and Related Research 355, S41-S55.

Carter, D.R., van der Meulen, M., Beaupre, G., 1998b. Mechanobiologic regulation of osteogenesis and arthrogenesis. Skeletal Growth and Development: Clinical Issues and Basic Science Advances. Rosemont, IL: AAOS, 99-130.

Carter, D.R., Wong, M., 1988b. Mechanical stresses and endochondral ossification in the chondroepiphysis. Journal of Orthopaedic Research 6, 148-154.

Chan, A., McCaul, K.A., Cundy, P.J., Haan, E.A., Byron-Scott, R., 1997. Perinatal risk factors for developmental dysplasia of the hip. Archives of Disease in Childhood-Fetal and Neonatal Edition 76, F94-F100.

Christie, A., 1949. Prevalence and distribution of ossification centers in the newborn infant. American Journal of Diseases of Children 77, 355-361.

Claes, L.E., Heigele, C.A., 1999. Magnitudes of local stress and strain along bony surfaces predict the course and type of fracture healing. Journal of Biomechanics 32, 255-266.

Correia, C., Pereira, A.L., Duarte, A.R., Frias, A.M., Pedro, A.J., Oliveira, J.T., Sousa, R.A., Reis, R.L., 2012. Dynamic culturing of cartilage tissue: the significance of hydrostatic pressure. Tissue Engineering Part A 18, 1979-1991.

Davisson, T., Kunig, S., Chen, A., Sah, R., Ratcliffe, A., 2002. Static and dynamic compression modulate matrix metabolism in tissue engineered cartilage. Journal of Orthopaedic Research 20, 842-848.

Dijkgraaf, L.C., de Bont, L.G., Boering, G., Liem, R.S., 1995. Normal cartilage structure, biochemistry, and metabolism: a review of the literature. Journal of oral and maxillofacial surgery 53, 924-929.

Doubilet, P.M., Benson, C.B., Nadel, A.S., Ringer, S.A., 1997. Improved birth weight table for neonates developed from gestations dated by early ultrasonography. Journal of ultrasound in medicine 16, 241-249.

Drachman, D., and Sokoloff, L., 1966. The role of movement in embryonic joint development. Dev Biol 14, 401-410.

Elgenmark, O., 1945. The normal development of the ossific centres during infancy and childhood. Acta Paediatrica Scandinavica.

Farquhar, T., Todhunter, R.J., Fubini, S.L., Burton-Wurster, N., Lust, G., 1996. Effect of methylprednisolone and mechanical loading on canine articular cartilage in explant culture. Osteoarthritis and Cartilage 4, 55-62.

Fisher, J., P, , Mikos, A., G, , Bronzino, J., D.. 2007. Tissue Engineering. CRC Press, Taylor & Francis Group.

Gardner, E., Gray, D., 1950. Prenatal development of the human hip joint. American Journal of Anatomy 87, 163-211.

Gardner, E., Gray, D., 1953. Prenatal development of the human shoulder and acromioclavicular joints. American Journal of Anatomy 92, 219-276.

Gardner, E., Gray, D., 1970. The prenatal development of the human femur. American Journal of Anatomy 129, 121-140.

Gardner, E., O'Rahilly, R., 1968. The early development of the knee joint in staged human embryos. Journal of Anatomy 102, 289.

Gillard, G.C., Reilly, H.C., Bell-booth, P.G., Flint, M.H., 1979. The influence of mechanical forces on the glycosaminoglycan content of the rabbit flexor digitorum profundus tendon. Connective tissue research 7, 37-46.

Giorgi, M., Carriero, A., Shefelbine, S., Nowlan, N., Year The role of fetal movement in prenatal hip joint morphogenesis. In International Journal of Experimental Pathology.

Giorgi, M., Carriero, A., Shefelbine, S.J., Nowlan, N.C., 2014. Mechanobiological simulations of prenatal joint morphogenesis. Journal of Biomechanics 47, 989-995.

Giorgi, M., Carriero, A., Shefelbine, S.J., Nowlan, N.C., 2015b. Effects of normal and abnormal loading conditions on morphogenesis of the prenatal hip joint: application to hip dysplasia. Journal of Biomechanics.

Giorgi, M., Innocenti, B., Luc, L., Alessandro, A., Cristina, B., 2011. Identification Of Landmarks On Lower Limb Joint From CT Images For Kinematics Studies: A Totally Semi-automatic Procedure. WIT Press.

Grodzinsky, A.J., Levenston, M.E., Jin, M., Frank, E.H., 2000. Cartilage tissue remodeling in response to mechanical forces. Annual Review of Biomedical Engineering 2, 691-713.

Guilak, F., Meyer, B.C., Ratcliffe, A., Mow, V.C., 1994. The effects of matrix compression on proteoglycan metabolism in articular cartilage explants. Osteoarthritis and Cartilage 2, 91-101.

Hall, B.K., 1983. Cartilage V1: Structure, Function, and Biochemistry. Academic Press.

Hansson, L., Menander-Sellman, K., Stenström, A., Thorngren, K.-G., 1972. Rate of normal longitudinal bone growth in the rat. Calcified tissue research 10, 238-251.

Harrison, T., 1958. The growth of the pelvis in the rat—a mensural and morphological study. Journal of Anatomy 92, 236.

Hayat, T., Nihat, A., Martinez-Biarge, M., McGuinness, A., Allsop, J., Hajnal, J., Rutherford, M., 2011. Optimization and initial experience of a multisection balanced steady-state free precession cine sequence for the assessment of fetal behavior in utero. American Journal of Neuroradiology 32, 331-338.

Health, W.H.O.R., 2003. Managing complications in pregnancy and childbirth: a guide for midwives and doctors. World Health Organization.

Heegaard, J.H., Beaupré, G.S., Carter, D.R., 1999. Mechanically modulated cartilage growth may regulate joint surface morphogenesis. Journal of Orthopaedic Research 17, 509-517.

Henderson, J., Carter, D., 2002. Mechanical induction in limb morphogenesis: the role of growth-generated strains and pressures. Bone 31, 645-653.

Herberhold, C., Stammberger, T., Faber, S., Putz, R., Englmeier, K.H., Reiser, M., Eckstein, F., 1998. An MR-based technique for quantifying the deformation of articular cartilage during mechanical loading in an intact cadaver joint. Magnetic resonance in medicine 39, 843-850.

Hill, A.H., 1939. Fetal age assessment by centers of ossification. American Journal of Physical Anthropology 24, 251-272.

Hogervorst, T., Eilander, W., Fikkers, J.T., Meulenbelt, I., 2012. Hip Ontogenesis: How Evolution, Genes, and Load History Shape Hip Morphotype and Cartilotype. Clinical Orthopaedics and Related Research 470, 3284-3296.

Homer, C., Baltz, R., Hickson, G., Miles, P., Shook, J., 2000. Clinical practice guideline: early detection of developmental dysplasia of the hip. Committee on Quality Improvement, Subcommittee on Developmental Dysplasia of the Hip. American Accademy of Pediatrics, 896-905.

Huiskes, R., Driel, W.D.V., Prendergast, P.J., SØBalle, K., 1997. A biomechanical regulatory model for periprosthetic fibrous-tissue differentiation. Journal of Materials Science: Materials in Medicine 8, 785-788.

Hunziker, E.B., 2000. Articular cartilage repair: problems and perspectives. Biorheology 37, 163-164.

Ippolito, E., Tovaglia, V., Caterini, R., 1984. Mechanisms of acetabular growth in the foetus in relation to the pathogenesis and treatment of congenital dislocation of the hip. Italian journal of orthopaedics and traumatology 10, 501-510.

Isaksson, H., Wilson, W., van Donkelaar, C.C., Huiskes, R., Ito, K., 2006. Comparison of biophysical stimuli for mechano-regulation of tissue differentiation during fracture healing. Journal of Biomechanics 39, 1507-1516.

Kahn, J., Shwartz, Y., Blitz, E., Krief, S., Sharir, A., Breitel, D.A., Rattenbach, R., Relaix, F., Maire, P., Rountree, R.B., 2009. Muscle contraction is necessary to maintain joint progenitor cell fate. Developmental Cell 16, 734-743.

Khan, I., Redman, S., williams, R., Dowthwaite, G., Oldfield, S., Archer, C., 2007. The development of synovial joints. Current topics in developmental biology 79, 1-36.

Kim, Y.J., Sah, R.L.Y., Grodzinsky, A.J., Plaas, A.H.K., Sandy, J.D., 1994. Mechanical Regulation of Cartilage Biosynthetic Behavior: Physical Stimuli. Archives of Biochemistry and Biophysics 311, 1-12.

Klein-Nulend, J., Veldhuijzen, J., Burger, E., 1986. Increased calcification of growth plate cartilage as a result of compressive force in vitro. Arthritis & Rheumatism 29, 1002-1009.

Koob, T.J., Clark, P.E., Hernandez, D.J., Thurmond, F.A., Vogel, K.G., 1992. Compression loading in vitro regulates proteoglycan synthesis by tendon fibrocartilage. Archives of Biochemistry and Biophysics 298, 303-312.

Korver, T., Van de Stadt, R., Kiljan, E., Van Kampen, G., Van der Korst, J., 1992. Effects of loading on the synthesis of proteoglycans in different layers of anatomically intact articular cartilage in vitro. The Journal of rheumatology 19, 905-912.

Kronenberg, H.M., 2003. Developmental regulation of the growth plate. Nature 423, 332-336.

Lacroix, D., Prendergast, P.J., 2002. A mechano-regulation model for tissue differentiation during fracture healing: analysis of gap size and loading. Journal of Biomechanics 35, 1163-1171.

Lacroix, D., Prendergast, P.J., Li, G., Marsh, D., 2002. Biomechanical model to simulate tissue differentiation and bone regeneration: Application to fracture healing. Med. Biol. Eng. Comput. 40, 14-21.

Larsson, T., Aspden, R.M., Heinegård, D., 1991. Effects of Mechanical Load on Cartilage Matrix Biosynthesis In Vitro. Matrix 11, 388-394.

Leck, I., 2000. Congenital dislocation of the hip. In: Antenatal and Neonatal Screening. Oxford University Press.

Lee, M.C., Eberson, C.P., 2006. Growth and development of the child's hip. Orthopedic Clinics of North America 37, 119-132.

Li, K.W., Williamson, A.K., Wang, A.S., Sah, R.L., 2001. Growth responses of cartilage to static and dynamic compression. Clinical Orthopaedics and Related Research 391, S34-S48.

Lorenzo, P., Bayliss, M.T., Heinegård, D., 2004. Altered patterns and synthesis of extracellular matrix macromolecules in early osteoarthritis. Matrix biology 23, 381-391.

Lu, X., Mow, V., 2008. Biomechanics of articular cartilage and determination of material properties. Medicine+ Science in Sports+ Exercise 40, 193.

Luterkort, M., Persson, P., Polberg, S., Bjerre, I., 1986. Hip joint instability in breech pregnancy. Acta Paediatrica 75, 860-863.

Mankin, H.J., 1982. Current concepts review. The response of articular cartilage to mechanical injury. J Bone Joint Surg Am 64, 460-466.

Maxian, T.A., Brown, T.D., Weinstein, S.L., 1995. Chronic stress tolerance levels for human articular cartilage: two nonuniform contact models applied to long-term follow-up of CDH. Journal of Biomechanics 28, 159-166.

McCarty, W.J., Masuda, K., Sah, R.L., 2011. Fluid movement and joint capsule strains due to flexion in rabbit knees. Journal of Biomechanics 44, 2761-2767.

Mikic, B., Wong, M., Chiquet, M., Hunziker, E.B., 2000. Mechanical modulation of tenascin-C and collagen-XII expression during avian synovial joint formation. Journal of Orthopaedic Research 18, 406-415.

Mow, V.C., Holmes, M.H., Michael Lai, W., 1984. Fluid transport and mechanical properties of articular cartilage: a review. Journal of Biomechanics 17, 377-394.

Muller, G., Seddon, H., 1953. Late results of treatment of congenital dislocation of the hip. J Bone Joint Surg Br 35, 342-362.

Murray, P.D., Drachman, D.B., 1969. The role of movement in the development of joints and related structures: the head and neck in the chick embryo. J Embryol Exp Morphol 22, 349-371.

Nowlan, N.C., Bourdon, C., Dumas, G., Tajbakhsh, S., Prendergast, P.J., Murphy, P., 2010a. Developing bones are differentially affected by compromised skeletal muscle formation. Bone 46, 1275-1285.

Nowlan, N.C., Chandaria, V., Sharpe, J., 2014. Immobilized chicks as a model system for early-onset developmental dysplasia of the hip. Journal of Orthopaedic Research 32, 777-785.

Nowlan, N.C., Murphy, P., Prendergast, P.J., 2008. A dynamic pattern of mechanical stimulation promotes ossification in avian embryonic long bones. Journal of Biomechanics 41, 249-258.

Nowlan, N.C., Sharpe, J., 2014. Joint shape morphogenesis precedes cavitation of the developing hip joint. Journal of Anatomy 224, 482-489.

Nowlan, N.C., Sharpe, J., Roddy, K.A., Prendergast, P.J., Murphy, P., 2010b. Mechanobiology of embryonic skeletal development: Insights from animal models. Birth Defects Research Part C: Embryo Today: Reviews 90, 203-213.

O'Rahilly, R., Gardner, E., 1975. The timing and sequence of events in the development of the limbs in the human embryo. Anatomy and embryology 148, 1-23.

O'Rahilly, R., Gardner, E., Gray, D., 1956. The ectodermal thickening and ridge in the limbs of staged human embryos. Journal of Embryology and Experimental Morphology 4, 254-264.

O'Rahilly, R., Müller, F., 1996. Human embryology & teratology. Wiley-Liss.

Osborne, A.C., Lamb, K.J., Lewthwaite, J.C., Dowthwaite, G.P., Pitsillides, A.A., 2002. Short-term rigid and flaccid paralyses diminish growth of embryonic chick limbs and abrogate joint cavity formation but differentially preserve pre-cavitated joints. J Musculoskelet Neuronal Interact 2, 448-456.

Pacifici, M., Koyama, E., Iwamoto, M., 2005. Mechanisms of synovial joint and articular cartilage formation: Recent advances, but many lingering mysteries. Birth Defects Research Part C: Embryo Today: Reviews 75, 237-248.

Palmoski, M.J., Brandt, K.D., 1984. Effects of static and cyclic compressive loading on articular cartilage plugs in vitro. Arthritis & Rheumatism 27, 675-681.

Parkkinen, J.J., Lammi, M.J., Helminen, H.J., Tammi, M., 1992. Local stimulation of proteoglycan synthesis in articular cartilage explants by dynamic compression in vitro. Journal of Orthopaedic Research 10, 610-620.

Platzer, W., Spitzer, G., 2003. Color atlas of human anatomy-Volume 1: Locomotor system. Thieme Verlag, Stuttgart New York.

Ponseti, I.V., 1978. Morphology of the acetabulum in congenital dislocation of the hip. J Bone Joint Surg [Am] 60, 586-599.

Portinaro, N., Matthews, S., Benson, M., 1994. The acetabular notch in hip dysplasia. Journal of Bone & Joint Surgery, British Volume 76, 271-273.

Prendergast, P.J., Huiskes, R., Søballe, K., 1997. Biophysical stimuli on cells during tissue differentiation at implant interfaces. Journal of Biomechanics 30, 539-548.

Ráliš, Z., McKibbin, B., 1973. Changes in shape of the human hip joint during its development and their relation to its stability. Journal of Bone & Joint Surgery, British Volume 55, 780-785.

Ralphs, J.R., Benjamin, M., 1994. The joint capsule: structure, composition, ageing and disease. Journal of Anatomy 184, 503-509.

Reddy, J.N., 1993. An introduction to the finite element method. McGraw-Hill New York.

Riboni, G., Bellini, A., Serantoni, S., Rognoni, E., Bisanti, L., 2003. Ultrasound screening for developmental dysplasia of the hip. Pediatric radiology 33, 475-481.

Roddy, K.A., Kelly, G.M., van Es, M.H., Murphy, P., Prendergast, P.J., 2011a. Dynamic patterns of mechanical stimulation co-localise with growth and cell proliferation during morphogenesis in the avian embryonic knee joint. Journal of Biomechanics 44, 143-149.

Roddy, K.A., Prendergast, P.J., Murphy, P., 2011b. Mechanical Influences on Morphogenesis of the Knee Joint Revealed through Morphological, Molecular and Computational Analysis of Immobilised Embryos. PLoS ONE 6, e17526.

Ryder, C.T., Mellin, G.W., 1966. A prospective epidemiological study of the clinical and roentgenological characteristics of the hip joint in the first year of life. Bone and Joint Surgery 48A.

Sah, R.L.Y., Kim, Y.-J., Doong, J.-Y.H., Grodzinsky, A.J., Plass, A.H.K., Sandy, J.D., 1989. Biosynthetic response of cartilage explants to dynamic compression. Journal of Orthopaedic Research 7, 619-636.

Sandell, L.J., 2012. Etiology of osteoarthritis: genetics and synovial joint development. Nat Rev Rheumatol 8, 77-89.

Sarin, V.K., Carter, D.R., 2000. Mechanobiology and joint conformity regulate endochondral ossification of sesamoids. Journal of Orthopaedic Research 18, 706-712.

Scheuer, L., Black, S., 2004. The Juvenile Skeleton. Elsevier Ltd.

Schuh, A., Doleschal, S., Schmickal, T., 2009. Anterior Hip Dislocation in a Football Player: A Case Report. Case Reports in Medicine 2009.

Sharpe, J., Ahlgren, U., Perry, P., Hill, B., Ross, A., Hecksher-Sørensen, J., Baldock, R., Davidson, D., 2002. Optical Projection Tomography as a Tool for 3D Microscopy and Gene Expression Studies. Science 296, 541-545.

Shefelbine, S.J., Carter, D.R., 2004. Mechanobiological predictions of growth front morphology in developmental hip dysplasia. Journal of Orthopaedic Research 22, 346-352.

Silver, F.H., Glasgold, A.I., 1995. Cartilage wound healing. An overview. Otolaryngologic Clinics of North America 28, 847-864.

Sival, D., Visser, G., Prechtl, H., 1990. Does reduction of amniotic fluid affect fetal movements? Early human development 23, 233-246.

Steinmeyer, J., Ackermann, B., Raiss, R.X., 1997. Intermittent cyclic loading of cartilage explants modulates fibronectin metabolism. Osteoarthritis and Cartilage 5, 331-341.

Stevens, S.S., Beaupré, G.S., Carter, D.R., 1999. Computer model of endochondral growth and ossification in long bones: Biological and mechanobiological influences. Journal of Orthopaedic Research 17, 646-653.

Stevenson, D.A., Mineau, G., Kerber, R.A., Viskochil, D.H., Schaefer, C., Roach, J.W., 2009. Familial predisposition to developmental dysplasia of the hip. Journal of Pediatric Orthopaedics 29, 463-466.

Storm, E.E., Kingsley, D.M., 1996. Joint patterning defects caused by single and double mutations in members of the bone morphogenetic protein (BMP) family. Development 122, 3969-3979.

Strayer Jr, L.M., 1943. The embryology of the human hip joint. The Yale journal of biology and medicine 16, 13.

Tachdjian, M.O., Wenger, D.R., 1983. Congenital Dislocation of the Hip. Journal of Pediatric Orthopaedics 3, 254.

Tanck, E., Blankevoort, L., Haaijman, A., Burger, E.H., Huiskes, R., 2000. Influence of muscular activity on local mineralization patterns in metatarsals of the embryonic mouse. Journal of Orthopaedic Research 18, 613-619.

Tanck, E., Van Donkelaar, C.C., Jepsen, K.J., Goldstein, S.A., Weinans, H., Burger, E.H., Huiskes, R., 2004. The mechanical consequences of mineralization in embryonic bone. Bone 35, 186-190.

Tanck, E., Van Driel, W., Hagen, J., Burger, E., Blankevoort, L., Huiskes, R., 1999. Why does intermittent hydrostatic pressure enhance the mineralization process in fetal cartilage? Journal of Biomechanics 32, 153-161.

Torzilli, P.A., Grigiene, R., Huang, C., Friedman, S.M., Doty, S.B., Boskey, A.L., Lust, G., 1997. Characterization of cartilage metabolic response to static and dynamic stress using a mechanical explant test system. Journal of Biomechanics 30, 1-9.

Vaal, J., van Soest, A., Hopkins, B., 2000. Spontaneous kicking behavior in infants: Age-related effects of unilateral weighting. Developmental psychobiology 36, 111-122.

Ward, A., Pitsillides, A., 1998. Development Immobilization Induces Failure of Joint Cavity Formation by a Process Involving Selective Local Changes in Glycosaminoglycan Synthesis. Transactions of the annual meeting-orthopaedic research society, 199-199.

Witters, I., Moerman, P., Fryns, J.P., 2002. Fetal akinesia deformation sequence: a study of 30 consecutive in utero diagnoses. American journal of medical genetics 113, 23-28.

Wong, M., Carter, D., 1990a. A theoretical model of endochondral ossification and bone architectural construction in long bone ontogeny. Anat Embryol 181, 523-532.

Wong, M., Carter, D., 1990b. Theoretical stress analysis of organ culture osteogenesis. Bone 11, 127-131.

Wong, M., Ponticiello, M., Kovanen, V., Jurvelin, J., 2000. Volumetric changes of articular cartilage during stress relaxation in unconfined compression. Journal of Biomechanics 33, 1049-1054.

Woo, S.L.Y., Buckwalter, J.A., 1988. Injury and repair of the musculoskeletal soft tissues. Savannah, Georgia, June 18–20, 1987. Journal of Orthopaedic Research 6, 907-931.

Wynne-Davies, R., 1970. Acetabular dysplasia and familial joint laxity: two etiological factors in congenital dislocation of the hip A review of 589 patients and their families. Journal of Bone & Joint Surgery, British Volume 52, 704-716.

Yamamuro, T., Ishida, K., 1984. Recent advances in the prevention, early diagnosis, and treatment of congenital dislocation of the hip in Japan. Clinical Orthopaedics and Related Research 184, 24-40.

Ziegler, J., Thielemann, F., Mayer-Athenstaedt, C., Günther, K., 2008. The natural history of developmental dysplasia of the hip. A meta-analysis of the published literature. Der Orthopade 37, 515-516, 518-524.

9 Appendix 1 - Copyright Permissions

Figure Number	Type of work	Source work	Copyright holder & years	Work out of copyright
2.3	Figure	(Pacifici et al., 2005)	©2005 John Wiley and Sons	X
2.4	Figure	(Drachman et al., 1966)	©1966 Elsevier Limited	X
2.5	Figure	(Mikic et al., 2000)	©2005 John Wiley and Sons	X
2.6	Figure	(Tachdjian et al., 1983)	©1983 Wolters Kluwer Health	X
2.7	Figure	(Tachdjian et al., 1983)	©1983 Wolters Kluwer Health	X
2.8	Figure	(Ralis et al., 1973)	©	X
2.9	Figure	(Lee et al., 2006)	©2006 Elsevier Limited	X
2.10	Figure	(Tachdjian et al., 1983)	©1983 Wolters Kluwer Health	X
2.12	Figure	(Shefelbine et al., 2004)	©2006 John Wiley and Sons	X
2.13	Figure	(Heegaard et. al, 1999)	©2005 John Wiley and Sons	X
2.15	Figure	(Henderson et. al, 2002)	©2002 Elsevier Limited	X
3.1	Figure	(Heegaard et. al, 1999)	©2005 John Wiley and Sons	X
3.2	Figure	(Heegaard et. al, 1999)	©2005 John Wiley and Sons	X
3.3	Figure	(Heegaard et. al, 1999)	©2005 John Wiley and Sons	X
3.9	Figure	(Heegaard et. al, 1999)	©2005 John Wiley and Sons	X
3.25	Figure	(Mikic et al., 2000)	©2005 John Wiley and Sons	X
3.27	Figure	(Heegaard et. al, 1999)	©2005 John Wiley and Sons	X
5.13	Figure	(Heegaard et. al, 1999)	©2005 John Wiley and Sons	X

10 Appendix 2 - Published and under review papers

Journal of Biomechanics 47 (2014) 989–995

Contents lists available at ScienceDirect

Journal of Biomechanics

journal homepage: www.elsevier.com/locate/jbiomech
www.JBiomech.com

Mechanobiological simulations of prenatal joint morphogenesis

Mario Giorgi [a], Alessandra Carriero [a], Sandra J. Shefelbine [a,b], Niamh C. Nowlan [a,*]

[a] Department of Bioengineering, Imperial College London SW7 2AZ, UK
[b] Department of Mechanical and Industrial Engineering, Northeastern University, USA

ARTICLE INFO

Article history:
Accepted 6 January 2014

Keywords:
Joint shape
Cartilage growth
Chondrogenesis
Computational model
Joint biomechanics

ABSTRACT

Joint morphogenesis is the process in which prenatal joints acquire their reciprocal and interlocking shapes. Despite the clinical importance of the process, it remains unclear how joints acquire their shapes. In this study, we simulate 3D mechanobiological joint morphogenesis for which the effects of a range of movements (or lack of movement) and different initial joint shapes are explored. We propose that static hydrostatic compression inhibits cartilage growth while dynamic hydrostatic compression promotes cartilage growth. Both pre-cavitational (no muscle contractions) and post-cavitational (with muscle contractions) phases of joint development were simulated. Our results showed that for hinge type motion (planar motion from 45° to 120°) the proximal joint surface developed a convex profile in the posterior region and the distal joint surface developed a slightly concave profile. When 3D movements from 40° to −40° in two planes were applied, simulating a rotational movement, the proximal joint surface developed a concave profile whereas the distal joint surface rudiment acquire a rounded convex profile, showing an interlocking shape typical of a ball and socket joint. The significance of this research is that it provides new and important insights into normal and abnormal joint development, and contributes to our understanding of the mechanical factors driving very early joint morphogenesis. An enhanced understanding of how prenatal joints form is critical for developing strategies for early diagnosis and preventative treatments for congenital musculoskeletal abnormalities such as developmental dysplasia of the hip.

1. Introduction

Joint morphogenesis is the process in which a distinct and functional joint shape starts to appear during prenatal joint development. Pacifici et al. (2005) describe the process of synovial joint formation as a well-defined sequence of three events: (1) a layer of compact and closely associated mesenchymal cells form the interzone, (2) cavitation results in the physical separation of the adjacent skeletal elements within the interzone, and (3) joint shape occurs through the process of morphogenesis. Recent studies, however, have shown that joint morphogenesis starts before cavitation (Nowlan and Sharpe, advance online publication). The consequences of incomplete or abnormal morphogenesis can be debilitating, such as in the case of developmental dysplasia of the hip (DDH) which has a frequency of 5 per 1000 hips (Bialik et al., 1999). Despite the clinical relevance of joint morphogenesis there is very little understanding about the factors that drive the process (Pacifici et al., 2005).

A small number of studies have shown that foetal immobilisation can alter joint shape development. Studies using neuromuscular blocking agents to immobilise chicks embryos have found a reduction in width of the intercondylar fossa of the distal femur and of the proximal epiphysis of the tibiotarsus and fibula during knee joint morphogenesis (Roddy et al., 2011b), and up to a 50% reduction in the epiphyseal width of the proximal and distal regions of the knee, tibiotarsus and metatarsus (Osborne et al., 2002). Mikic et al. (2000) reported morphological abnormalities including joint fusion and non-interlocking joint shapes in the post-cavitational stages of joint development. Similarly, studies of genetically modified "muscleless limb" mice have revealed changes in joint morphogenesis, particularly in the elbow and shoulder (Kahn et al., 2009; Nowlan et al., 2010). Though it is clear that lack of motion affects joint shape morphogenesis, few studies have explored the role of motion or loading on joint shape in depth.

Only one computational study has explored the role of motion on joint morphogenesis (Heegaard et al., 1999). An idealised planar biomechanical model of the proximal interphalangeal joint was used to simulate epiphyseal growth using a modified version of the endochondral ossification theory proposed by Carter et al. (1987), in which growth and shape depends on the biological

* Corresponding author. Tel.: +44 0 2075945189.
E-mail address: n.nowlan@imperial.ac.uk (N.C. Nowlan).

http://dx.doi.org/10.1016/j.jbiomech.2014.01.002
0021-9290

growth (i.e. the intrinsic growth due to hormones, genes and nutrients), and mechanical growth (i.e. region-specific growth due to muscle, ligament and joint forces). The model predicted the development of congruent surfaces within the joint region and was the first mechanobiological simulation of any aspect of prenatal joint development. While the Heegaard et al. (1999) study was undeniably ground-breaking, there are a number of ways in which it can be advanced upon. Firstly, examining pre-cavitation time-points would show the influence of static loads before motion occurs. Morphogenesis has been shown to commence prior to cavitation (Nowlan and Sharpe, advance online publication), and therefore static loading prior to cavitation may play a role in early joint shape. Secondly, experimental studies indicate that static compressive loading inhibits cartilage growth (Burton-Wurster et al., 1993; Guilak et al., 1994) while cyclic compressive loading promotes growth (Kim et al., 1994; Korver et al., 1992; Parkkinen et al., 1992), and so a mechanobiological theory specific to these properties of cartilage growth would provide a significant insight. Finally, using multiple loading conditions and longer iteration times could enable a range of realistic joint shapes to be obtained.

In this study, we propose a 3D mechanobiological simulation of joint morphogenesis in which the effects of a range of movements and different initial joint shapes are explored. Following previous studies, growth and adaptation are directed by biological and mechanobiological factors. Both pre- and post-cavitational phases of joint development are simulated, representing static and dynamic loading phases respectively. Prior to the onset of spontaneous muscle contracts in the limb, we assume that pre-cavitational joints experience static loading due to growth related strains (Henderson and Carter, 2002). We use idealised shapes to represent a generic ball and socket joint and a generic hinge joint, and apply movement patterns typical for these joints in order to predict the effects on shape development. We also examine the effect of rigid paralysis on joint shape by growing a joint when no movement is applied.

2. Methods

2.1. Model geometry and material properties

Three idealised geometries of common joint configurations were created in Abaqus (Dassault Systemes, CAE module, version 6.12), where all configurations consisted of two opposing cartilage rudiments and a synovial capsule. A hinge joint configuration was composed of two cylindrical rudiments of the same dimensions with hemispherical opposing ends, with the distal rudiment at an initial angle of 45° to the vertical proximal rudiment, as shown in Fig. 1-A. A ball-and-socket configuration was composed of a distal cylindrical rudiment opposed to a flat proximal rudiment representing a bone such as the pelvis or shoulder, as shown in Fig. 1-B. A similar configuration to the hinge was used for the rigid paralysis configuration, except that the two rudiments were aligned, as shown in Fig. 1-C. As these configurations are intended to be generic and not to be representative of any particular species or animal, the initial dimensions (as shown in Fig. 1) were arbitrary, and size changes due to growth or adaptation were analysed as relative to the initial size. For the purposes of performing sensitivity analyses, 2D versions of the 3D models were used. The 2D models predicted the same geometrical changes as a midline longitudinal section of the 3D versions for the range of loading regimes.

The synovial capsule was modelled as a sphere surrounding the joint, (truncated at its extremes in order to decrease the number of elements) with a maximal diameter of 10 mm and large enough to contain the joint throughout movement sequences (Fig. 1-D). In order to quantify the effects of inclusion of the synovial capsule, 2D hinge simulations were run both with and without the capsule. Based on the stage of joint development being modelled, the rudiments were assumed to be fully cartilaginous (Gardner and O'Rahilly, 1968). All cartilage material properties were assumed to be linear elastic, isotropic and homogeneous. The Young's modulus for cartilage (E=1.1 MPa) was taken from four-point bending tests on un-mineralised embryonic mouse ribs (Tanck et al., 2004) and the cartilage Poisson's ratio taken as ν=0.49 to reflect the incompressibility of the fluid in the cartilage at short time scales (Armstrong et al., 1984; Carter and Beaupré, 1999; Wong et al., 2000). The Young's modulus of the synovial capsule was E=0.287 kPa (Roddy et al., 2011a), and its Poisson's ratio was ν=0.4 (McCarty et al., 2011).

2.2. Loading conditions

In all models, the proximal rudiment was fixed at its proximal end. At rest, the bottom rudiment was located 0.2 mm from the top rudiment's lower surface (Fig. 1). Static and dynamic loading were represented by an applied displacement of the distal rudiment towards the proximal (upper fixed) rudiment. In the pre-cavitational phase, prior to the onset of muscle contractions, static loading due to growth-related strains (Henderson and Carter, 2002) was represented by the constant application of an axial displacement on the distal rudiment towards the proximal rudiment in the starting configuration. In the post-cavitational phase, after the onset of muscle contractions, joint loads were represented by a number of steps during which a displacement was applied to the lower surface of the distal rudiment towards the proximal element, with the angle and position of the displacement determined by the type of movement being applied. The magnitude of the displacement applied, 10 μm, remained constant throughout all simulations. Based on approximations of muscle cross sectional area (as a percentage of rudiment width) and allowable maximum embryonic muscle stress of S= 1.11 mN/mm^2 (Nowlan et al., 2008), we estimated the likely muscle force to be on the order of 0.1 mN. An applied displacement of 10 μm resulted in a force of approximately this magnitude. In the absence of data on the magnitude of growth related strains in the developing joint, the same displacement was used for the static phase. Two static iterations (pre-cavitation with no motion) and eight dynamic iterations (post-cavitation with motion) were included in the hinge and ball-and-socket simulations. In the hinge model, a single plane motion was applied from 45° to 120° in each iteration, as shown in Fig. 1-A, at angles of 45°, 90° and 120°, while the ball-and-socket model was loaded under a multi-plane motion

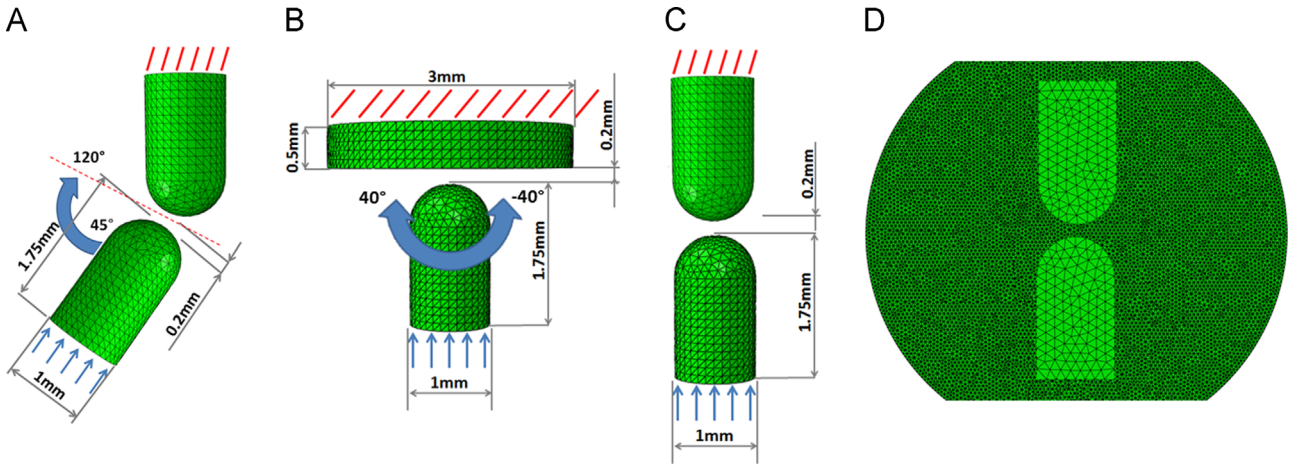

Fig. 1. Configuration of the models. (A) Hinge model configuration, with the initial rudiment at an initial angle of 45° to the vertical proximal rudiment. (B) Ball-and-socket configuration with a distal cylindrical rudiment opposed to a flat proximal rudiment. (C) Rigid paralysis configuration, the two rudiments are aligned along their vertical axis. (D) Section of the rigid paralysis configuration with synovial capsule.

from 40° to 0° to −40° in two planes perpendicular to each other as shown in Fig. 1-B. Rigid paralysis, where the muscles are in continuous tetanus (Roddy et al., 2011b) was represented by the constant application of an axial displacement, as shown in Fig. 1-C, assumed to be static loading due to the lack of dynamic muscle contractions. The paralysis model was also run in 2D with the distal rudiment at −60° to the proximal rudiment. Frictionless impenetrable contact was modelled between all the components of the models.

2.3. Growth rate

Growth and morphogenesis of the rudiments were controlled by biological and mechanical growth rates so that the growth rate $d\varepsilon/dt$ was as follows:

$$\frac{d\varepsilon}{dt}=\frac{d(\varepsilon_b)}{dt}+\frac{d(\varepsilon_m)}{dt}$$

with $\dot{\varepsilon}_b$ the biological contribution to growth and $\dot{\varepsilon}_m$ the mechanical contribution to growth (Shefelbine and Carter, 2004). Following Heegaard et al. (1999), $\dot{\varepsilon}_b$ was considered to be proportional to the chondrocyte density. The equation for local chondrocyte density along the long axis of a rudiment was calculated by Heegaard et al. (1999) by fitting a polynomial curve to the grey level distribution on a sagittal micrograph of a joint, where darker areas indicated higher chondrocyte density. The chondrocyte density C_d is greater towards the ends of the rudiments and lower towards the diaphysis, and therefore expressed by the formula

$$\dot{\varepsilon}_b = C_d = k(0.14-0.87\xi+4.40\xi^2-2.66\xi^3)$$

with C_d being the chondrocyte density, $k=11\times10^3$ being a constant determining the amount of biological growth, which is maintained in the range of 75–85% of the total growth (Germiller and Goldstein, 1997), and ξ the distance along the proximal-distal axis of the rudiment starting from the distal end (Heegaard et al., 1999). The biological contribution to growth was assumed to be constant during static and dynamic loading phases. The effects of alternative equations for the chondrocyte density were also analysed in 2D versions of the hinge simulation.

The mechanical growth rate, $\dot{\varepsilon}_m$, was proportional to the compressive hydrostatic stress, σ_h. Previous experimental studies have found that static compression significantly inhibits the synthesis of cartilage matrix proteins (Burton-Wurster et al., 1993; Guilak et al., 1994) while dynamic compression stimulates matrix production (Kim et al., 1994; Korver et al., 1992; Parkkinen et al., 1992). Accordingly, we implemented a mechanobiological theory in which static hydrostatic compression inhibits cartilage growth while dynamic hydrostatic compression promotes cartilage growth. The mechanobiological growth rate was also considered to be proportional to the chondrocyte density, based on the assumption that the greater the number of cells, the greater the adaptation to mechanical loading. The overall mechanobiological contribution to growth was therefore calculated at each node of the model as the average stresses throughout a full joint motion using the formulae below

$$\dot{\varepsilon}_m = C_d\left(\frac{\sum_{i=1}^{N}\sigma_{hi}}{N}\right), \text{for static loads}$$

$$\dot{\varepsilon}_m = -C_d\left(\frac{\sum_{i=1}^{N}\sigma_{hi}}{N}\right), \text{for dynamic loads}$$

where σ_h is the compressive hydrostatic stress, N the number of movement per step and C_d the chondrocyte density.

2.4. Model implementation

During each iteration, the orthonormal thermal expansion capabilities of the FE solver were utilised to allow isotropic expansion of the proximal and distal rudiments with the sum of the biological and mechanobiological growth rates used as the 'temperature' for expansion. This expansion occurred within an unconstrained volume, representing the growth of the entire limb, which ensured that the mechanical stresses due to motion were the dominant stimulus for shape change rather than stresses due to contact of the two rudiments during growth. The new geometry was then re-meshed and the two rudiments were automatically realigned, so that the loading conditions could be applied again for another step of growth. The size and shape of the synovial capsule remained the same for the entire simulation. A simulation using biological growth rates only was also performed for comparative purposes.

3. Results

3.1. Hydrostatic stress distribution

In all the models, the hydrostatic stresses close to the contact regions were always compressive, as shown in Fig. 2. High compressive hydrostatic stresses were also seen at the anterior corner of the proximal rudiment of the hinge model due to the fixed boundary condition (Fig. 2, arrows). The simulation in which rigid paralysis was modelled induced a symmetric stress pattern on the rudiments, as shown in the first (static) phase of the hinge simulation (Fig. 2, left).

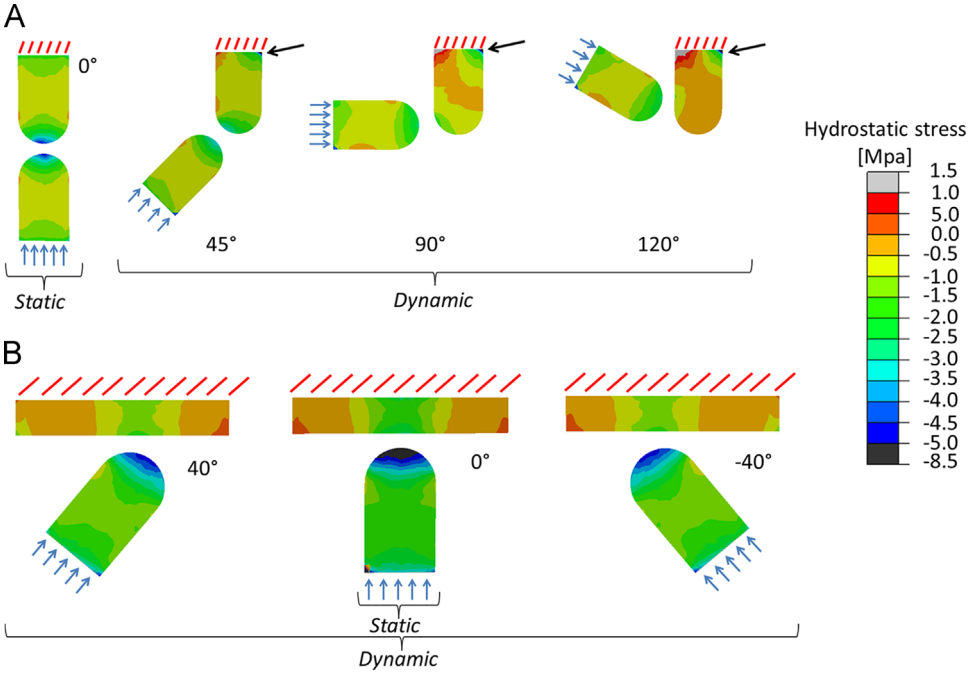

Fig. 2. Hydrostatic stress distribution during the first step of static and dynamic loading for the (A) hinge and the (B) ball-and-socket joint, respectively. In both joint models, the highest hydrostatic compression stresses are seen within the region of contact between the two rudiments.

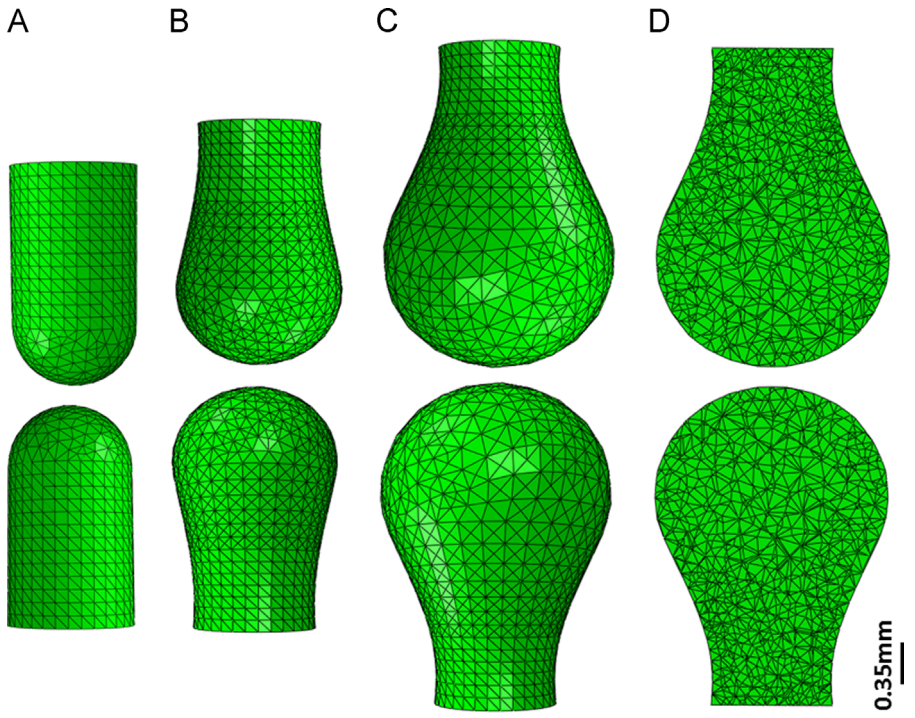

Fig. 3. Joint morphogenesis prediction when only the biological contribution to growth was considered. (A) Sagittal view of the initial model. (B) Sagittal view of the predicted joint shape after 2 steps. (C) Sagittal view of the predicted joint shape after 10 steps of growth. (D) Sagittal section after 10 steps of growth. Scale bar = 0.35 mm.

3.2. Morphogenesis

When biological growth alone was applied, the rudiments preserved their initial opposing convex surfaces as shown in Fig. 3. In contrast, when the mechanical stimulus was included in the simulation, the shape of the predicted growing joints changed according to the movement pattern applied. When a single plane motion from 45° to 120° was applied, the proximal rudiment showed a rounded convex profile in both posterior and anterior regions, with more pronounced growth posteriorly (Fig. 4, arrowhead). The distal rudiment showed similar features with a less pronounced rounded convex profile in its posterior region and the acquisition of a slight concave profile in the mid-line section (Fig. 4, arrow). When a multi-plane motion from 40° to −40° degrees was applied between a flat and a cylindrical rudiment, the flat rudiment showed a concave profile which partially enclosed the rounded convex profile of the cylindrical rudiment (Fig. 5). When only axial forces were applied under static loading conditions, reproducing rigid paralysis, both the rudiments acquired a flat shape within the joint region as shown in Fig. 6, similar to the experimental results of Mikic et al. (2000). Flat opposing surfaces were also predicted when the same simulation was run in 2D with the distal rudiment at −60° to the proximal rudiment (data not shown).

3.3. Sensitivity analyses

When simulations were run without a synovial capsule, small differences in shape were found due to stress concentrations at the contact regions, but similar patterns of growth for the models with and without synovial capsule were predicted. Similarly, when a linear approximation of the polynomial equation for chondrocyte density was used there was no major effect on joint shape or growth. Analysis of the effects of varying the relative influence of the biological and mechanobiological contributions demonstrated that with a higher biological contribution, the mechanobiological contribution was too low to have an influence on the total growth and joint morphology. With a lower weighting for the biological contribution, the effects of the mechanobiological stimulus were more evident with more extreme changes at the epiphyses and decreased growth overall (data not shown for sensitivity analyses).

4. Discussion

We have developed the first 3D mechanobiological models of prenatal joint shape development, which are capable of predicting a range of joint shapes based on the starting joint configuration and applied movements.

When a hinge movement from 45° to 120° was applied, the proximal rudiment acquired a rounded convex profile in its posterior and anterior regions with a more pronounced growth posteriorly, and the distal rudiment acquired a slight concave profile in the middle, as shown in Fig. 4, suggesting the generation of an interlocking joint shape such as the knee. When a rotational movement from 40° to −40° was applied, the proximal rudiment developed a clear concave profile in which the rounded convex profile of the distal rudiment was contained at its proximal end, as shown in Fig. 5, suggesting the generation of an interlocking joint shape such as the hip or shoulder joint. When only axial forces were applied under static loading conditions, reproducing rigid paralysis, both the rudiments acquired a flat shape within the joint region (Fig. 6) similar to the experimental results of Mikic et al. (2000) for the immobilised interphalangeal joint.

Based on recent evidence that joint shape initiates prior to cavitation (Nowlan and Sharpe, advance online publication), we have modelled the development of the joint under both static and dynamic loads, characteristic of pre- and post- cavitation, respectively. We have developed a novel mechanobiology theory of cartilage growth, based on experimental evidence from *in vitro* stimulation of chondrocytes (Burton-Wurster et al., 1993; Guilak et al., 1994; Kim et al., 1994; Korver et al., 1992; Parkkinen et al., 1992). Despite the abundance of mechanobiological theories and mechanobiological simulations relating to endochondral

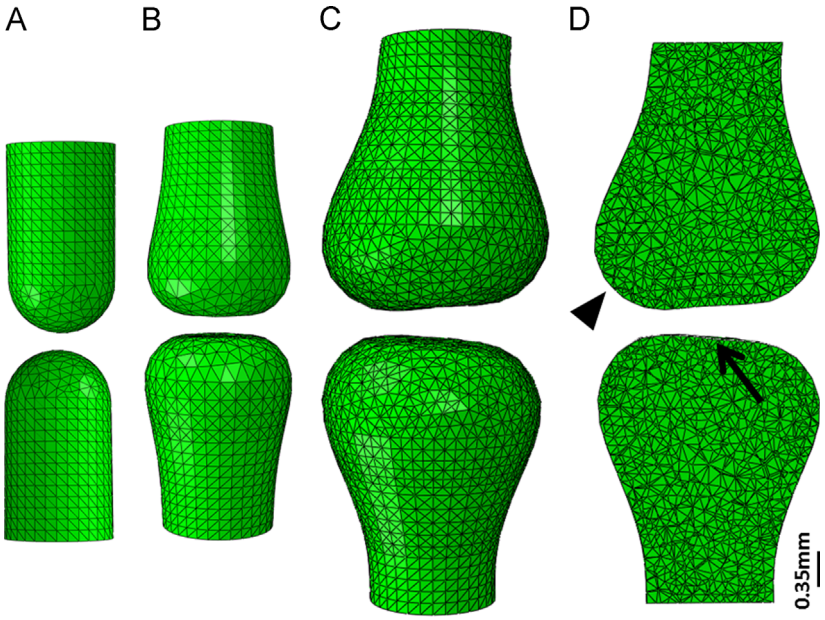

Fig. 4. Joint morphogenesis prediction when a single plane motion from 45° to 120° is applied. (A) Sagittal view of the initial model. (B) Sagittal view of the predicted joint shape after 2 static steps of growth. (C) Sagittal view of the predicted joint shape after 2 static and 8 dynamic steps of growth. (D) Sagittal section after 2 static+8 dynamic steps of growth. Scale bar=0.35 mm.

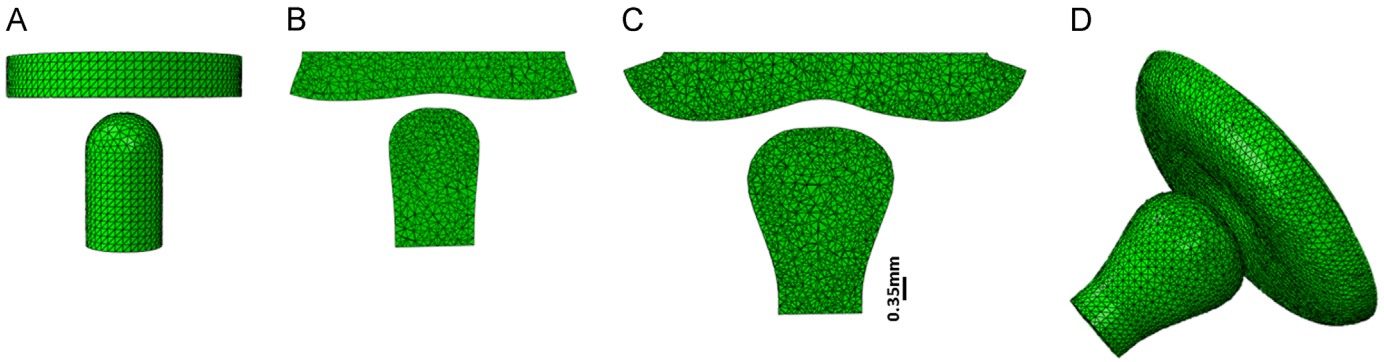

Fig. 5. Joint morphogenesis prediction when a multi plane motion from 40° to −40° is applied. (A) Sagittal view of the initial model. (B) Sagittal section of the predicted joint shape after 2 static steps of growth. (C) Sagittal section of the predicted joint shape after 2 static and 8 dynamic steps of growth. (D) Rotated view after 2 static+8 dynamic steps of growth. Scale bar=0.35 mm.

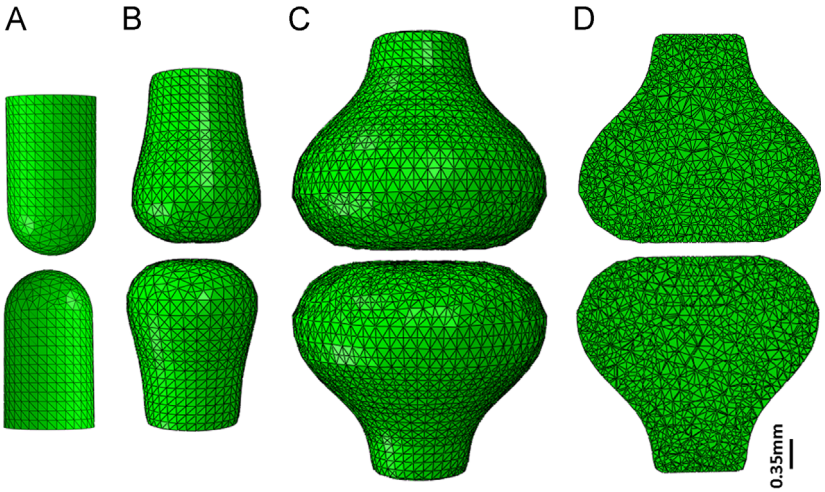

Fig. 6. Joint morphogenesis when the rigid paralysis was simulated. (A) Sagittal view of the initial model. (B) Sagittal view of the predicted joint shape after 2 static steps of growth. (C) Sagittal view of the predicted joint shape after 10 static steps of growth. (D) Sagittal section after 10 static steps of growth. Scale bar=0.35 mm.

ossification (Carter et al., 1998; Claes and Heigele, 1999; Huiskes et al., 1997; Lacroix and Prendergast, 2002; Lacroix et al., 2002; Prendergast et al., 1997; Sarin and Carter, 2000; Stevens et al., 1999), we are unaware of any mechanoregulation algorithm specific to cartilage growth in a non-endochondral ossification context. The growth law proposed by Heegaard et al. (1999) was based upon a theory developed for endochondral ossification (Carter et al., 1987), where hydrostatic compressive stress inhibits and tensile stress promotes cartilage growth and ossification. In contrast, our simulations focus specifically on joint epiphyses which are entirely cartilaginous at the stages modelled (Gardner and O'Rahilly, 1968), and it is likely that the mechanical stimuli for growth and adaptation of epiphyseal cartilage are different than those which influence endochondral growth and ossification. These two processes are biologically distinct, as growth at the growth plate is primarily due to chondrocyte hypertrophy (Kronenberg, 2003), while cartilage growth at the epiphysis is likely due to cell proliferation (Pacifici et al., 2005). Therefore, the mechanobiological growth law proposed here is specific to epiphyseal cartilage and is based upon experimental data showing that cyclic hydrostatic compression stimulates matrix production (Kim et al., 1994; Korver et al., 1992; Parkkinen et al., 1992) and static compression inhibits the synthesis of cartilage matrix proteins (Burton-Wurster et al., 1993; Guilak et al., 1994). However, the new theory which we propose in not in conflict with the theories previously proposed for growth plate cartilage, as in both cases, compression provides a favourable environment for cartilage. In endochondral ossification, hydrostatic compression maintains the cartilage at the growth plate, while during epiphyseal cartilage growth, hydrostatic compression promotes the formation of more cartilage. This new theory for cartilaginous joint morphogenesis differentiates between static and dynamic loading conditions, where static compressive loading inhibits cartilage growth while dynamic compressive loading promotes it. In proposing a mechanobiological theory for epiphyseal cartilage growth and adaptation, we offer a biomechanical understanding of the influence of mechanical loading on joint morphogenesis.

Material properties of synovial capsule and cartilage were assumed to be linear elastic, isotropic and homogeneous. Although cartilage is a biphasic material (Roddy et al., 2011a), and the synovial capsule is also likely to be the same (Roddy et al., 2011a), we modelled our cartilage as single phase and near incompressible (Poisson′s ratio of 0.49), based on previous studies which showed that the fluid pressure in biphasic models is comparable to the hydrostatic stress in the single phase models when loaded at frequencies of 1 Hz (Carter and Wong, 2003; Shefelbine and Carter, 2004), which is close to the frequency of muscle contraction in utero (Vaal et al., 2000) Muscles and ligaments were not explicitly modelled as acting at specific location of the rudiment. However, since our models are of generic joint shapes and configurations, and do not apply to one specific species (or even limb) we focussed on the joint motion likely to result from approximations of common movement sequences.

In conclusion, this study presents how stresses generated during static growth-related loading and dynamic post-cavitational movements can influence prenatal joint morphogenesis. This study predicts joint shape morphogenesis in 3D using a novel mechanobiology theory for cartilage growth. Our simulations predict a range of anatomically recognisable joint shapes based on the starting joint configuration and applied movement. The significance of this research is that it provides new and important insights into normal and abnormal joint development. Understanding the factors driving joint morphogenesis at a very early stage is critical for developing strategies for early diagnosis and preventative treatments for congenital musculoskeletal abnormalities, such as developmental dysplasia of the hip.

Conflict of interest

The authors have no conflicts of interests relating to this research.

Acknowledgements

This research was funded by a Departmental Studentship from the Department of Bioengineering at Imperial College London.

References

Armstrong, C.G., Lai, W.M., Mow, V.C., 1984. An analysis of the unconfined compression of articular cartilage. J. Biomech. Eng. 106, 165–173.
Bialik, V., Bialik, G.M., Blazer, S., Sujov, P., Wiener, F., Berant, M., 1999. Developmental dysplasia of the hip: a new approach to incidence. Pediatrics 103, 93–99.
Burton-Wurster, N., Farquhar, V.-S.M., Lust G., T., 1993. Effect of compressive loading and unloading on the synthesis of total protein, proteoglycan, and fibronectin by canine cartilage explants. J. Orthop. Res. 11, 717–729.
Carter, D., Orr, T., Fyhrie, D., Schurman, D., 1987. Influences of mechanical stress on prenatal and postnatal skeletal development. Clin. Orthop. Relat 15, 237–250.
Carter, D., Wong, M., 2003. Modelling cartilage mechanobiology. R. Soc. 358, 1461–1471.
Carter, D.R., Beaupré, G.S., 1999. Linear elastic and poroelastic models of cartilage can produce comparable stress results: a comment on Tanck et al. J. Biomech. 32, 153–161.
Carter, D.R., Beaupré, G.S., Giori, N.J., Helms, J.A., 1998. Mechanobiology of skeletal regeneration. Clin. Orthop. Relat. Res. 355, S41–S55.
Claes, L.E., Heigele, C.A., 1999. Magnitudes of local stress and strain along bony surfaces predict the course and type of fracture healing. J. Biomech. 32, 255–266.
Gardner, E., O'Rahilly, R., 1968. The early development of the knee joint in staged human embryos. J. Anat. 102, 289–299.
Germiller, J.A., Goldstein, S.A., 1997. Structure and function of embryonic growth plate in the absence of functioning skeletal muscle. J. Orthop. Res. 15, 362–370.
Guilak, F., Meyer, B.C., Ratcliffe, A., Mow, V.C., 1994. The effects of matrix compression on proteoglycan metabolism in articular cartilage explants. Osteoarthr. Cartil. 2, 91–101.
Heegaard, J.H., Beaupré, G.S., Carter, D.R., 1999. Mechanically modulated cartilage growth may regulate joint surface morphogenesis. J. Orthop. Res. 17, 509–517.
Henderson, J.H., Carter, D.R., 2002. Mechanical induction in limb morphogenesis: the role of growth-generated strains and pressures. Bone 31, 645–653.
Huiskes, R., Driel, W.D.V., Prendergast, P.J., SØBalle, K., 1997. A biomechanical regulatory model for periprosthetic fibrous-tissue differentiation. J. Mater. Sci.: Mater. Med. 8, 785–788.
Kahn, J., Shwartz, Y., Blitz, E., Krief, S., Sharir, A., Breitel, D.A., Rattenbach, R., Relaix, F., Maire, P., Rountree, R.B., Kingsley, D.M., Zelzer, E., 2009. Muscle contraction is necessary to maintain joint progenitor cell fate. Dev. Cell 16, 734–743.
Kim, Y.J., Sah, R.L.Y., Grodzinsky, A.J., Plaas, A.H.K., Sandy, J.D., 1994. Mechanical regulation of cartilage biosynthetic behavior: physical stimuli. Arch. Biochem. Biophys. 311, 1–12.
Korver, T.H., Van de Stadt, R.J., Kiljan, E., Van Kampen, G.P., Van der Korst, J.K., 1992. Effects of loading on the synthesis of proteoglycans in different layers of anatomically intact articular cartilage in vitro. J. Rheumatol. 19, 905–912.
Kronenberg, H.M., 2003. Developmental regulation of the growth plate. Nature.
Lacroix, D., Prendergast, P.J., 2002. A mechano-regulation model for tissue differentiation during fracture healing: analysis of gap size and loading. J. Biomech. 35, 1163–1171.
Lacroix, D., Prendergast, P.J., Li, G., Marsh, D., 2002. Biomechanical model to simulate tissue differentiation and bone regeneration: application to fracture healing. Med. Biol. Eng. Comput. 40, 14–21.
McCarty, W.J., Masuda, K., Sah, R.L., 2011. Fluid movement and joint capsule strains due to flexion in rabbit knees. J. Biomech. 44, 2761–2767.
Mikic, B., Wong, M., Chiquet, M., Hunziker, E.B., 2000. Mechanical modulation of tenascin-C and collagen-XII expression during avian synovial joint formation. J. Orthop. Res. 18, 406–415.
Nowlan, N.C., Bourdon, C., Dumas, G., Tajbakhsh, S., Prendergast, P.J., Murphy, P., 2010. Developing bones are differentially affected by compromised skeletal muscle formation. Bone 46, 1275–1285.
Nowlan, N.C., Murphy, P., Prendergast, P.J., 2008. A dynamic pattern of mechanical stimulation promotes ossification in avian embryonic long bones. J. Biomech. 41, 249–258.
Nowlan, N.C., Sharpe, J., Joint shape morphogenesis precedes cavitation of the developing hip joint. J. Anat, http://dx.doi.org/10.1111/joa.12143, in press.
Osborne, A.C., Lamb, K.J., Lewthwaite, J.C., Dowthwaite, G.P., Pitsillides, A.A., 2002. Short-term rigid and flaccid paralyses diminish growth of embryonic chick limbs and abrogate joint cavity formation but differentially preserve pre-cavitated joints. J. Musculoskelet. Neuronal Interact. 2, 448–456.

Pacifici, M., Koyama, E., Iwamoto, M., 2005. Mechanisms of synovial joint and articular cartilage formation: recent advances, but many lingering mysteries. Birth Defects Res. Part C: Embryo Today: Rev. 75, 237–248.
Parkkinen, J.J., Lammi, M.J., Helminen, H.J., Tammi, M., 1992. Local stimulation of proteoglycan synthesis in articular cartilage explants by dynamic compression in vitro. J. Orthop. Res. 10, 610–620.
Prendergast, P.J., Huiskes, R., Søballe, K., 1997. Biophysical stimuli on cells during tissue differentiation at implant interfaces. J. Biomech. 30, 539–548.
Roddy, K.A., Kelly, G.M., van Es, M.H., Murphy, P., Prendergast, P.J., 2011a. Dynamic patterns of mechanical stimulation co-localise with growth and cell proliferation during morphogenesis in the avian embryonic knee joint. J. Biomech. 44, 143–149.
Roddy, K.A., Prendergast, P.J., Murphy, P., 2011b. Mechanical influences on morphogenesis of the knee joint revealed through morphological, molecular and computational analysis of immobilised embryos. PLoS ONE 6, e17526.
Sarin, V.K., Carter, D.R., 2000. Mechanobiology and joint conformity regulate endochondral ossification of sesamoids. J. Orthop. Res. 18, 706–712.
Shefelbine, S.J., Carter, D.R., 2004. Mechanobiological predictions of growth front morphology in developmental hip dysplasia. J. Orthop. Res. 22, 346–352.
Stevens, S.S., Beaupré, G.S., Carter, D.R., 1999. Computer model of endochondral growth and ossification in long bones: biological and mechanobiological influences. J. Orthop. Res. 17, 646–653.
Tanck, E., Van Donkelaar, C.C., Jepsen, K.J., Goldstein, S.A., Weinans, H., Burger, E.H., Huiskes, R., 2004. The mechanical consequences of mineralization in embryonic bone. Bone 35, 186–190.
Vaal, J., van Soest, A.J.K., Hopkins, B., 2000. Spontaneous kicking behavior in infants: age-related effects of unilateral weighting. Dev. Psychobiol. 36, 111–122.
Wong, M., Ponticiello, M., Kovanen, V., Jurvelin, J.S., 2000. Volumetric changes of articular cartilage during stress relaxation in unconfined compression. J. Biomech. 33, 1049–1054.

www.elsevier.com/locate/jbiomech

Effects of normal and abnormal loading conditions on morphogenesis of the prenatal hip joint: application to hip dysplasia

Mario Giorgi, Alessandra Carriero, Sandra J. Shefelbine, Niamh C. Nowlan

PII: S0021-9290(15)00339-5
DOI: http://dx.doi.org/10.1016/j.jbiomech.2015.06.002
Reference: BM7203

To appear in: *Journal of Biomechanics*

Received date: 29 January 2015
Revised date: 4 June 2015
Accepted date: 15 June 2015

Cite this article as: Mario Giorgi, Alessandra Carriero, Sandra J. Shefelbine and Niamh C. Nowlan, Effects of normal and abnormal loading conditions on morphogenesis of the prenatal hip joint: application to hip dysplasia, *Journal of Biomechanics,* http://dx.doi.org/10.1016/j.jbiomech.2015.06.002

Title: Effects of normal and abnormal loading conditions on morphogenesis of the prenatal hip joint: application to hip dysplasia

Authors: Mario Giorgi[1], Alessandra Carriero[1,2], Sandra J. Shefelbine[1,3], Niamh C. Nowlan[1]

[1] Department of Bioengineering, Imperial College London, UK

[2] Department of Biomedical Engineering, Florida Institute of Technology, USA

[3] Department of Mechanical and Industrial Engineering, Northeastern University, USA

Corresponding Author: Dr. Niamh C. Nowlan
Department of Bioengineering
Imperial College London
London, SW7 2AZ, UK
Email: n.nowlan@imperial.ac.uk
Tel: +44 (0) 2075945189

Word count: 3500

Keywords: joint shape; joint biomechanics; joint development; developmental dysplasia of the hip; DDH; computational model;

Abstract

Joint morphogenesis is an important phase of prenatal joint development during which the opposing cartilaginous rudiments acquire their reciprocal and interlocking shapes. At an early stage of development, the prenatal hip joint is formed of a deep acetabular cavity that almost totally encloses the head. By the time of birth, the acetabulum has become shallower and the femoral head has lost substantial sphericity, reducing joint coverage and stability. In this study, we use a dynamic mechanobiological simulation to explore the effects of normal (symmetric), reduced and abnormal (asymmetric) prenatal movements on hip joint shape, to understand their importance for postnatal skeletal malformations such as developmental dysplasia of the hip (DDH). We successfully predict the physiological trends of decreasing sphericity and acetabular coverage of the femoral head during fetal development. We show that a full range of symmetric movements helps to maintain some of the acetabular depth and femoral head sphericity, while reduced or absent movements can lead to decreased sphericity and acetabular coverage of the femoral head. When an abnormal movement pattern was applied, a deformed joint shape was predicted, with an opened asymmetric acetabulum and the onset of a malformed femoral head. This study provides evidence for the importance of fetal movements in the prevention and manifestation of congenital musculoskeletal disorders such as DDH.

Introduction

During prenatal joint development, the two opposing cartilaginous rudiments of a joint develop their reciprocal and interlocking shapes through a process known as morphogenesis (Pacifici et al., 2005). Joint morphogenesis is a continuous process which commences prior to, and continues after, joint cavitation (Nowlan and Sharpe, 2014). Human hip joint morphogenesis has been described by Ralis and McKibbin (1973). At gestational week 11, a globular femoral head is almost completely enclosed by a deep-set acetabulum. From that time until birth, the acetabulum becomes shallower and the femoral head loses substantial sphericity, becoming more hemi-spherical. The coverage of the femoral head is at its lowest at birth (Ráliš and McKibbin, 1973), which most likely means that the hip joint is at its most unstable shape at this time. Alterations of the normal process of joint morphogenesis are highly relevant to postnatal skeletal malformations, particularly to developmental dysplasia of the hip (DDH). DDH occurs when the hip joint is malformed, unstable or dislocated, and occurs in 1.3 per 1000 births (Leck, 2000). Two types of dislocation have been defined (American Academy of Pediatrics, 2000). Teratologic dislocations occur early in utero, and are usually associated with neuromuscular abnormalities, while typical dislocations occur *in utero* or after birth in otherwise healthy infants. In the most severe cases of DDH, the femoral head is completely dislocated from the acetabulum, while in less severe manifestations, the femoral head is partially dislocated or easily dislocatable from the acetabulum (Ponseti, 1978). The risk of DDH increases with abnormal fetal movements or suboptimal intrauterine conditions. Fetal breech position, particularly extended breech where the hips are flexed and knees extended, has been shown to increase the risk of hip instability and dysplasia (Luterkort et al., 1986; Muller and Seddon, 1953). Portinaro et al. (1994) hypothesised that ligamentous laxity or malpositioning in utero can lead to abnormal joint loading, where the femoral head can displace and encourage deformity. First-born infants are twice as likely to

be affected by DDH compared with the successive siblings (Record and Edwards, 1958), likely due to a narrower intra-uterine cavity in these pregnancies (Hinderaker et al., 1994). It has been proposed that the reason why the left hip has a higher risk of DDH than the right is due to the common position of the fetal left leg beside the mother's spine, which limits hip abduction (Aronsson et al., 1994; Ward and Pitsillides, 1998).

Despite the acknowledged influence of fetal movements on hip joint formation, the mechanism by which these movements affect joint morphogenesis is still unknown. Previous studies suggest that prenatal joint growth and shape depend on two major factors, the biological (i.e. intrinsic) growth, due to hormones, genes and nutrients, and the mechanobiological growth, due to muscle, ligament and joint forces (Giorgi et al., 2014; Heegaard et al., 1999). In this study, we develop a mechanobiological simulation of prenatal hip joint morphogenesis with which to propose and test hypotheses on how fetal movements impact upon the shape of the developing hip joint, in order to provide new insights into the normal physiology of joint morphogenesis and into the etiology of DDH. We predict growth and shape change of an idealised hip joint, correlate our predictions with human hip joint shape data, and investigate the effects of reduced, or asymmetric, movement at various stages of fetal development. We hypothesise that reduced movements due to suboptimal intrauterine conditions, or asymmetric loading on the acetabulum due to fetal breech position or increased joint laxity, may negatively influence hip joint shape at birth.

Methods

Model geometry and material properties

An idealised 2D geometry of a simplified hip joint was created in Abaqus (Dassault Systemes, CAE module, version 6.12). The joint consisted of two opposing cartilage rudiments: the proximal femur and the pelvis, which included a concave acetabular region

(Figure 1-A). The interlocking shape was designed with the same proportions of a human hip joint at gestational week (GW) 11 of development (Ráliš and McKibbin, 1973), while the initial dimensions were arbitrary (Figure 1-A). The initial depth-to-diameter ratio of the acetabulum was approximately 75%, and the femoral head perfectly matched the acetabular shape with a height-to-diameter ratio of approximately 85% (Figure 1-A, B). The junction of the three cartilagineous ends of the ilium, ischium and pubis, known as the triradiate cartilage, is the site of radial acetabular growth during the fetal period (Portinaro et al., 1994; Scheuer and Black, 2004). The femoral head does not undergo secondary ossification until after birth (Scheuer and Black, 2004), and the models were entirely cartilaginous for the duration of the simulations. Cartilage (E= 1.1 MPa, υ =0.49) (Tanck et al., 2004; Wong et al., 2000) was assumed to be linear elastic, isotropic and homogeneous (Carter and Beaupre, 1999; Shefelbine and Carter, 2004).

Movements and boundary conditions

The pelvis was fixed for all translations and rotations at its proximal end and at its sides. In the case of normal (symmetric) movement, the shaft of the femur was initially aligned with the vertical axis of the pelvis in order to obtain a perfect match between the femoral head and the acetabulum (Figure 1-A). The explicit module of Abaqus (Dassault Systemes, CAE module, version 6.12) was used to simulate dynamic joint movements by applying a rotation to the centre of the femoral head. A complete cycle of motion included four different phases, a pre-load phase followed by three rotations of the femoral head around its centre. During the pre-load phase, an axial displacement of 1μm was applied on the distal rudiment towards the proximal rudiment, and this displacement was maintained through the entire motion to generate contact between the two rudiments. The three rotations were as follows: 1) anticlockwise rotation of the femoral head, from the midline position to the extreme left; 2) clockwise rotation, from left to right; 3) anticlockwise rotation of the femoral head to the

initial midline position. Frictionless, impenetrable contact was modelled between the two components of the model.

Growth and morphogenesis of the hip joint from GW 11 to birth were modelled with 28 cycles, where one cycle was equivalent to approximately one week. Two variables were identified as decreasing over the course of development, namely the rate of fetal growth (and therefore the rate of *rudiment expansion*) and the *range of hip motion* (Figure 1-C). By plotting the fetal weight change (Doubilet et al., 1997) on a logarithmic scale, we identified three stages during which the fetus grows at different rates (Figure 1-C), namely: 1) early stage, from GW 11 to 18; 2) middle stage, from GW 19 to 34; 3) late stage, from GW 35 to birth. The rate of *rudiment expansion* in the model was adapted according to the rate of fetal growth (Figure 1-C) and was implemented by varying the orthonormal thermal expansion capabilities of the finite element solver.

There is very little information on the range of motion of the prenatal hip joint. However, fetal cine-MRI can now be used for viewing and assessing fetal movements (Hayat et al., 2011). Using fetal cine-MRI data obtained from our collaborators (Profs Hajnal and Rutherford, King's College London, UK), we were able to make a realistic estimate of the range of motion at the hip over gestation. Five MR images sequences, corresponding to 5 subjects, were analysed and the maximum range of hip motion over the 1.5 minute average time frame of the scan was calculated. Scans were taken with a slice thickness of 30-40 mm (Hayat et al., 2011). The angle generated by the intersection of the spine line and the longitudinal axis of the femur was used to quantify the hip motion as shown in Figure 2-A, B. All the image sequences belonged to the middle stage of development: three in the early-middle (GW: 21- 22) and two in the late-middle (GW: 29, 34) stages. The first set showed a maximum range of motion of 90° with an average value over the three sequences of 52°. The second set showed a maximum range of motion of 15° with an average value of 12.5°.

Because all the scans belonged to the middle stage, we assumed higher and lower range of motion for the early and late stages, with an intermediate value for the middle stage. Therefore, symmetrical movements from +/- 40° in the early stage, +/- 30° in the middle stage, and +/- 5° in the late stage were used to simulate the physiological range of hip motion over the course of development. In addition to physiological loading conditions, we explored the effects of altering movement patterns. Reduced movements were simulated by decreasing joint motion by approximately 80% at each of the three stages of development, as described in Table 1. Absent movements were simulated by retaining the femoral head in its initial position for the entire simulation without any rotation applied (but still maintaining the pre-load compression). The effects of asymmetric movements were also simulated. Asymmetric movements differed from symmetric movements only for the initial configuration, where the longitudinal axis of the femoral head was rotated by 20° to the right of the vertical axis of the acetabulum (Figure 1-D). Rotations occurred about this new offset axis instead of the vertical axis. This new setup was also used to explore the effect of reduced asymmetric movements at each of the three stages of development as described in Table 1. Finally, simulations with a constant rate of rudiment expansion were run in order to separate out the influences of growth rate and range of movements on the resulting joint shape.

Growth & Morphogenesis

Growth and morphogenesis of the rudiments were controlled by biological and mechanobiological growth rates (Giorgi et al., 2014). The biological contribution was considered to be proportional to the chondrocyte density (Heegaard et al., 1999). For the femoral head, the chondrocyte density was greatest at the proximal epiphysis of the rudiment (Heegaard et al., 1999), while for the pelvic rudiment, the chondrocyte density was greatest at the acetabulum, as shown in Figure 3-A. We are unaware of any study quantifying the rate of expansion at the triradiate cartilage. However, by comparing the rates of growth of the

murine long bones (Hansson et al., 1972) and the pelvis (Harrison, 1958), we calculated that during very early postnatal development, the pelvis grows at a rate which is close to the half that of the femur in the mouse. Therefore, we implemented our model so that the maximum value for the biological contribution at the acetabulum was half that of the femur. For sensitivity analysis purposes, simulations were also run with the same biological contribution between the pelvis and femur. The mechanobiological growth rate was proportional to the dynamic compressive hydrostatic stress generated by the movements (Giorgi et al., 2014). The overall mechanobiological contribution to growth was calculated at each node of the model as the average stresses throughout a full joint motion and was also weighted by the chondrocyte density, based on the assumption that the greater the number of cells, the greater the potential to respond to mechanical loading (Giorgi et al., 2014). The total growth was the sum of the biological and mechanobiological contributions as shown by the equations below (Giorgi et al., 2014):

$$\frac{d\varepsilon}{dt} = \frac{d(\varepsilon_b)}{dt} + \frac{d(\varepsilon_m)}{dt}$$

where:

$$\frac{d(\varepsilon_b)}{dt} = \dot{\varepsilon}_b = C_d = (0.14 - 0.87\xi^2 - 2.66\xi^3)$$

$$\frac{d(\varepsilon_m)}{dt} = \dot{\varepsilon}_m = -C_d * \left(\frac{\sum_{i=1}^{N} \sigma_{hi}}{N} \right)$$

Where $\dot{\varepsilon}_b$ and $\dot{\varepsilon}_m$ are the biological and mechanobiological contribution to growth respectively (Shefelbine and Carter, 2004), C_d the chondrocyte density, which is a function of

ξ, the distance from the end of the rudiment. σ_h the compressive hydrostatic stress, and N the number of movements per step.

Morphological changes due to growth or adaptation were analysed relative to the initial shape of the joint. The changes in shape were assessed over time by looking at two parameters, the "acetabular ratio" and the "femoral head ratio". These parameters are derived from the measurements proposed by Ralis & McKibbin (1973) and as shown in figure 1-B. The congruence of the joint over the developmental period was assessed as the degree of joint coverage, which was measured as the length of the edges in common between the acetabulum and the femoral head. As a measure of asymmetry, we calculated the acetabular and femoral head skew factors (Figure 1-E). A reference point was identified using the centre of the initial acetabular cavity, the crossing point between its vertical and horizontal axes (Figure 1-A, E). This reference point was then kept constant over development, and the skew factor was calculated as the distance between this point and its most left and right extremities (Figure 1-E). The same technique was used for the femoral head, where the skew factor was calculated as the distance between the rotational center, and the left and right extremes on the horizontal line through the reference point.

Results

Hydrostatic stress distribution

The resulting hydrostatic stresses of an entire cycle of motion were always compressive, as shown by Figure 3-B, due to the two rudiments being always in contact. Stresses due to symmetric movements, when applied to the initial geometry, were higher in the acetabulum (especially in its rim) and along the distal curvature of the femoral head. When combined with the biological growth rates, the stresses generated by one full cycle of physiological

motion showed higher values of growth at the most proximal part of the femoral head and at the middle of the acetabulum (as shown in Figure 3-C).

Morphogenesis

When growth due to physiological symmetric movements was simulated, the model predicted a progressive opening of the acetabulum, making it increasingly shallow up to birth, and a gradual decrease in roundness of the femoral head with the onset of a flatter surface at its most proximal region (Figure 4–A, B). The predicted joint at birth had roughly half the acetabular coverage of the initial shape, but maintained a clear interlocking shape (Figure 4-A). The predicted trends showed a striking similarity with the experimental data (Ráliš and McKibbin, 1973), as shown in Figure 4-B, C. The predicted decrease in the acetabular ratio over the course of the simulation is almost identical (although slightly shifted) as compared to the experimental curve, while our model predicts a faster decrease in femoral head roundness in the early phase of gestation than for the experimental data. When reduced movements at the early stage were simulated, the femoral head roundness decreased further and the acetabulum became shallower compared to the physiological predictions (Figure 5-A, B), resulting in a 60% decrease in acetabular coverage of the femoral head (as compared with the initial shape), and therefore potentially a less stable joint at birth. Reduced movements at the middle or late stage of development resulted in minimal joint shape changes from the physiological joint prediction (Figure 5-A). When absent movements were simulated the acetabulum became even shallower and the femoral head ratio decreased even further compared with the predicted shape for early reduced movements (Figure 5-A). Therefore, the presence of movements at the early stage were most critical in maintaining acetabular coverage of the femoral head, with reduced or absent movements in the early stage contributing to decreased coverage of the femoral head, and a likely reduction in joint stability. When, simulations were run with the same biological contribution between the

pelvis and femur, the results showed the onset of a non-interlocking joint shape (Supplementary Figure 1). When a constant rate of rudiment expansion was implemented, the results showed that the rates at which the acetabular ratio and the femoral head ratio decreased were inversely proportional to the ranges of movement (Supplementary Figure 2). Therefore, the reason why movement is most critical at the early stage of development is due to the higher rate of fetal growth (rudiment expansion) used during this stage.

When an asymmetric movement pattern was applied, the acetabulum became increasingly open in the direction of the applied loads (Figure 6-A), leading to development of an asymmetric shape. The shape of the femoral head was also affected, showing a loss of head roundness and the onset of a malformed overall shape (Figure 6-A). The predicted shape is similar to the deformed shape typical of a dysplastic hip joint as shown in figure 6-B. When asymmetric movements were reduced, or absent completely, a deeper acetabulum was predicted for simulations with reduced early, or absent movements, than for simulations with a full range of asymmetric movements, or reduced movements in the middle or late stages (Figure 7-A). By measuring the acetabular skew factor (Figure 1-E), we observed that the simulations with a full range of asymmetric movement throughout, or full asymmetric movement at the early stage, resulted in a more asymmetric acetabular shape compared with other asymmetric simulations (Figure 7-B). This suggests that, in case of asymmetric loading, the higher the range of movement at an early stage, the higher the likelihood of a skewed, shallower acetabulum. Therefore, asymmetric movements have the opposite effect on acetabular shape than symmetric movements. No influence of reduced or absent asymmetric movements, as compared to a full range of asymmetric movements, was found for the femoral head roundness or skew factor (data not shown), which always exhibited the asymmetric profile shown in Figure 6.

Discussion

In this study we describe a dynamic mechanobiological simulation of the prenatal hip joint with which we explore the effects of normal, reduced and asymmetric fetal movements on hip joint growth and morphogenesis, providing insight into the normal physiology of the hip joint and the etiology of DDH. The predicted joint shapes when physiological, symmetric movements was applied well approximated the anatomical changes in shape reported in the literature for fetal human hip joint development (Ráliš and McKibbin, 1973). In our predictions, the acetabulum progressively opened and the femoral head showed the onset of a flatter surface at its proximal end over development (Figure 4-A, B). The overall joint shape changes replicated the trends of human hip joint development, where its natural growth and development leads to a decrease in coverage of the femoral head while maintaining its interlocking shape (Figure 4-A, B, C).

When reduced symmetric movements at the early stage of development were simulated, the joint maintained its interlocking shape at birth but the femoral head roundness decreased and the acetabulum became shallower (Figure 5-A, B). Our results suggest that fetal movements tend to minimise the natural trend of decreasing stability (Figure 5-A). When, for sensitivity analysis, symmetric movements with a constant growth rate (rudiment expansion) were simulated, the rates at which the acetabular ratio and the femoral head ratio decreased were inversely proportional to the ranges of movement. This indicates that, with a constant growth rate, the larger the range of movement, the greater the acetabular depth and femoral head roundness. The shape predicted under early reduced movements would likely be less stable at birth than under normal physiological conditions due to the loss of joint coverage, which would increase the risk of subluxation or dislocation of the hip. When reduced movements at the middle or late stage of development were simulated, minimal changes in joint shape compared to growth under physiological movement were observed (Figure 5-A), suggesting

that movement in the early stage of development is the most critical for joint shape. This may explain why the hip joint is so severely affected in cases of paralytic dislocations, where movement may have been reduced or absent from an early stage of development. When an asymmetric movement pattern was simulated, the predicted joint shape was abnormal: the acetabulum opened in the same direction as the applied loads and the femoral head lost its roundness, showing an overall deformed shape of the joint typical of hip dysplasia as shown in Figure 6-B. Acetabular depth and skew were exacerbated with greater asymmetric movement ranges (Figure 7-B), suggesting that increased movements in the case of mal-positioning or joint laxity in utero may actually increase the risk of DDH.

Although the shape of the joint and movement patterns have been simplified in this model, our simulations predicted similar anatomical changes in shape to the experimental measurements presented by Ralis & McKibbin (1973) (Figure 4-C) allowing us to explore the effects of normal, reduced and abnormal prenatal movements on hip joint shape. While the predicted decrease in the acetabular ratio was almost identical (although slightly shifted), the decrease in femoral head ratio was faster, especially in the early phase of gestation, compared to the experimental curve (Figure 4-B, C). The difference in the predictions may be due to the shapes used, as while the simple profile used for the acetabulum is likely to represent the structure fairly well, the symmetric shape used for the femoral head is much simpler than the reality. Accurate 3D shapes of prenatal joints are currently not available, but we expect that if a more realistic femoral head shape were to be included in our model, more accurate results would be obtained from our simulations. We are unaware of any previous studies showing the physiological range of motion of the prenatal hip. For this study, the maximum range of hip motion at different stages was gathered by analysing different MR imaging sequences of the developing fetus. Even if the actual range of motion used may not perfectly match with the real physiological motion, the reduced trend of physiological symmetric movements over

time reflect the finding of Hayat et al. (2011). In this study, we assumed that during normal development the movement at the fetal hip joint is symmetric, based on previous observations that at the very early prenatal age the femoral head is almost fully covered by the acetabular cavity (Ráliš and McKibbin, 1973) minimising all translations. Conditions such as fetal breech position or joint laxity (Luterkort et al., 1986; Muller and Seddon, 1953; Portinaro et al., 1994) which are risk factors for DDH (Ponseti, 1978; Portinaro et al., 1994), were assumed to lead to asymmetric movements at the hip, due to the loss of the distributed pressure patterns that these conditions may generate. All the simulations were run using 2D dynamic models, due to the lack of access to fetal realistic hip joint shapes. However, as stated in our previous study (Giorgi et al., 2014), minimal additional insights on the effects of joint motion on shape could have be gained by using 3D simulations in the absence of realistic joint shape.

In conclusion, this study demonstrates that normal fetal movements are important for the emergence of hip joint shape and coverage. The natural tendency of the developing hip joint is to decrease in sphericity and acetabular coverage of the femoral head between 11 gestational weeks and birth (Ráliš and McKibbin, 1973) and our model predicted these physiological trends. We show that physiological, symmetric movements help to maintain some of the acetabular depth and femoral head sphericity while reduced movements at an early stage of development or completely absent movements, such as could occur from a neuromuscular disorder, lead to decreased sphericity and acetabular coverage of the femoral head, increasing the risk of subluxation or dislocation of the hip. We also show that asymmetric movements, which we hypothesise to result from fetal breech position or increased joint laxity, lead to an abnormal hip joint shape with characteristics of DDH such as a malformed femoral head and an asymmetric shallower acetabulum which increase the likelihood for the femoral head to dislocate (Larsson et al., 1991; Ziegler et al., 2008).

Therefore, this research provides evidence for the importance of fetal movements in promoting normal hip joint morphogenesis, particularly joint coverage, and an explanation how abnormal movements could lead to joint instability and DDH in the infantile hip.

Acknowledgements: The authors express their gratitude to Prof Jo Hajnal and Prof Mary Rutherford (King's College London, UK) for providing access to the fetal cine-MRI data used as part of this study. This research was funded by the European Research Council under the European Union's Seventh Framework Programme (ERC Grant agreement n° [336306]). The funders had no role in study design, data collection and analysis, decision to publish, or preparation of the manuscript.

Conflict of interest: The authors have no conflicts of interest relating to this research.

References

American Academy of Pediatrics, 2000. Committee on Quality Improvement, Subcommittee on Developmental Dysplasia of the Hip. Clinical practice guideline: early detection of developmental dysplasia of the hip. Pediatrics 105, 896-905.

Aronsson, D., Goldberg, M., Kling Jr, T., Roy, D., 1994. Developmental dysplasia of the hip. Pediatrics 94, 201.

Carter, D., Beaupre, G., 1999. Linear elastic and poroelastic models of cartilage can produce comparable stress results: a comment on Tanck et al.(J Biomech 32: 153-161, 1999). Journal of Biomechanics 32, 1255-1257.

Doubilet, P.M., Benson, C.B., Nadel, A.S., Ringer, S.A., 1997. Improved birth weight table for neonates developed from gestations dated by early ultrasonography. Journal of ultrasound in medicine 16, 241-249.

Giorgi, M., Carriero, A., Shefelbine, S.J., Nowlan, N.C., 2014. Mechanobiological simulations of prenatal joint morphogenesis. Journal of Biomechanics 47, 989-995.

Hansson, L., Menander-Sellman, K., Stenström, A., Thorngren, K.-G., 1972. Rate of normal longitudinal bone growth in the rat. Calcified tissue research 10, 238-251.

Harrison, T., 1958. The growth of the pelvis in the rat—a mensural and morphological study. Journal of Anatomy 92, 236.

Hayat, T., Nihat, A., Martinez-Biarge, M., McGuinness, A., Allsop, J., Hajnal, J., Rutherford, M., 2011. Optimization and initial experience of a multisection balanced steady-state free precession cine sequence for the assessment of fetal behavior in utero. American Journal of Neuroradiology 32, 331-338.

Heegaard, J.H., Beaupré, G.S., Carter, D.R., 1999. Mechanically modulated cartilage growth may regulate joint surface morphogenesis. Journal of Orthopaedic Research 17, 509-517.

Hinderaker, T., Daltveit, A.K., Irgens, L.M., Udén, A., Reikeräs, O., 1994. The impact of intra-uterine factors on neonatal hip instability. Acta Orthopaedica 65, 239-242.

Larsson, T., Aspden, R.M., Heinegård, D., 1991. Effects of Mechanical Load on Cartilage Matrix Biosynthesis In Vitro. Matrix 11, 388-394.

Leck, I., 2000. Congenital dislocation of the hip. In: Antenatal and Neonatal Screening. Oxford University Press.

Luterkort, M., Persson, P.H., Polberger, S., Bjerre, I., 1986. Hip joint instability in breech pregnancy. Acta pædiatrica Scandinavica 75, 860-863.

Muller, G., Seddon, H., 1953. Late results of treatment of congenital dislocation of the hip. J Bone Joint Surg Br 35, 342-362.

Nowlan, N.C., Sharpe, J., 2014. Joint shape morphogenesis precedes cavitation of the developing hip joint. Journal of Anatomy 224, 482-489.

Pacifici, M., Koyama, E., Iwamoto, M., 2005. Mechanisms of synovial joint and articular cartilage formation: Recent advances, but many lingering mysteries. Birth Defects Research Part C: Embryo Today: Reviews 75, 237-248.

Ponseti, I.V., 1978. Morphology of the acetabulum in congenital dislocation of the hip. J Bone Joint Surg [Am] 60, 586-599.

Portinaro, N., Matthews, S., Benson, M., 1994. The acetabular notch in hip dysplasia. Journal of Bone & Joint Surgery, British Volume 76, 271-273.

Ráliš, Z., McKibbin, B., 1973. Changes in shape of the human hip joint during its development and their relation to its stability. Journal of Bone & Joint Surgery, British Volume 55, 780-785.

Record, R., Edwards, J., 1958. Environmental influences related to the aetiology of congenital dislocation of the hip. British journal of preventive & social medicine 12, 8-22.

Scheuer, L., Black, S., 2004. The Juvenile Skeleton. Elsevier Ltd.

Shefelbine, S.J., Carter, D.R., 2004. Mechanobiological predictions of growth front morphology in developmental hip dysplasia. Journal of Orthopaedic Research 22, 346-352.

Tanck, E., Van Donkelaar, C.C., Jepsen, K.J., Goldstein, S.A., Weinans, H., Burger, E.H., Huiskes, R., 2004. The mechanical consequences of mineralization in embryonic bone. Bone 35, 186-190.

Ward, A., Pitsillides, A., 1998. Development Immobilization Induces Failure of Joint Cavity Formation by a Process Involving Selective Local Changes in Glycosaminoglycan Synthesis. Transactions of the annual meeting-orthopaedic research society, 199-199.

Wong, M., Ponticiello, M., Kovanen, V., Jurvelin, J., 2000. Volumetric changes of articular cartilage during stress relaxation in unconfined compression. Journal of Biomechanics 33, 1049-1054.

Ziegler, J., Thielemann, F., Mayer-Athenstaedt, C., Günther, K., 2008. The natural history of developmental dysplasia of the hip. A meta-analysis of the published literature. Der Orthopade 37, 515-516, 518-524.

List of Figures:

Figure 1. A) Dimensions of initial model of concave pelvis and spherical femoral head region. B) Changes in shape were assessed by the measurements proposed by Ralis & McKibbin (1973), where the acetabular shape was assessed by the ratio between the deepest height (a_2) to the greatest width (a_1) of the acetabular cavity, and the femoral head shape was assessed as the ratio between the greatest height (h_2) as measured perpendicularly to the greatest diameter, and the greatest diameter (h_1) of the femoral head. C) Changes in fetal weight on a logarithmic scale (extracted from data from (Doubilet et al., 1997) taken as a measure of the rate of fetal growth. Three stages of fetal growth were identified by fitting lines to regions of the growth curve; the movements applied for each stage are superimposed. D) Initial configuration used for the abnormal (asymmetric) movement; the femoral head is rotated 20° to the right of the vertical axis of the acetabulum. E) Method used to calculate the acetabular and femoral head skew factors; the former measured as the ratio of the distances between a reference point, calculated as the centre of the initial acetabular cavity, and the left (x_1) and right (x_2) extremities of the acetabular space, the latter as the ratio of the distances between a reference point, calculated as the centre of the initial femoral head, and the left (y_1) and right (y_2) extremities which lie on the horizontal line passing through the reference point of the femoral head.

Figure 2. A) Two timeframes from a fetal cine-MRI at 22 gestational weeks showing a hip flexion-extension range of 88°. B) Timeframes from a fetal cine-MRI at 34 gestational weeks showing a hip flexion-extension of 11°. These data were used to estimate the range of motion at the hip over gestation. Fetal cine-MR images courtesy of Professors Hajnal and Rutherford, Kings College London, UK.

Figure 3. A) Biological contribution to growth; for the femoral head the chondrocyte density was greatest at the proximal end of the epiphysis, while for the pelvis the density was highest at the centre of the acetabulum. B) Resulting hydrostatic stresses, averaged over the first full cycle of physiological motion. Stresses were higher along the acetabular rim and at the regions of curvature of the distal femoral head. C) The stresses generated by the combination of biological and hydrostatic stresses lead to higher values of growth at the proximal end of the femoral head and at the center of the acetabulum.

Figure 4. A) Predicted hip joint morphogenesis under physiological symmetric movements; a progressive opening of the acetabulum and a gradual decrease in roundness of the femoral head were predicted. B) Quantification of the changes in shape based on the acetabular shape and femoral head roundness parameters. C) Changes in human hip joint shape over development measured experimentally by Ralis & McKibbin (1973).

Figure 5. A) The effects on acetabular and femoral head shape of reduced movements at each stage of development (early, middle and late) and of a complete absence of movements. When movements were reduced at the early stage, the acetabulum became shallower and the femoral head roundness decreased compared to the predictions for physiological movements. Reduced movements in the middle and late stages of development resulted in minimal joint shape changes. When absent movements were simulated, the shape changes were similar to those of the early reduction simulation, with the predicted joint shape for absent movement having a slightly shallower acetabulum than that of the early reduction. B) Predicted shapes under physiological movements (blue) and early reduction of movements (red). When movements were reduced in the early stage, a less rounded femoral head and a shallower acetabulum were predicted.

Figure 6. A) Predicted joint morphogenesis under asymmetric movements; a progressive opening of the acetabulum in the direction of the applied loads was predicted, while the femoral head showed a loss of head sphericity and malformation on the medial side. B) The predicted hip joint shape at birth when asymmetric loading occurs is similar to the hip joint of a 30 month old infant affected by DDH. Image adapted with permission from Dr Frank Gaillard from website www.radiopaedia.org.

Figure 7. A) The effects of reduced asymmetric movements on acetabular shape and B) skew factor at each stage of development (early, middle and late) and under a complete absence of movements. With a full range of asymmetric movement, or reduced movement at the middle or late stages, the predicted acetabular shape was shallower than for simulations with no movement or with reduced movement in the early stage.

List of Tables:

Table 1 – Ranges of motion, in degrees, applied about an axis during each stage of development for simulations involving symmetric and asymmetric movements. When symmetric movements were applied, the centre of the axis of rotation was through the midline of the femoral head, with the initial position of the femoral head being perpendicular to the acetabulum. Equivalent reductions in the early, middle, late stages, and absent movements, were also simulated for the abnormal initial position of the femur which was rotated 20^0 to the right.

Figure 1

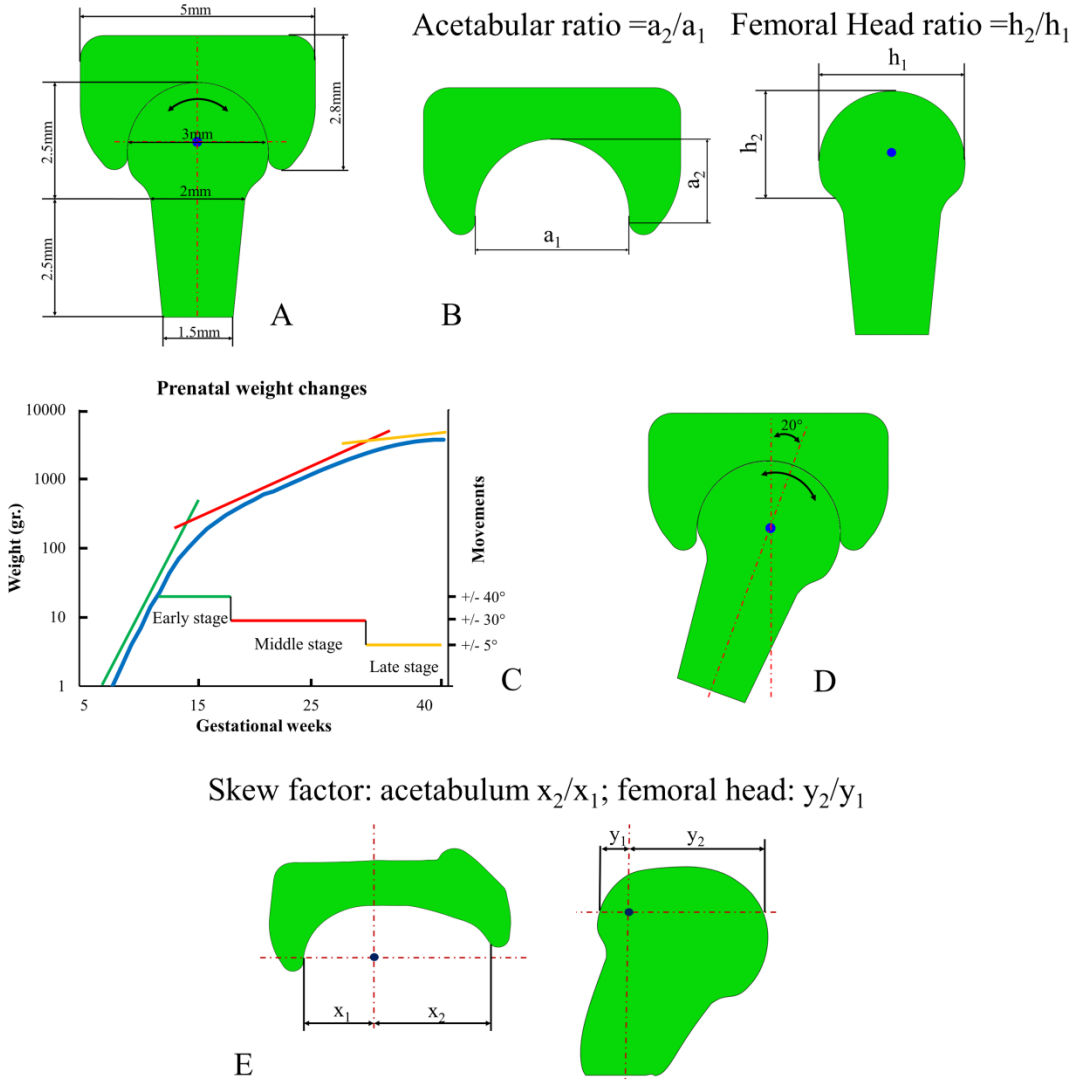
5mm
2.8mm
3mm
2.5mm
2mm
2.5mm
1.5mm
A
Acetabular ratio =a_2/a_1
a_2
a_1
B
Femoral Head ratio =h_2/h_1
h_1
h_2
Prenatal weight changes
Weight (gr.)
10000
1000
100
10
1
5
15
25
40
Gestational weeks
Movements
+/- 40°
+/- 30°
+/- 5°
Early stage
Middle stage
Late stage
C
20°
D
Skew factor: acetabulum x_2/x_1; femoral head: y_2/y_1
x_1
x_2
E
y_1
y_2

Figure 2

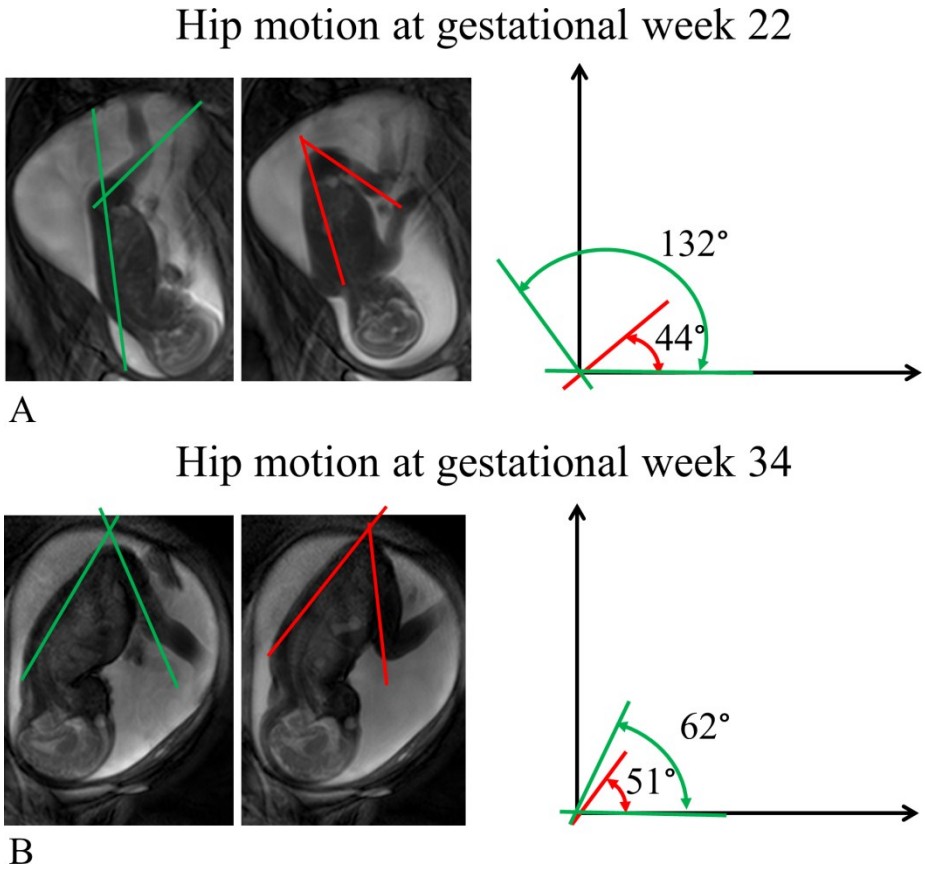
Hip motion at gestational week 22
132°
44°
A
Hip motion at gestational week 34
62°
51°
B

Figure 3

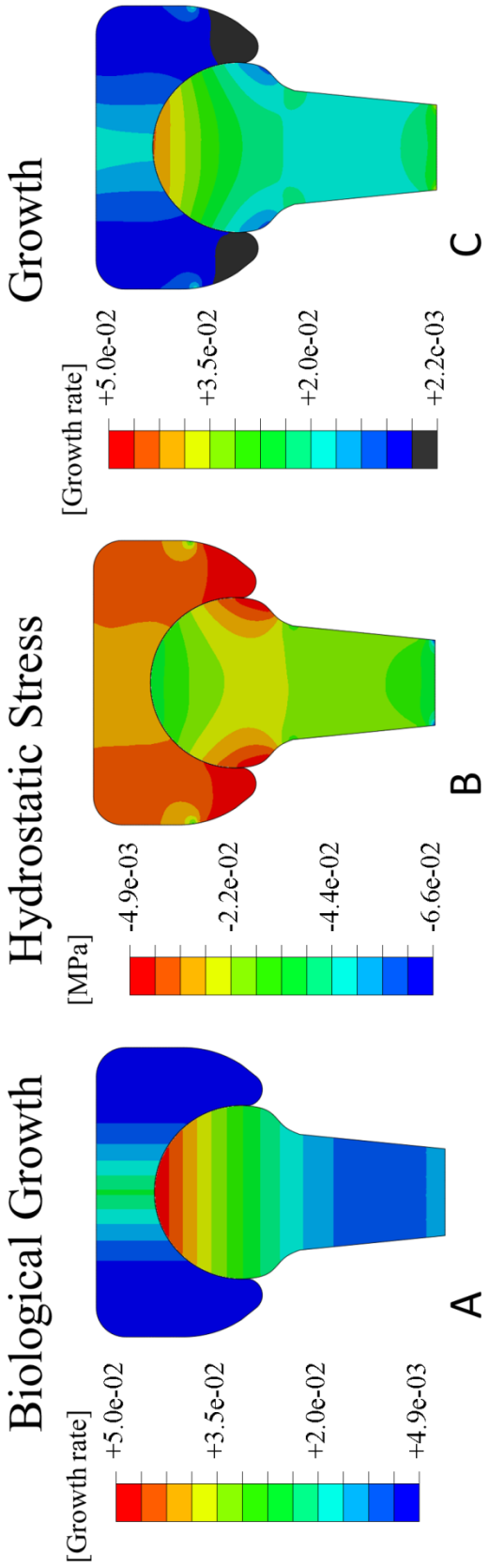
Biological Growth
[Growth rate]
+5.0e-02
+3.5e-02
+2.0e-02
+4.9e-03
A
Hydrostatic Stress
[MPa]
-4.9e-03
-2.2e-02
-4.4e-02
-6.6e-02
B
Growth
[Growth rate]
+5.0e-02
+3.5e-02
+2.0e-02
+2.2e-03
C

Figure 4

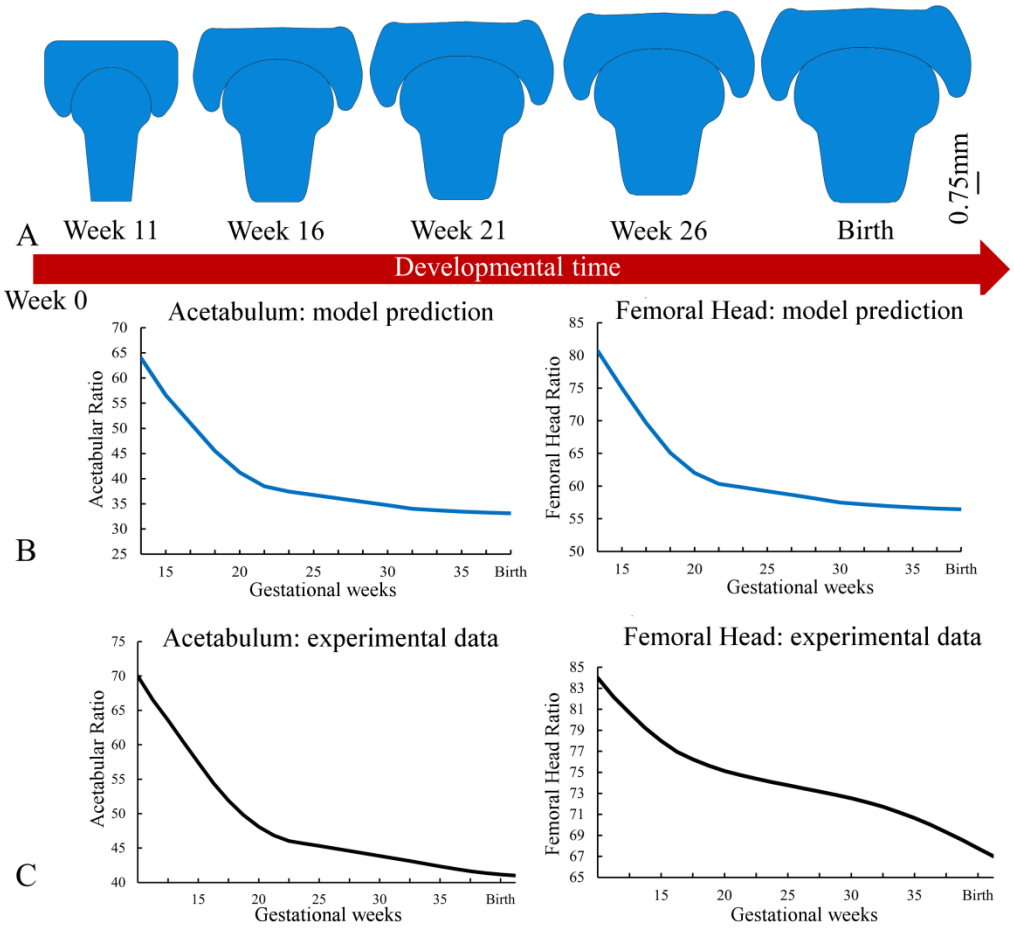
A
Week 11
Week 16
Week 21
Week 26
Birth
0.75mm
Developmental time
Week 0
B
Acetabulum: model prediction
Acetabular Ratio
Gestational weeks
Birth
Femoral Head: model prediction
Femoral Head Ratio
Gestational weeks
Birth
C
Acetabulum: experimental data
Acetabular Ratio
Gestational weeks
Birth
Femoral Head: experimental data
Femoral Head Ratio
Gestational weeks
Birth

Figure 5

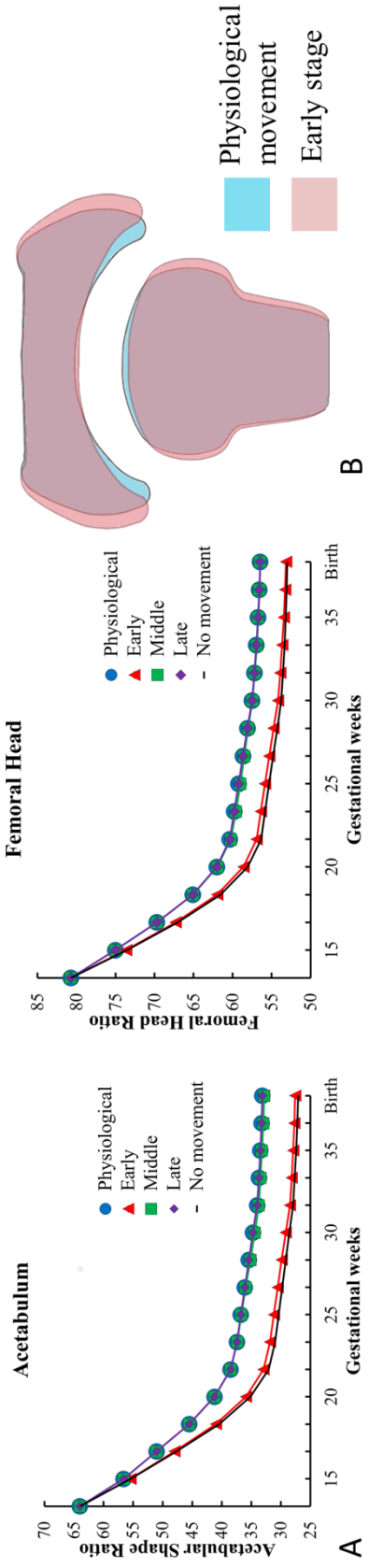
Physiological movement
Early stage
B
Femoral Head
Femoral Head Ratio
85
80
75
70
65
60
55
50
15
20
25
30
35
Birth
Gestational weeks
Physiological
Early
Middle
Late
No movement
Acetabulum
Acetabular Shape Ratio
70
65
60
55
50
45
40
35
30
25
15
20
25
30
35
Birth
Gestational weeks
Physiological
Early
Middle
Late
No movement
A

Figure 6

0.75mm
A
Week 0
Week 11
Week 16
Week 21
Week 26
Birth
Developmental time
B

Figure 7

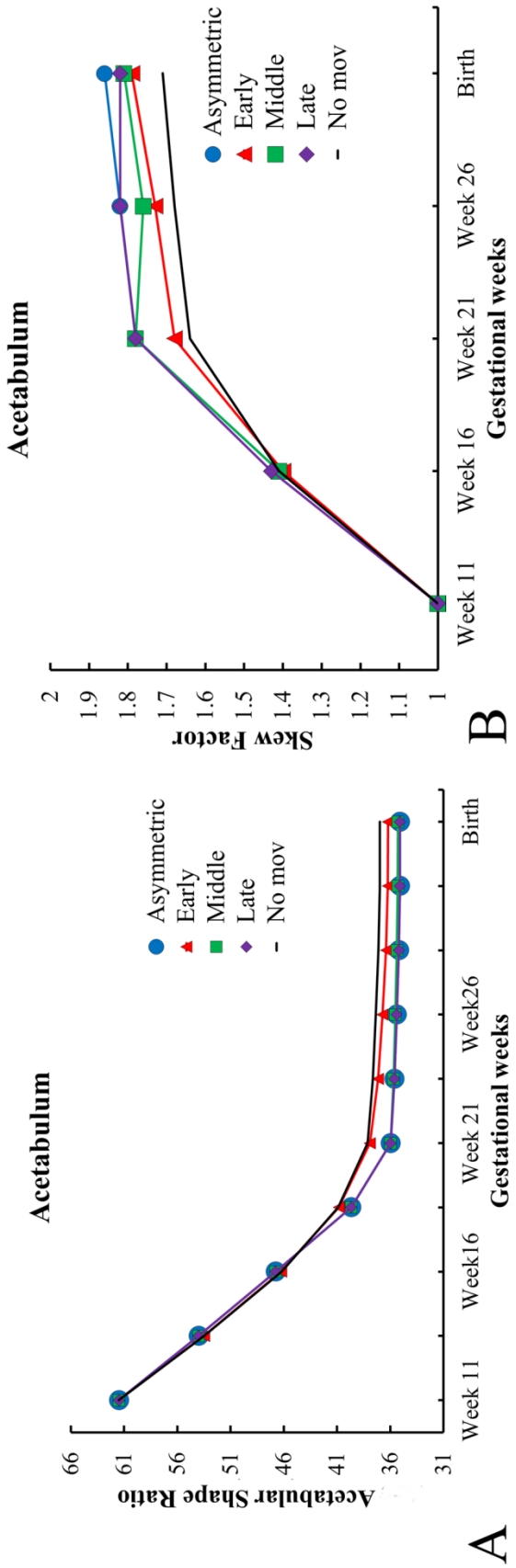
Acetabulum
Asymmetric
Early
Middle
Late
No mov
Skew Factor
2
1.9
1.8
1.7
1.6
1.5
1.4
1.3
1.2
1.1
1
Week 11
Week 16
Week 21
Week 26
Birth
Gestational weeks
B
Acetabulum
Asymmetric
Early
Middle
Late
No mov
Acetabular Shape Ratio
66
61
56
51
46
41
36
31
Week 11
Week16
Week 21
Week26
Birth
Gestational weeks
A

Type of movements	Early 11th–18th Weeks	Middle 19th–34th Weeks	Late 35th–birth
Symmetric movements [°]			
Physiological	+/- 40	+/- 30	+/- 5
Early reduction	+/- 10	+/- 30	+/- 5
Middle reduction	+/- 40	+/- 8	+/- 5
Late reduction	+/- 40	+/- 30	+/- 1
No movements	0	0	0

Table 1